Chapter 2
Gravity methods

2.1 INTRODUCTION

Gravity surveying measures variations in the Earth's gravitational field caused by differences in the density of sub-surface rocks. Although known colloquially as the 'gravity' method, it is in fact the variation of the *acceleration* due to gravity that is measured. Gravity methods have been used most extensively in the search for oil and gas, particularly in the early twentieth century. While such methods are still employed very widely in hydrocarbon exploration, many other applications have been found (Table 2.1), some examples of which are described in more detail in Section 2.7.

Micro-gravity surveys are those conducted on a very small scale – of the order of hundreds of square metres – and which are capable of detecting cavities, for example, as small as 1 m in diameter within 5 m of the surface.

Perhaps the most dramatic change in gravity exploration in the 1980s has been the development of instrumentation which now permits *airborne* gravity surveys to be undertaken routinely and with a high degree of accuracy (see Section 2.5.7). This has allowed aircraft-borne gravimeters to be used over otherwise inaccessible terrain and has led to the discovery of several small but significant areas with economic hydrocarbon potentials.

Table 2.1 Applications of gravity surveying

Hydrocarbon exploration
Regional geological studies
Isostatic compensation determination
Exploration for, and mass estimation of, mineral deposits
Detection of sub-surface cavities (micro-gravity)
Location of buried rock-valleys
Determination of glacier thickness
Tidal oscillations
Archaeogeophysics (micro-gravity); e.g. location of tombs
Shape of the earth (geodesy)
Military (especially for missile trajectories)
Monitoring volcanoes

2.2 PHYSICAL BASIS

2.2.1 Theory

The basis on which the gravity method depends is encapsulated in two laws derived by Sir Isaac Newton, which he described in *Principia Mathematica* (1687) – namely his Universal Law of Gravitation, and his Second Law of Motion.

The first of these two laws states that the force of attraction between two bodies of known mass is directly proportional to the product of the two masses and inversely proportional to the square of the distance between their centres of mass (Box 2.1). Consequently, the greater the distance separating the centres of mass, the smaller is the force of attraction between them.

Box 2.1 Newton's Universal Law of Gravitation

$$\text{Force} = \text{gravitational constant} \times \frac{\text{mass of Earth } (M) \times \text{mass } (m)}{(\text{distance between masses})^2}$$

$$F = \frac{G \times M \times m}{R^2} \qquad \text{(equation (1))}$$

where the gravitational constant $(G) = 6.67 \times 10^{-11}\ \text{N m}^2\ \text{kg}^{-2}$

Newton's law of motion states that a force (F) is equal to mass (m) times acceleration (Box 2.2). If the acceleration is in a vertical direction, it is then due to gravity (g).

Box 2.2 Newton's Second Law of Motion

$$\text{Force} = \text{mass } (m) \times \text{acceleration } (g)$$

$$F = m \times g \qquad \text{(equation (2))}$$

Equations (1) and (2) can be combined to obtain another simple relationship:

$$F = \frac{G \times M \times m}{R^2} = m \times g; \quad \text{thus } g = \frac{G \times M}{R^2} \qquad \text{(equation (3)).}$$

This shows that the magnitude of the acceleration due to gravity on Earth (g) is directly proportional to the mass (M) of the Earth and inversely proportional to the square of the Earth's radius (R). Theoretically, acceleration due to gravity should be constant over the Earth. In reality, gravity varies from place to place because the Earth has the shape of a flattened sphere (like an orange or an inverted pear),

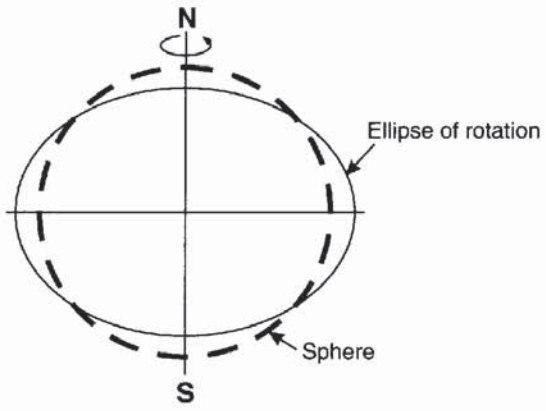

Figure 2.1 Exaggerated difference between a sphere and an ellipse of rotation (spheroid)

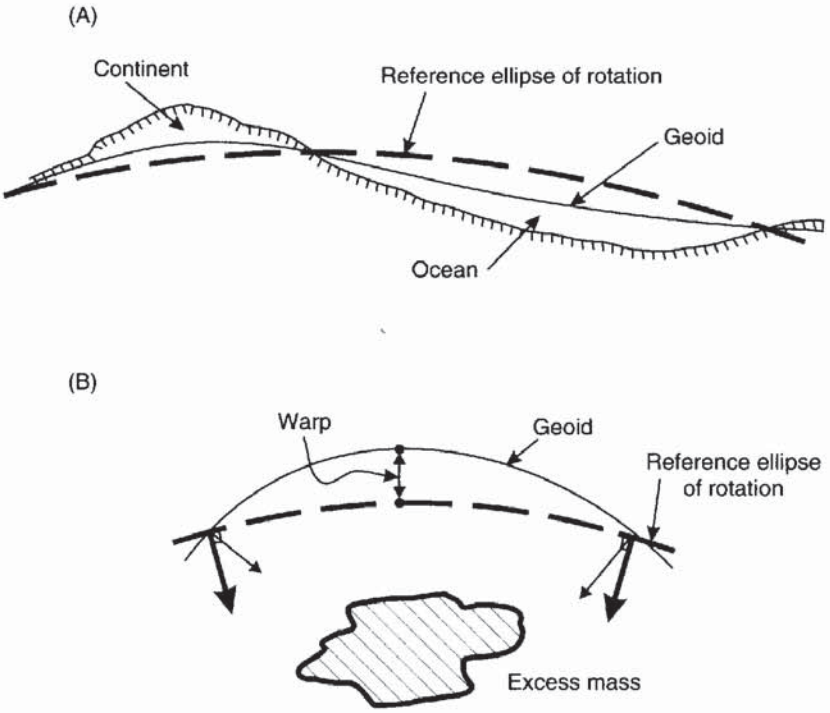

Figure 2.2 Warping of the geoid: (A) continental-scale effects, and (B) localised effects due to a sub-surface excess mass

rotates, and has an irregular surface topography and variable mass distribution (especially near the surface).

The shape of the Earth is a consequence of the balance between gravitational and centrifugal accelerations causing a slight flattening to form an oblate spheroid. Mathematically it is convenient to refer to the Earth's shape as being an *ellipse of rotation* (Figure 2.1).

The sea-level surface, if undisturbed by winds or tides, is known as the *geoid* and is particularly important in gravity surveying as it is horizontal and at right angles to the direction of the acceleration due

to gravity everywhere. The geoid represents a surface over which the gravitational field has equal value and is called an *equipotential surface*. The irregular distribution of mass, especially near the Earth's surface, warps the geoid so that it is not identical to the ellipse of rotation (Figure 2.2). Long-wavelength anomalies, which can be mapped using data from satellites (Wagner *et al.* 1977), relate to very deep-seated masses in the mantle (Figure 2.2A), whereas density features at shallow depths cause shorter-wavelength warps in the geoid (Figure 2.2B). Consequently, anomalies within the gravitational field can be used to determine how mass is distributed. The particular study of the gravitational field and of the form of the Earth is called *geodesy and is used to determine exact geographical locations and to* measure precise distances over the Earth's surface (*geodetic surveying*).

2.2.2 Gravity units

The first measurement of the acceleration due to gravity was made by Galileo in a famous experiment in which he dropped objects from the top of the leaning tower of Pisa. The normal value of g at the Earth's surface is 980 cm/s^2. In honour of Galileo, the c.g.s. unit of acceleration due to gravity (1 cm/s^2) is the *Gal*. Modern gravity meters (gravimeters) can measure extremely small variations in acceleration due to gravity, typically 1 part in 10^9 (equivalent to measuring the distance from the Earth to the Moon to within a metre). The sensitivity of modern instruments is about ten parts per million. Such small numbers have resulted in sub-units being used such as the milliGal (1 mGal = 10^{-3} Gals) and the microGal (1 μGal = 10^{-6} Gals). Since the introduction of SI units, acceleration due to gravity is measured in μm/s^2, which is rather cumbersome and so is referred to as the *gravity unit* (g.u.); 1 g.u. is equal to 0.1 mGal [10 g.u. = 1 mGal]. However, the gravity unit has not been universally accepted and 'mGal' and 'μGal' are still widely used.

2.2.3 Variation of gravity with latitude

The value of acceleration due to gravity varies over the surface of the Earth for a number of reasons, one of which is the Earth's shape. As the polar radius (6357 km) is 21 km shorter than the equatorial radius (6378 km) the points at the poles are closer to the Earth's centre of mass (so smaller value of R) and, therefore, the value of gravity at the poles is greater (by about 0.7%) than that at the equator (Figure 2.3) (see equation (3) under Box 2.2). Furthermore, as the Earth rotates once per sidereal day around its north–south axis, there is a centrifugal acceleration acting which is greatest where the rotational velocity is largest, namely at the equator (1674 km/h; 1047 miles/h) and decreases to zero at the poles (Figure 2.3). The centrifugal

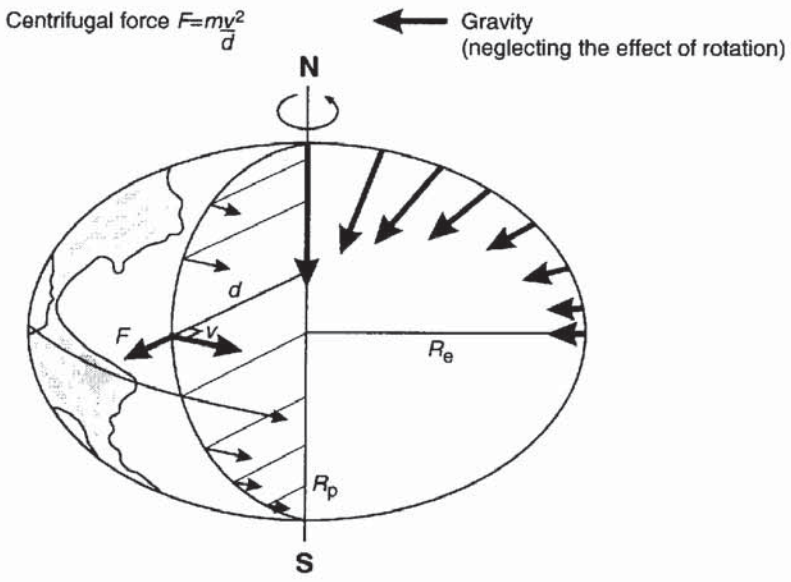

Figure 2.3 Centrifugal acceleration and the variation of gravity with latitude ϕ (not to scale)

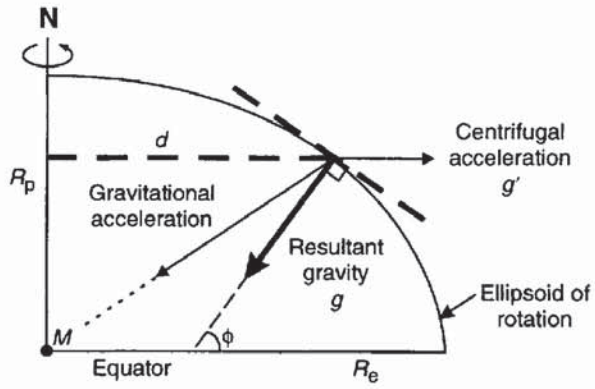

Figure 2.4 Resultant of centrifugal acceleration (g') and the acceleration due to gravity (g) (not to scale); the geographic (geodetic) latitude is given by ϕ. After Robinson and Coruh (1988)

acceleration, which is equal to the rotational velocity (ω) squared times the distance to the rotational axis (d), serves to decrease the value of the gravitational acceleration. It is exactly the same mechanism as that which keeps water in a bucket when it is being whirled in a vertical plane.

The value of gravity measured is the resultant of that acting in a line with the Earth's centre of mass with the centrifugal acceleration (Figure 2.4). The resultant acts at right-angles to the ellipsoid of rotation so that a plumb line, for example, hangs vertically at all locations at sea level. The angle ϕ in Figure 2.4 defines the geodetic (ordinary or geographic) latitude. The resultant gravity at the poles is 5186 mGal (51 860 g.u.) greater than at the equator and varies systematically with latitude in between, as deduced by Clairaut in 1743.

Subsequent calculations in the early twentieth century, based on Clairaut's theory, led to the development of a formula from which it was possible to calculate the theoretical acceleration due to gravity (g_ϕ) at a given geographic latitude (ϕ) relative to that at sea level (g_0). Parameters α and β are constants which depend on the amount of flattening of the spheroid and on the speed of rotation of the Earth.

Box 2.3 General form of the International Gravity Formula

$$g_\phi = g_0(1 + \alpha \sin^2 \phi - \beta \sin^2 2\phi)$$

In 1930 the International Union of Geodesy and Geophysics adopted the form of the *International Gravity Formula* (Nettleton 1971; p. 20) shown in Box 2.3. This became the standard for gravity work. However, refined calculations using more powerful computers and better values for Earth parameters resulted in a new formula – known as the *Geodetic Reference System 1967* (GRS67) – becoming the standard (Woollard 1975) (Box 2.4). If gravity surveys using the 1930 gravity formula are to be compared with those using the 1967 formula, then the third formula (Kearey and Brooks 1991) in Box 2.4 should be used to compensate for the differences between them. Otherwise, discrepancies due to the differences in the equations may be interpreted wrongly as being due to geological causes.

Box 2.4 Standard formulae for the theoretical value of g at a given latitude ϕ

$$g_\phi(1930) = 9.78049\,(1 + 0.0052884 \sin^2 \phi - 0.0000059 \sin^2 2\phi)\ \text{m/s}^2$$

$$\mathbf{g_\phi(1967) = 9.78031846\,(1 + 0.005278895 \sin^2 \phi + 0.000023462 \sin^4 \phi)\ m/s^2}$$

$$g_\phi(1967) - g_\phi(1930) = (-172 + 136 \sin^2 \phi)\ \mu\text{m/s}^2\ \text{(g.u.)}$$

2.2.4 Geological factors affecting density

Gravity surveying is sensitive to variations in rock density, so an appreciation of the factors that affect density will aid the interpretation of gravity data. Ranges of bulk densities for a selection of different material types are listed in Table 2.2 and shown graphically in Figure 2.5.

It should be emphasised that in gravity surveys, the determination of densities is based on rocks that are accessible either at the surface, where they may be weathered and/or dehydrated, or from boreholes, where they may have suffered from stress relaxation and be far more

Table 2.2 Densities of common geologic materials (data from Telford *et al.* 1990)

Material type	Density range (Mg/m^3)	Approximate average density (Mg/m^3)
Sedimentary rocks		
Alluvium	1.96–2.00	1.98
Clay	1.63–2.60	2.21
Gravel	1.70–2.40	2.00
Loess	1.40–1.93	1.64
Silt	1.80–2.20	1.93
Soil	1.20–2.40	1.92
Sand	1.70–2.30	2.00
Sandstone	1.61–2.76	2.35
Shale	1.77–3.20	2.40
Limestone	1.93–2.90	2.55
Dolomite	2.28–2.90	2.70
Chalk	1.53–2.60	2.01
Halite	2.10–2.60	2.22
Glacier ice	0.88–0.92	0.90
Igneous rocks		
Rhyolite	2.35–2.70	2.52
Granite	2.50–2.81	2.64
Andesite	2.40–2.80	2.61
Syenite	2.60–2.95	2.77
Basalt	2.70–3.30	2.99
Gabbro	2.70–3.50	3.03
Metamorphic rocks		
Schist	2.39–2.90	2.64
Gneiss	2.59–3.00	2.80
Phylite	2.68–2.80	2.74
Slate	2.70–2.90	2.79
Granulite	2.52–2.73	2.65
Amphibolite	2.90–3.04	2.96
Eclogite	3.20–3.54	3.37

cracked than when *in situ*. Consequently, errors in the determination of densities are among the most significant in gravity surveying. This should be borne in mind when interpreting gravity anomalies so as not to over-interpret the data and go beyond what is geologically reasonable.

There are several crude 'rules of thumb' which can be used as general guides (Dampney 1977; Telford *et al.* 1990; Nettleton 1971, 1976). Sedimentary rocks tend to be the least dense (average density about $2.1 \pm 0.3\ Mg/m^3$). Within the three fundamental rock classifications there are crude trends and associations which are outlined in the next section. Commonly, units are quoted in terms of grams per cubic centimetre (g/cm^3) but are herein referred to in the SI derived units of Mg/m^3 which are numerically equivalent.

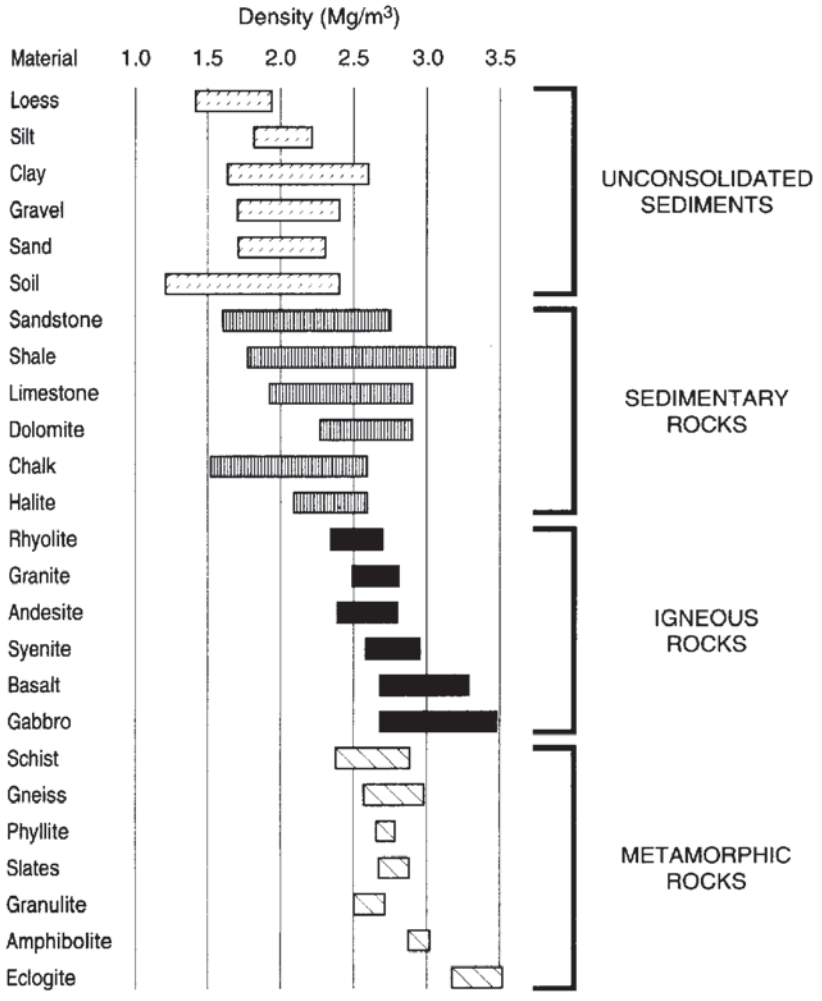

Figure 2.5 Variations in rock density for diffeent rock types. Data from Telford *et al.* (1990)

2.2.4.1 Sedimentary rocks

At least seven factors affect the density of sedimentary materials: composition, cementation, age and depth of burial, tectonic processes, porosity and pore-fluid type. Any or all of these may apply for a given rock mass. The degree to which each of these factors affects rock density is given in Table 2.3; but experience shows that, under normal circumstances, the density contrast between adjacent sedimentary strata is seldom greater than 0.25 Mg/m^3.

Density varies depending on the material of which the rock is made, and the degree of consolidation. Four groups of materials are listed in order of increasing density in Table 2.4. Sediments that remain buried for a long time consolidate and lithify, resulting in reduced porosity and consequently an increased density.

Table 2.3 The effect of different physical factors on density

Factor	Approximate percentage change in density
Composition	35
Cementation	10
Age and depth of burial	25
Tectonic processes	10
Porosity and pore fluids	10

Table 2.4 Approximate average densities of sedimentary rocks

Material type	Approximate average Density (Mg/m^3)
Soils and alluvium	2.0
Shales and clays	2.3
Sandstones and conglomerates	2.4
Limestone and dolomite	2.6

In sandstones and limestones, densification is achieved not by volume change but by pore spaces becoming infilled by natural cement. In shales and clays, the dominant process is that of compaction and, ultimately, recrystallisation into minerals with greater densities.

2.2.4.2 Igneous rocks

Igneous rocks tend to be denser than sedimentary rocks although there is overlap. Density increases with decreasing silica content, so basic igneous rocks are denser than acid ones. Similarly, plutonic rocks tend to be denser than their volcanic equivalents (see Table 2.5).

Table 2.5 Variation of density with silica content and crystal size for selected igneous rocks; density ranges and, in parentheses, average densities are given in Mg/m^3. Data from Telford *et al.* (1990)

Crystal size	Silica content		
	Acid	Intermediate	Basic
Fine-grained (volcanic)	Rhyolite 2.35–2.70 (2.52)	Andesite 2.4–2.8 (2.61)	Basalt 2.70–3.30 (2.99)
Coarse-grained (plutonic)	Granite 2.50–2.81 (2.64)	Syenite 2.60–2.95 (2.77)	Gabbro 2.70–3.50 (3.03)

2.2.4.3 Metamorphic rocks

The density of metamorphic rocks tends to increase with decreasing acidity and with increasing grade of metamorphism. For example, schists may have lower densities than their gneissose equivalents. However, variations in density within metamorphic rocks tend to be far more erratic than in either sedimentary or igneous rocks and can vary considerably over very short distances.

2.2.4.4 Minerals and miscellaneous materials

As the gravity survey method is dependent upon contrast in densities, it is appropriate to highlight some materials with some commercial

Table 2.6 Densities of a selection of metallic and non-metallic minerals and some miscellaneous materials. Data from Telford *et al.* (1990)

Material type	Density range (Mg/m^3)	Approximate average density (Mg/m^3)
Metallic minerals		
Oxides, carbonate		
Manganite	4.2–4.4	4.32
Chromite	4.2–4.6	4.36
Magnetite	4.9–5.2	5.12
Haematite	4.9–5.3	5.18
Cuprite	5.7–6.15	5.92
Cassiterite	6.8–7.1	6.92
Wolframite	7.1–7.5	7.32
Uraninite	8.0–9.97	9.17
Copper	n.d.	8.7
Silver	n.d.	10.5
Gold	15.6–19.4	17.0
Sulphides		
Malachite	3.9–4.03	4.0
Stannite	4.3–4.52	4.4
Pyrrhotite	4.5–4.8	4.65
Molybdenite	4.4–4.8	4.7
Pyrite	4.9–5.2	5.0
Cobaltite	5.8–6.3	6.1
Galena	7.4–7.6	7.5
Cinnabar	8.0–8.2	8.1
Non-metallic minerals		
Gypsum	2.2–2.6	2.35
Bauxite	2.3–2.55	2.45
Kaolinite	2.2–2.63	2.53
Baryte	4.3–4.7	4.47
Miscellaneous materials		
Snow	0.05–0.88	n.d.
Petroleum	0.6–0.9	n.d.
Lignite	1.1–1.25	1.19
Anthracite	1.34–1.8	1.50

value for which the method can be used for exploration purposes. Gravity surveying becomes increasingly appropriate as an exploration tool for those ore materials with greatest densities. The densities of a selection of metallic and non-metallic minerals and of several other materials are listed in Table 2.6.

2.3 MEASUREMENT OF GRAVITY

2.3.1 Absolute gravity

Determination of the acceleration due to gravity in absolute terms requires very careful experimental procedures and is normally only undertaken under laboratory conditions. Two methods of measurement are used, namely the falling body and swinging pendulum methods. However, it is the more easily measured *relative* variations in gravity that are of interest and value to explorationists. More detailed descriptions of how absolute gravity is measured are given by Garland (1965), Nettleton (1976) and Robinson and Coruh (1988). A popular account of gravity and its possible non-Newtonian behaviour has been given by Boslough (1989); see also Parker and Zumberge (1989).

A network of gravity stations has been established worldwide where absolute values of gravity have been determined by reference to locations where absolute gravity has been measured, such as at the National Bureau of Standards at Gaithersburg, USA, the National Physical Laboratory at Teddington, England, and Universidad Nationale de Columbia, Bogata, Columbia. The network is referred to as the *International Gravity Standardisation Net 1971* (IGSN 71) (Morelli 1971) and was established in 1963 by Woollard and Rose (1963). It is thus possible to tie in any regional gravity survey to absolute values by reference to the IGSN 71 and form a primary network of gravity stations.

2.3.2 Relative gravity

In gravity exploration it is not normally necessary to determine the absolute value of gravity, but rather it is the relative variation that is measured. A base station (which can be related to the IGSN 71) is selected and a secondary network of gravity stations is established. All gravity data acquired at stations occupied during the survey are reduced relative to the base station. If there is no need for absolute values of g to be determined, the value of gravity at a local base station is arbitrarily designated as zero. Details of the data reduction procedure are given in Section 2.5.

The spacing of gravity stations is critical to the subsequent interpretation of the data. In regional surveys, stations may be located

with a density of 2–3 per km^2, whereas in exploration for hydrocarbons, the station density may be increased to 8–10 per km^2. In localised surveys where high resolution of shallow features is required, gravity stations may be spaced on a grid with sides of length 5–50 m. In micro-gravity work, the station spacing can be as small as 0.5 m.

For a gravity survey to achieve an accuracy of ± 0.1 mGal, the latitudinal position of the gravimeter must be known to within ± 10 m and the elevation to within ± 10 mm. Furthermore, in conjunction with multiple gravity readings and precision data reduction, gravity data can be obtained to within $\pm 5\,\mu$Gal (Owen 1983). The most significant causes of error in gravity surveys on land are uncertainties in station elevations. At sea, water depths are measured easily by using high-precision echo sounders. Positions are determined increasingly by satellite navigation; and in particular, the advent of the Global Positioning System (GPS) (Bullock 1988), with its compact hardware and fast response time, is resulting in GPS position-fixing becoming more precise. This is particularly true with reference to airborne gravity measurements.

2.4 GRAVITY METERS

No single instrument is capable of meeting all the requirements of every survey, so there are a variety of devices which serve different purposes. In 1749, Pierre Bouguer found that gravity could be measured using a swinging pendulum. By the nineteenth century, the pendulum was in common use to measure relative variations in gravity. The principle of operation is simple. Gravity is inversely proportional to the square of the period of oscillation (T) and directly proportional to the length of the pendulum (L) (Box 2.5). If the same pendulum is swung under identical conditions at two locations where the values of accelerations due to gravity are g_1 and g_2, then the ratio of the two values of g is the same as the ratio of the two corresponding periods of oscillation T_1 and T_2.

Box 2.5 Acceleration due to gravity from pendulum measurements

$$\text{Gravity} = \text{constant} \times \text{pendulum length}/\text{period}^2 \qquad g = 4\pi^2 L/T^2$$

$$\frac{(\text{Period}_1)^2}{(\text{Period}_2)^2} = \frac{\text{gravity}_2}{\text{gravity}_1} \qquad \frac{T_2^2}{T_1^2} = \frac{g_2}{g_1}$$

Further, the size of the difference in acceleration due to gravity (δg) between the two locations is (to the first order) equal to the product of

gravity and twice the difference in periods ($T_2 - T_1$) divided by the first period (Box 2.6). This method is accurate to about 1 mGal if the periods are measured over at least half an hour. Portable systems were used in exploration for hydrocarbons in the 1930s.

Box 2.6 Differences in gravitational acceleration

$$\text{Gravity difference} = -2 \times \text{gravity} \times \frac{\text{difference in periods}}{\text{period}_1};$$

$$\delta g = -2g\frac{(T_2 - T_1)}{T_1}$$

Another method of determining relative gravity is that of the torsion balance (Figure 2.6). English physicist Henry Cavendish devised this system to measure the gravitational constant in 1791. The method was developed for geodetic purposes in 1880 by a Hungarian physicist, Baron Roland von Eötvös. After further modification it was used in exploration from 1915 to the late 1940s. The method, which measures variations in only the horizontal component of gravity due to terrain and not vertical gravity, is capable of very great sensitivity (to 0.001 mGal) but is awkward and very slow to use in the field. The method is described in more detail by Telford *et al.* (1990).

Since about the early 1930s, variations in relative gravity have been measured using gravity meters (gravimeters), firstly stable (static) and

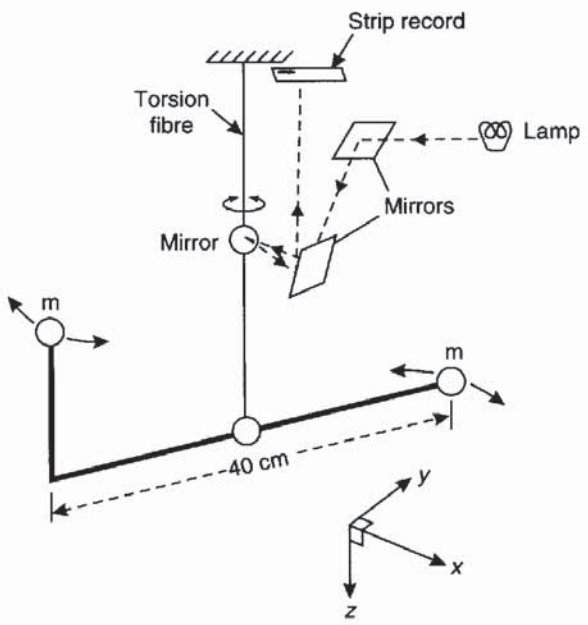

Figure 2.6 Schematic of a torsion balance

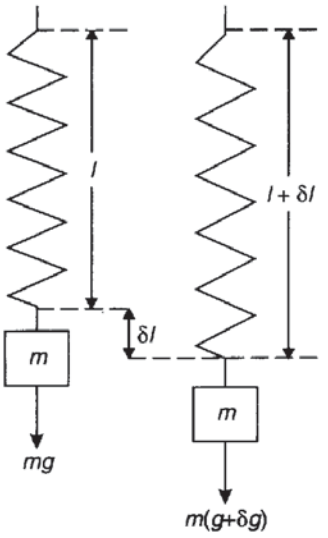

Figure 2.7 Extension (δl) of a spring due to additional gravitational pull (δg)

more recently unstable (astatic) types. Practical aspects of how to use such instruments have been detailed by Milsom (1989, Ch. 2). Gravimeters are sophisticated spring balances from which a constant mass is suspended (Figure 2.7). The weight of the mass is the product of the mass and the acceleration due to gravity. The greater the weight acting on the spring, the more the spring is stretched. The amount of extension (δl) of the spring is proportional to the extending force, i.e. the excess weight of the mass (δg). (Remember that weight equals mass times acceleration due to gravity.) The constant of proportionality is the elastic spring constant κ. This relationship is known as Hooke's Law (Box 2.7).

As the mass is constant, variations in weight are caused by changes in gravity (δg). By measuring the extension of the spring (δl), differences in gravity can then be determined. As the variations in g are very small (1 part in 10^8) the extension of any spring will also be extremely tiny. For a spring 30 cm long, changes in length of the order of 3×10^{-8} m (30 nanometres) have to be measured. Such small distances are even smaller than the wavelength of light (380–780 nm). Consequently, gravimeters use some form of system to amplify the movement so that it can be measured accurately.

Box 2.7 Hooke's Law

Extension to spring = mass $\times \dfrac{\text{change in gravity}}{\text{spring constant}}$	$\delta l = \dfrac{m\delta g}{\kappa}$
Change in gravity = constant $\times$ extension/mass	$\delta g = \kappa \delta l / m$

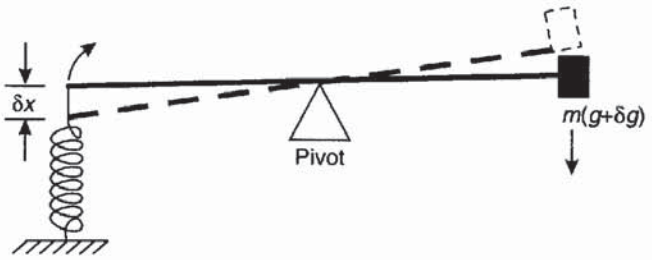

Figure 2.8 Basic principle of operation of a stable gravimeter

2.4.1 Stable (static) gravimeters

Stable gravimeters (Figure 2.8), which were developed in the 1930s, are less sensitive than their more modern cousins, the unstable gravimeters, which have largely superseded them. The stable gravimeter consists of a mass at the end of a beam which is pivoted on a fulcrum and balanced by a tensioned spring at the other end. Changes in gravity affect the weight of the mass which is counterbalanced by the restoring action of the spring. Different configurations of stable gravimeters are shown in Figure 2.9 and are discussed in more detail by Garland (1965), Nettleton (1976), Telford *et al.* (1990), and Parasnis (1986). A brief description of three stable gravimeters is given below.

2.4.1.1 Askania

A beam with a mass at one end is pivoted on a main spring S (Figure 2.9A). Changes in gravity cause the beam to tilt, so producing a deflection in a beam of light which is reflected off a mirror placed on the mass. A photoelectric cell, the output of which is displayed on a galvanometer, measures the displacement of the light beam. An auxiliary spring (AS) is retensioned using a micrometer to restore the mass to its rest position, which is indicted when the galvanometer reading is returned to zero (nulled).

2.4.1.2 Boliden

The Boliden gravimeter uses the principle that the capacitance of a parallel-plate capacitor changes with the separation of the plates (Figure 2.9B). The mass has the form of a bobbin with a plate at each end and is suspended by two springs between two other capacitor plates. With a change in gravity, the mass moves relative to the fixed plates, changing the capacitance between the upper plates; this movement can be detected easily using a tuned circuit. The lower plates are connected to a d.c. supply which supports the bobbin mass by electrostatic repulsion. With a change in gravity and the consequent displacement of the bobbin relative to the fixed plates, the original or

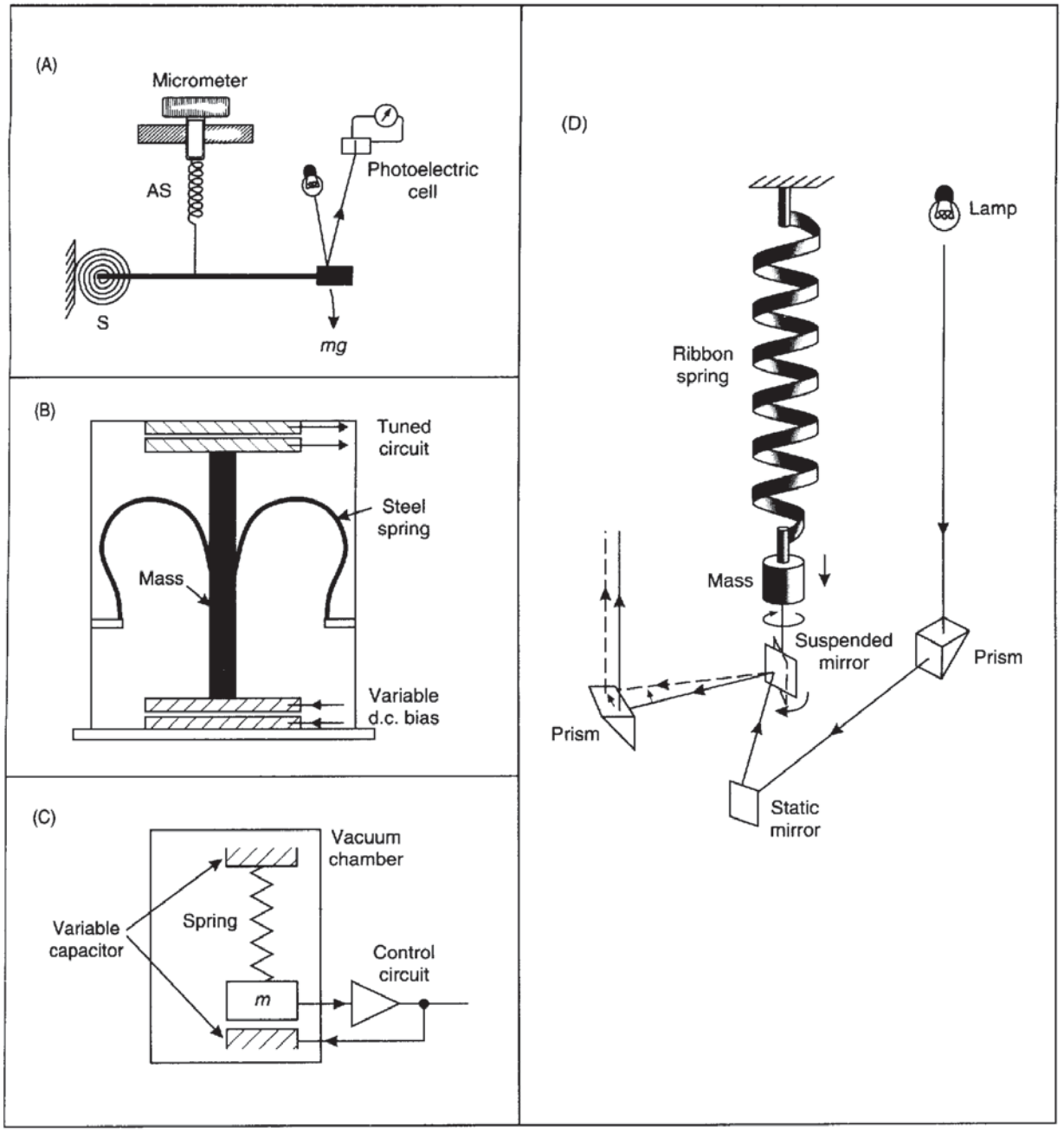

a reference position can be obtained by changing the direct voltage between the lower pair of plates. The overall sensitivity is about 1 g.u. (0.1 mGal). A modern version has been produced by Scintrex (Model CG-3) which operates on a similar principle (see Figure 2.9C). Any displacement of the mass due to a change in gravity is detected by

Figure 2.9 Types of stable gravimeter: (A) Askania; (B) Boliden; (C) Scintrex CG-3; and (D) Gulf (Hoyt). After Garland (1965), Telford *et al.* (1976), Robinson and Coruh (1988), by permission

a capacitor transducer and activates a feedback circuit. The mass is returned to its null position by the application of a direct feedback voltage (which is proportional to the change in gravity) to the plates of the capacitor which changes the electrostatic force between the plates and the mass (Robinson and Coruh 1988).

2.4.1.3 Gulf (Hoyt)

The Gulf gravimeter comprises a coiled helical ribbon spring which rotates as it changes length (Figure 2.9D). The rotation of the free end of the spring is much larger than the change in length and so is more easily measured. The range of measurement is quite small, being only 300 g.u. (30 mGal), although this can be overcome to some extent by retensioning the spring, and the accuracy of measurement is to within 0.2–0.5 g.u. (0.02–0.05 mGal).

2.4.2 Unstable (astatic) gravimeters

Since the 1930s, unstable gravimeters have been used far more extensively than their stable counterparts. In a stable device, once the system has been disturbed it will return to its original position, whereas an unstable device will move further away from its original position.

For example, if a pencil lying flat on a table is lifted at one end and then allowed to drop, the pencil will return to being flat on the table. However, if the pencil starts by being balanced on its end, once disturbed, it will fall over; i.e. it becomes unstable, rather than returning to its rest position. The main point of the instability is to exaggerate any movement, so making it easier to measure, and it is this principle on which the unstable gravimeter is based.

Various models of gravimeter use different devices to achieve the instability. The principle of an astatic gravimeter is shown in Figure 2.10. An almost horizontal beam hinged at one end supports a mass at the other. The beam is attached to a main spring which is connected at its upper end to a support above the hinge. The spring attempts to pull the beam up anticlockwise by its turning moment, which is equal to the restoring force in the spring multiplied by the perpendicular distance from the hinge (d). This turning moment is balanced by the gravitational turning moment which attempts to rotate the beam in a clockwise manner about the hinge and is equal to the weight of the mass (mg) times the length of the beam (l) multiplied by the cosine of the angle of the beam from the horizontal (θ) (i.e. $mgl\cos\theta$). If gravity changes, the beam will move in response but will be maintained in its new position because the main spring is a 'zero-length' spring. One virtue of such a spring is that it is pretensioned during manufacture so that the tension in the spring is proportional to its length. This means that if all forces were removed from the

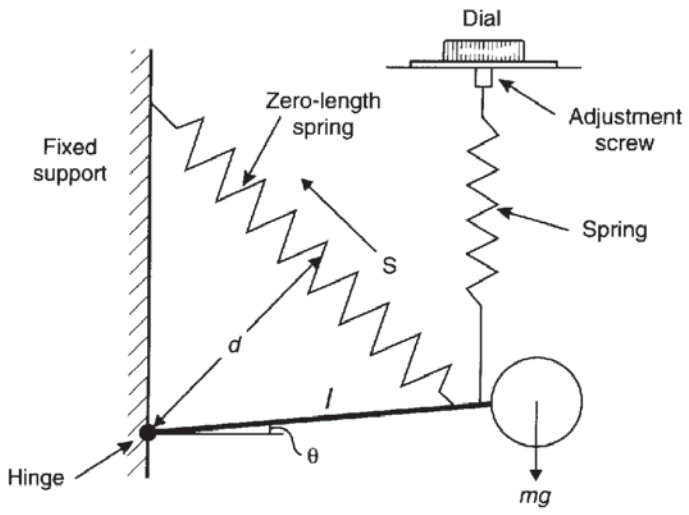

Figure 2.10 Principle of operation of an astatic gravimeter

spring it would collapse to zero length, something which is impossible in practice. Another virtue of the zero-length spring is that it results in an instrument which is linear and very responsive over a wide range of gravity values. Astatic gravimeters do not measure the movement of the mass in terms of changes in gravity but require the displaced mass to be restored to a null position by the use of a micrometer. The micrometer reading is multiplied by an instrumental calibration factor to give values of gravity, normally to an accuracy within 0.1 g.u. (0.01 mGal) and in some specialist devices to within 0.01 g.u. (0.001 mGal = 1 μGal).

2.4.2.1 Thyssen

Although obsolete, this gravimeter demonstrates the instability concept extremely well and is included for this reason. An extra mass is placed above a balanced beam (Figure 2.11) so producing the instability condition. If gravity increases, the beam tilts to the right and the

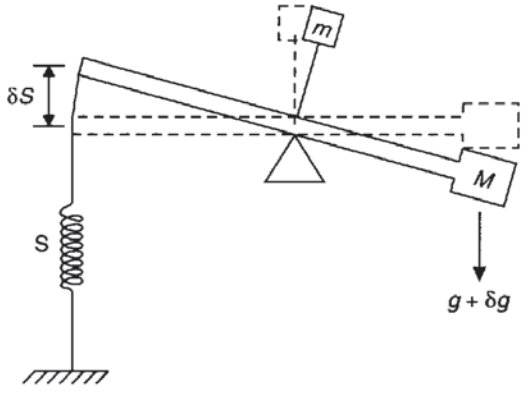

Figure 2.11 Schematic of a Thyssen gravimeter

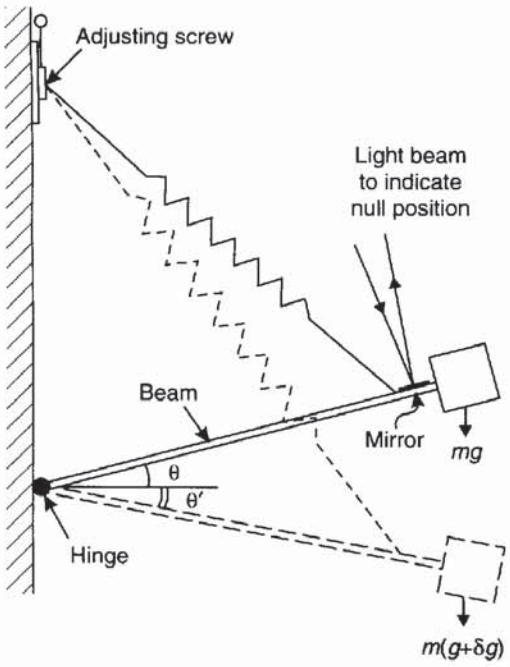

Figure 2.12 Schematic of a LaCoste-Romberg gravimeter. After Kearey and Brooks (1991), by permission

movement of the extra mass enhances the clockwise rotation about the pivot, and conversely for a reduction in gravity. When used, this type of gravimeter had a sensitivity of about 2.5 g.u. (0.25 mGal).

2.4.2.2 LaCoste–Romberg

This device is a development of LaCoste's long-period seismograph (LaCoste 1934) and is illustrated in Figure 2.12. The spring is made of metal with a high thermal conductivity but cannot be insulated totally to eradicate thermal effects and so has to be housed permanently in an enclosed container in which a stable temperature is maintained to within 0.002°C by a thermostat element. The null point is obtained by the observer viewing a scale through an eyepiece onto which a beam of light is reflected from the beam when it is in its rest position. In order to restore the position of the beam, the operator rotates a micrometer gauge on the outer casing which turns a screw which adjusts the beam position. The long length of the screw means that the gravimeter can be used worldwide without having to undergo any resets, which is a major advantage over other makes for surveys where this is important. When this type of gravimeter was manufactured in the 1930s it weighed a massive 30 kg, but modern technology has made it possible for the weight to be reduced to only about 2 kg, excluding the battery required to maintain the heating coils. The

springs can be clamped and so the gravimeter is more easily transportable than other makes and also less sensitive to vibration. It is possible for some models of LaCoste–Romberg gravimeters to measure to 3 μGal.

2.4.2.3 Worden

Unlike the LaCoste–Romberg gravimeter, the Worden is made entirely of quartz glass springs, rods and fibres (Figure 2.13). The quartz construction makes it much easier to reduce thermal effects. Indeed, the whole assembly is housed in a glass vacuum flask and some models have an electrical thermostat. As the spring cannot be clamped, the Worden gravimeter is sensitive to vibration and has to be transported extremely carefully. The range of the instrument is about 20 000 g.u. (2000 mGal) with an accuracy to within 0.1–0.2 g.u. (0.01–0.02 mGal). However, quartz gravimeters such as the Worden can be quite difficult for inexperienced operators to read and a realistic accuracy may be more like 1 g.u. (0.1 mGal). The Worden gravimeter has two auxiliary springs, one for coarse and the other for fine adjustments.

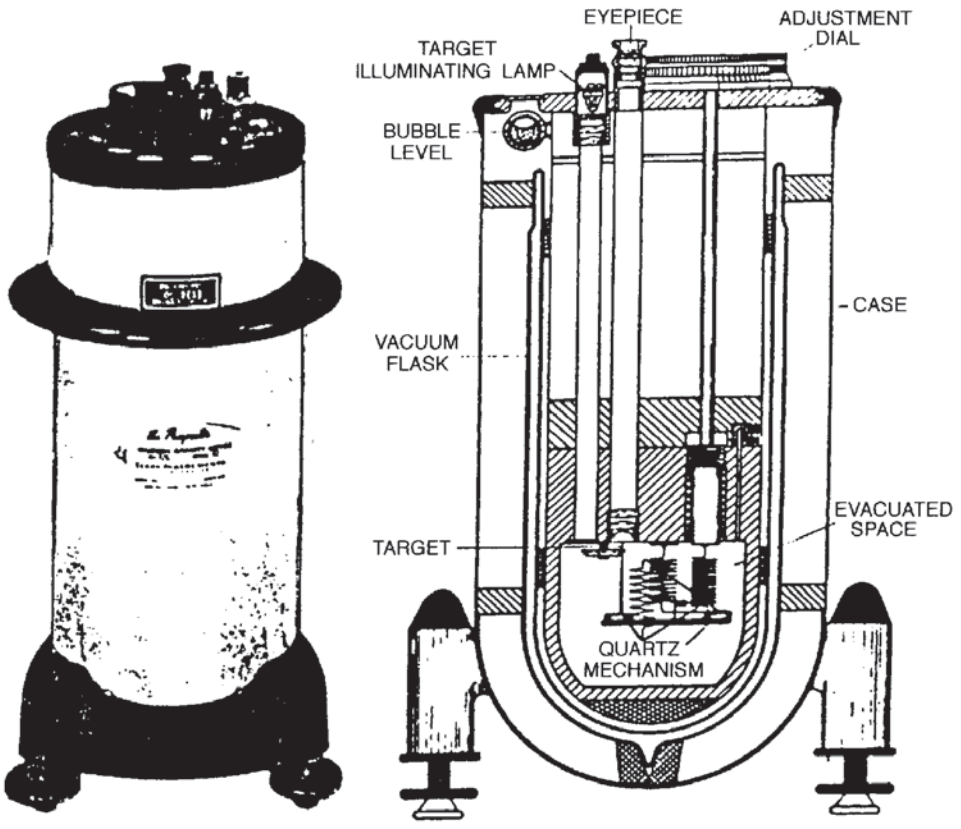

Figure 2.13 Cross-section through a Worden gravimeter (Texas Instruments Ltd). From Dunning (1970), by permission

2.4.2.4 Sodin

This is very comparable to the Worden and operates in similar ways. Further details are given by Robinson and Coruh (1988).

2.4.2.5 Vibrating string

If a mass is suspended on a fibre which is forced to oscillate by an a.c. circuit, then the frequency of vibration, which can be measured electronically, will vary with changes in gravity. For a fibre of length L, and mass per unit length m_s, from which a mass M is suspended, by measuring the frequency of vibration (f), gravity can be determined (Box 2.8). However, the technology is not sufficiently developed to provide the same resolution and accuracy as other gravimeters, but it does give the impression that even more compact and lightweight gravimeters may be forthcoming in the near future. There is potential for use in airborne survey systems.

Box 2.8 Determination of g using a vibrating string

$$\text{Gravity} = \frac{4 \times \text{string length}^2 \times \text{frequency}^2 \times \text{string mass}}{\text{suspended mass}};$$

$$g = \frac{4L^2 f^2 m_s}{M}$$

2.5 CORRECTIONS TO GRAVITY OBSERVATIONS

Gravimeters do not give direct measurements of gravity. Rather, a meter reading is taken which is then multiplied by an instrumental calibration factor to produce a value of observed gravity (g_{obs}). Before the results of the survey can be interpreted in geological terms, these raw gravity data have to be corrected to a common datum, such as sea level (geoid), in order to remove the effects of features that are only of indirect geological interest. The correction process is known as *gravity data reduction* or *reduction to the geoid*. The difference between the value of observed gravity (g_{obs}) and that determined either from the International Gravity Formula/Geodetic Reference System 67 for the same location, or relative to a local base station, is known as the *gravity anomaly*. The various corrections that can be applied are listed in Table 2.7 with the sections of this book in which each one is discussed.

Table 2.7 Corrections to gravity data

Correction	Book sections
Instrument drift	2.5.1
Earth tides	2.5.2
Eötvös	2.5.7
Latitude	2.2.3 and 2.5.3
Elevation	
Free-air correction	2.5.4
Bouguer correction	2.5.5
Terrain	2.5.6
Isostatic	2.5.8

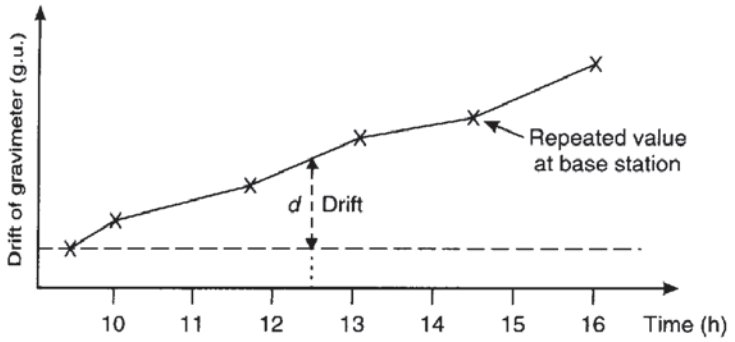

Figure 2.14 An instrumental drift curve

2.5.1 Instrumental drift

Gravimeter readings change (drift) with time as a result of elastic creep in the springs, producing an apparent change in gravity at a given station. The instrumental drift can be determined simply by repeating measurements at the same stations at different times of the day, typically every 1–2 hours. The differences between successive measurements at the same station are plotted to produce a *drift curve* (Figure 2.14). Observed gravity values from intervening stations can be corrected by subtracting the amount of drift from the observed gravity value. For example, in Figure 2.14 the value of gravity measured at an outlying station at 12.30 hours should be reduced by the amount of drift *d*. The range of drift of gravimeters is from a small fraction of one g.u. to about ten g.u. per hour. If the rate of drift is found to be irregular, return the instrument to the supplier – it is probably faulty!

2.5.2 Tides

Just as the water in the oceans responds to the gravitational pull of the Moon, and to a lesser extent of the Sun, so too does the solid earth.

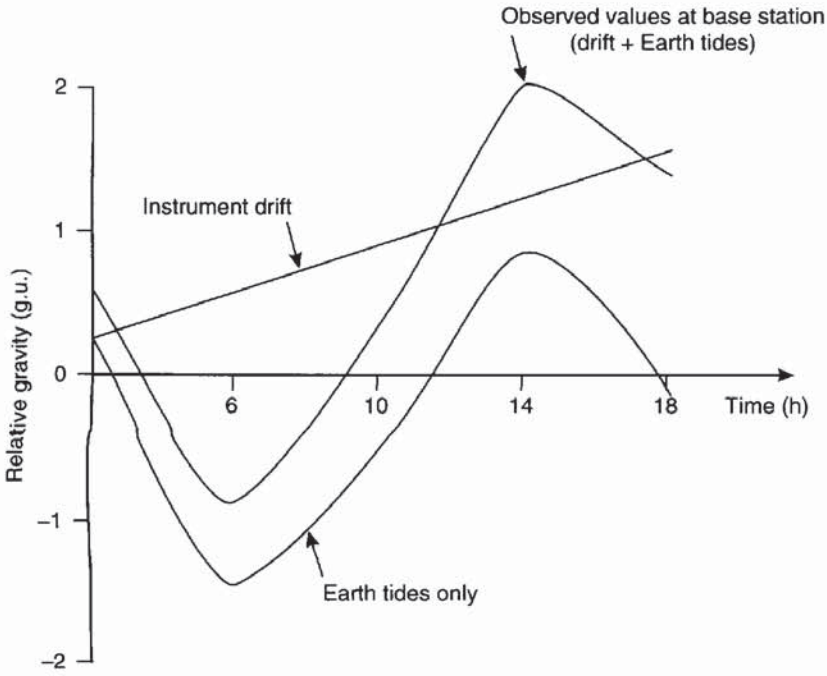

Figure 2.15 Graph of the effects of Earth tides and instrumental drift on the acceleration due to gravity

Earth tides give rise to a change in gravity of up to three g.u. with a minimum period of about 12 hours. Repeated measurements at the same stations permit estimation of the necessary corrections for tidal effects over short intervals, in addition to determination of the instrumental drift for a gravimeter (Figure 2.15). Alternatively, recourse can be made to published tide tables which are published periodically (e.g. *Tidal Gravity Corrections for 1991*, European Association of Exploration Geophysicists, The Hague).

2.5.3 Latitude

The latitude correction is usually made by subtracting the theoretical gravity calculated using the International Gravity Formula (g_ϕ) (Section 2.2.3) from the observed value (g_{obs}). For small-scale surveys which extend over a total latitude range of less than one degree, and not tied into the absolute gravity network, a simpler correction for latitude can be made. A local base station is selected for which the horizontal gravity gradient (δg_L) can be determined at a given degree of latitude (ϕ) by the expression in Box 2.9.

Box 2.9 Local latitude correction

$$\delta g_L = -8.108 \sin 2\phi \quad \text{g.u. per km N}$$

Note that the correction is negative with distance northwards in the northern hemisphere or with distance southwards in the southern hemisphere. This is to compensate for the increase in the gravity field from the equator towards the poles. For a latitude of 51°N, the local latitude correction is about 8 g.u./km. For gravity surveys conducted with an accuracy of ± 0.1 g.u., the latitudinal position of the gravity station needs to be known to within ± 10 m, which is well within the capability of modern position-fixing.

2.5.4 Free-air correction

The basis of this correction is that it makes allowance for the reduction in magnitude of gravity with height above the geoid (see Figure 2.16 and Box 2.10), irrespective of the nature of the rock below. It is analogous to measuring gravity in the basket of a hot-air balloon in flight – hence the term *free-air correction*. The free-air correction is the difference between gravity measured at sea level and at an elevation of h metres with no rock in between. A value of 3.086 g.u./m

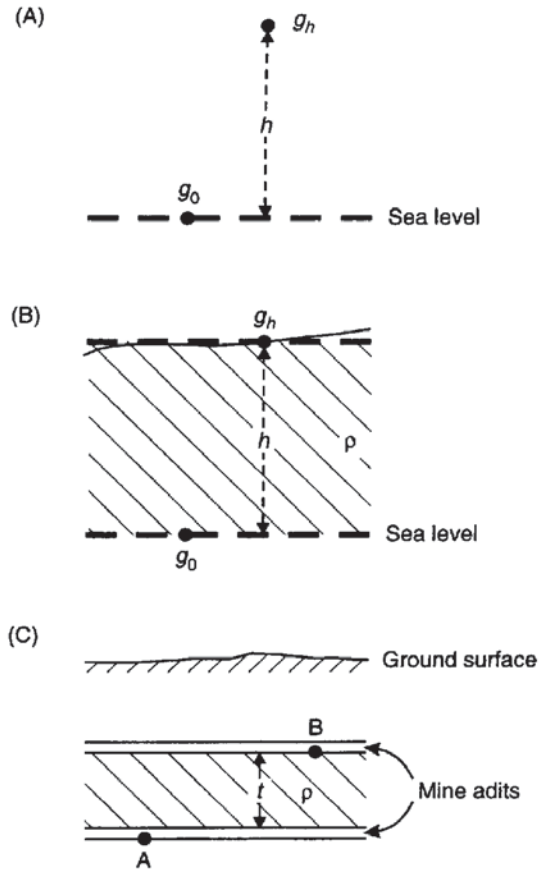

Figure 2.16 Schematic showing (A) the free-air correction, (B) the Bouguer correction, and (C) the Bouguer correction for measurements made underground

is accepted for most practical applications and is positive at elevations above sea level, and negative below. The free-air correction term varies slightly with latitude from 3.083 g.u./m at the equator to 3.088 g.u./m at the poles. With the normal measuring precision of modern gravimeters being around 0.1 g.u., elevations must be known to within 3–5 cm.

Box 2.10 Free-air correction (see also Figure 2.16)

Taking the Earth to be a sphere (rather than an oblate spheroid) with its mass concentrated at its centre of mass, then the value of gravity at sea level is:

$$g_0 = GM/R^2.$$

The value of gravity at a station at an elevation of h metres above sea level is:

$$g_h = GM/(R+h)^2 = \frac{GM}{R^2}\left(\frac{1-2h}{R}\cdots\right).$$

The difference in gravity between sea level and at h metres is the free-air correction:

$$\delta g_F = g_0 - g_h = \frac{2g_0 h}{R}.$$

With $g_0 = 9\,817\,855$ g.u., $R = 6\,371\,000$ M, and with h in metres,

$$\delta g_F = 3.082h \text{ g.u.}$$

Taking into account that the Earth is an oblate spheroid, rather than a sphere, the normally accepted value of the free-air correction is:

$$\boldsymbol{\delta g_F = 3.086\,h \text{ g.u.}}$$

The reduction in g with increasing height above the ground is important in airborne gravimetry. Anomalies detected by helicopter-mounted gravimeters will have decreased amplitudes and lengthened wavelengths compared with those obtained from land-based surveys. To compare land gravity survey data with airborne, it is necessary to correct for the free-air attenuation of the gravity anomaly by using *upward continuation*, which is discussed in Section 2.6.

The quantity calculated by applying both the latitude and the free-air corrections is called the *free-air anomaly* and is commonly

used to display corrected gravity data for oceans and continental shelves (see, e.g., Talwani *et al.* 1965).

2.5.5 Bouguer correction

Whereas the free-air correction compensates for the reduction in that part of gravity due only to increased distance from the centre of mass, the Bouguer correction (δg_B) is used to account for the rock mass between the measuring station and sea level (Figure 2.16).

The Bouguer correction calculates the extra gravitational pull exerted by a rock slab of thickness h metres and mean density ρ (Mg/m^3) which results in measurements of gravity (g_{obs}) being overestimated by an amount equal to $0.4192\rho h$ g.u. (Box 2.11). The Bouguer correction should be subtracted from the observed gravity value for stations above sea level. For an average rock density of 2.65 Mg/m^3, the Bouguer correction amounts to 1.12 g.u./m. For marine surveys, the Bouguer correction is slightly different in that the low density of sea water is effectively replaced by an equivalent thickness of rock of a specified density (Box 2.11).

Box 2.11 Bouguer correction

Bouguer correction $(\delta g_B) = 2\pi G\rho h = \beta\rho h$ (g.u.), where:

$$\beta = 2\pi G = 0.4192 \text{ g.u. m}^2 \text{ Mg}^{-1}$$
$$G = 6.67 \times 10^{-8} \text{ m}^3 \text{ Mg}^{-1} \text{ s}^{-2}.$$

Density (ρ) is in Mg m^{-3} and height (h) is in metres.

For marine surveys, the Bouguer correction is given by:

$$\delta g_B = \beta(\rho_r - \rho_w)h_w \text{ (g.u.)}.$$

where ρ_r and ρ_w are the densities of rock and sea water respectively, and h_w is the water depth in metres.

A further development of this correction has to be made for gravity measurements made underground (Figure 2.16C). In this case, the Bouguer correction has to allow for the extra gravitational pull ($=0.4191\rho t$ g.u.) on Station A caused by the slab of thickness t metres between the two stations A and B, whereas the value of gravity at Station A is underestimated by the equal but upward attraction of the same slab. The difference in gravity between the two stations is *twice* the normal Bouguer correction ($=0.8384\rho t$ g.u.). Allowances also have to be made for underground machinery, mine layout and the

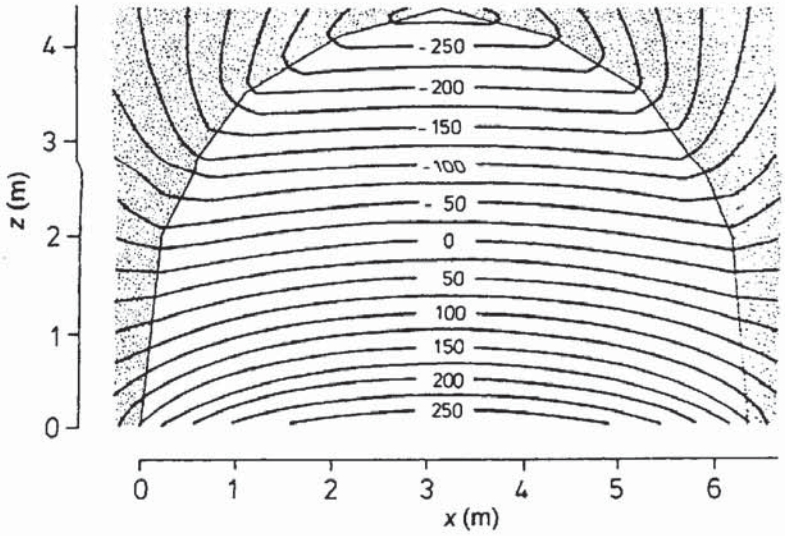

Figure 2.17 Micro-isogals for a typical gallery in a deep coal mine; the contour interval is 25 μGal and the density of the host rock is 2.65 Mg/m^3. From Casten and Gram (1989), by permission

variable density of local rocks, and this is sometimes referred to as the *Gallery correction* (Figure 2.17).

The Bouguer correction on land has to be modified by allowances for terrain roughness (see Section 2.5.6) in areas where there is a marked topographic change over a short distance, such as an escarpment of cliff. In such a situation the approximation of a semi-infinite horizontal slab of rock no longer holds true and more detailed calculations are necessary (Parasnis 1986; p. 72).

The free-air and Bouguer corrections are commonly combined into one *elevation correction* (δg_E) to simplify data handling (Box 2.12). It should be noted that in some cases, the resulting gravity anomaly may be misleading and the combined calculation should be used judiciously. For a density of 2.60 Mg/m^3, the total elevation correction is 2 g.u./m, which requires elevations to be known to an accuracy within 5 cm if gravity readings are to be made to within 0.1 g.u.

Box 2.12 Elevation correction

Elevation correction (δg_E) = (Free-air − Bouguer) corrections:

$$\delta g_E = \delta g_F - \delta g_B.$$

Substituting in the terms $\delta g_F = 3.086h$ and $\delta g_B = 0.4192\rho h$:

$$\boldsymbol{\delta g_E = (3.086 - 0.4192\rho)h \text{ (g.u.)}}$$

where ρ is the average rock density in Mg/m^3.

One of the main problems with the Bouguer correction is knowing which density to use. For example, a difference of 0.1 Mg/m^3 in density for a gravity measurement made at an elevation of 250 m will result in a discrepancy of more than 10 g.u. in the Bouguer correction. In many cases, it may be possible to obtain an estimate of rock densities from appropriate surface samples, or from borehole samples, if available. Caution should be used in the latter case as rock-core samples will relax mechanically, producing many cracks, and expanding slightly in response to the reduced pressure at the surface, giving rise to an underestimate of *in situ* density.

Nettleton (1939, 1940) found a very simple way of determining the appropriateness of the chosen density using a graphical method. Corrected gravity data should show no correlation with topography as all such effects should have been removed through the data reduction process. If a range of densities is chosen and the resulting elevation corrections computed along one gravity profile, the density that shows least correlation with topography is taken as the 'correct' one (Figure 2.18). It is known, however, that this method becomes less accurate if there is any topographic expression due to dipping beds with a significant density contrast to those above and below. Examples of where this might occur are in association with an inclined dense igneous intrusion, or in a marked structural feature with significant variations in density.

A generalised Nettleton method has been proposed by Rimbert *et al.* (1987) which allows for density to vary over a geographic area. The topographic data of an area are smoothed and reduced to produce a surface that lies just below the low topographic points on the survey, and which they refer to as the 'regional topography'. The density between the 'regional' and the actual topography is considered as constant (ρ_0) for a fixed radius around each station. The density below the 'regional' topography is taken as uniform throughout the area of the survey. The variations in density above the 'regional' topography are accounted for statistically but can be plotted in map form to demonstrate the areal variation in density which can be correlated independently with maps of the known geology. Rimbert *et al.* (1987) have achieved accuracies to within 3–4 g.u. with this method in an area in the south of France in which the observed gravity anomalies ranged from 40 to 150 g.u.

Another method to calculate density is to plot a graph of the latitude-corrected gravity data from an area without marked gravity anomalies, against station elevation (Reeves and MacLeod 1986). The resulting straight-line graph yields a gradient that is numerically equal to the elevation correction. Using the result in Box 2.16 and rearranging the equation to make density the subject of the equation, it is possible to solve and find a value for the density. Reeves and MacLeod used this method on data for a survey in Belgium, and produced a graphical elevation correction of 2.35 g.u./m which gave

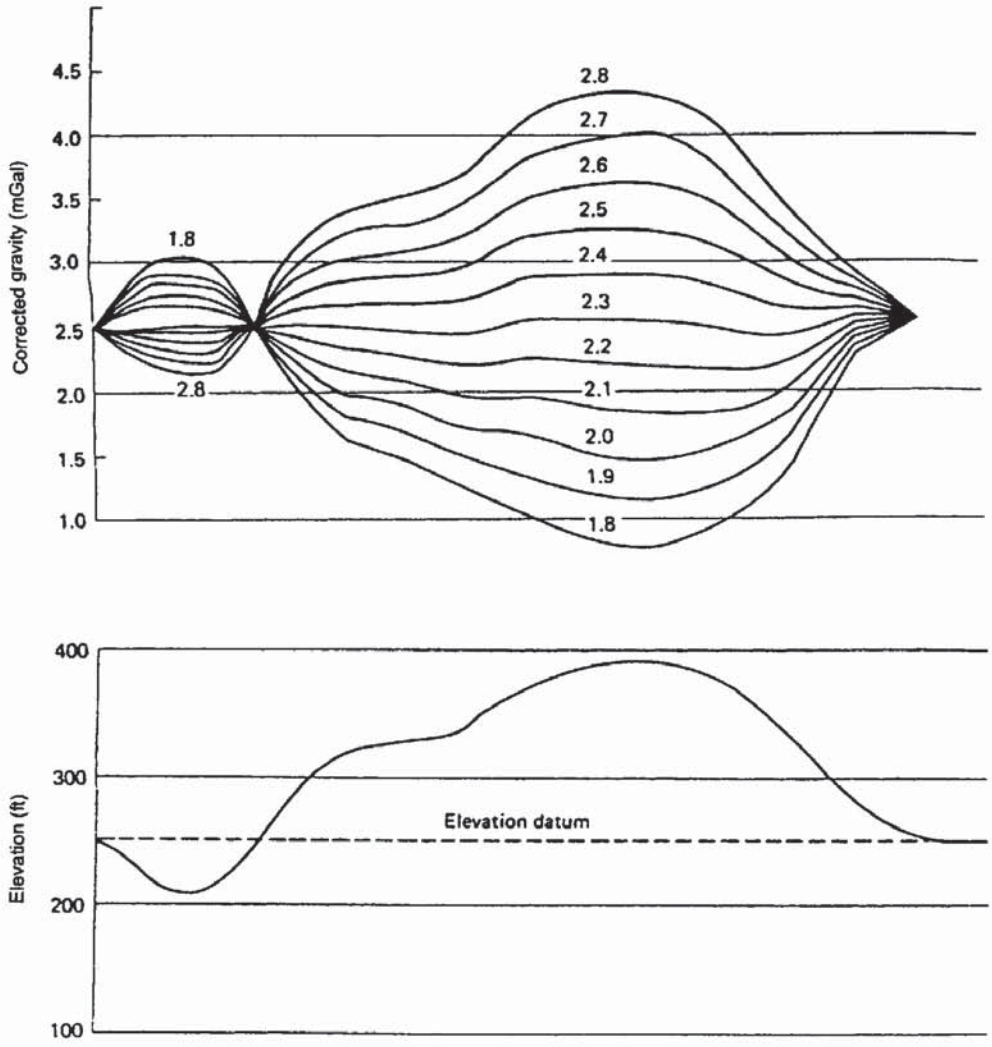

Figure 2.18 The Nettleton method for determining the density of near surface rock formations with the topography as shown. The most appropriate density is about 2.3 Mg/m^3 (least correlation with the topography). Corrections are referred to a height of 76 m. From Dobrin (1976), by permission

a density estimate of 1.74 Mg/m^3, compared with 1.6 Mg/m^3 determined using the Nettleton method.

The danger with a graphical method – even if linear regression statistics are used to determine the gradient of the best straight-line fit through the data – is that a small difference in the graphical gradient can result in an unacceptably large density discrepancy, and this makes the method rather insensitive to small changes in density. For example, the data presented by Reeves and MacLeod, rather than showing a single trend with elevation, indicate two: data up to an elevation of 215 m yield a density of 1.43 Mg/m^3 and the remaining data up to 280 m yield a density of 1.79 Mg/m^3, a difference of 0.36 Mg/m^3. Densities should be determined to better than 0.1 Mg/m^3 if possible.

In underground gravity surveys, a similar method is employed (Hussein 1983). The vertical gravity gradient (i.e. δg_E) is obtained by measuring g at two or more elevations separated by only 1.5–3 m at the same location within an underground chamber. The density can then be calculated as described above. As the measurements of g are strictly controlled, the error in density can be minimised routinely to within 0.08 Mg/m^3 (Casten and Gram 1989).

Rock densities for depths below which it is not possible to sample can also be estimated using the relationship of density with P-wave velocities as described, for example, by Nafe and Drake (1963), Woollard (1950, 1959, 1975), Birch (1960, 1961), and Christensen and Fountain (1975).

2.5.6 Terrain correction

In flat countryside, the elevation correction (the combined free-air and Bouguer correction) is normally adequate to cope with slight topographic effects on the acceleration due to gravity. However, in areas where there are considerable variations in elevation, particularly close to any gravity station, a special *terrain correction* must be applied. The Bouguer correction assumes an approximation to a semi-infinite horizontal slab of rock between the measuring station and sea level. It makes no allowance for hills and valleys and this is why the terrain correction is necessary.

The effect of topography on g is illustrated in Figure 2.19. Consider a gravity station beside a hill as in Figure 2.19A. The slab of rock which comprises the hill (mass M) has its centre of mass above the plane on which the gravimeter is situated. There is a force of attraction between the two masses. If the force is resolved into horizontal and vertical components and the latter only is considered, then it can be seen that the measurement of g at the gravity station will be underestimated by an amount δg. Conversely, if the gravity station is adjacent to a valley, as indicated in Figure 2.19B, then the valley represents a mass deficiency which can be represented by a negative mass ($-M$). The lack of mass results in the measurement of g to be underestimated by an amount δg. Consequently, a gravity measurement made next to either a hill or a valley requires a correction to be added to it to make allowance for the variable distribution of mass. The correction effectively removes the effects of the topography to fulfil the Bouguer approximation of a semi-infinite rock slab.

Physical computation of the terrain correction is extremely laborious as it has to be carried out for each and every station in an entire survey. A special transparent template, known as a *Hammer chart* after its originator Sigmund Hammer (1939), consists of a series of segmented concentric rings (Figure 2.20). This is superimposed over a topographic map and the average elevation of each segment of the

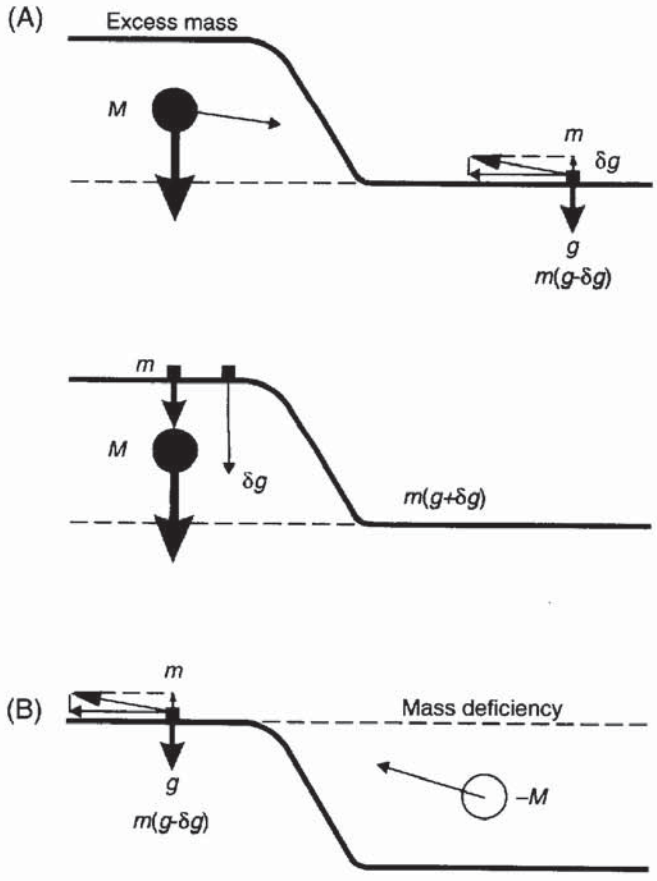

Figure 2.19 The effects of a hill and a valley on the measurement of gravity, illustrating the need for terrain corrections

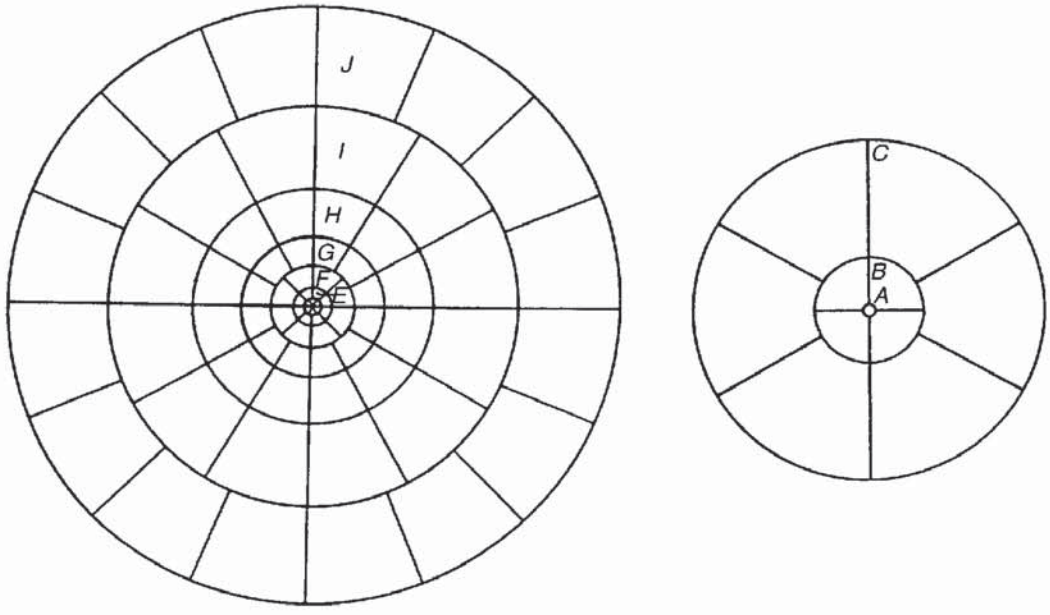

Figure 2.20 Hammer terrain correction chart with inner rings A–C shown expanded for clarity. After Dobrin (1976) and Milsom (1989), by permission

Table 2.8 Terrain corrections for Hammer zones B to M. From Milsom (1989), by permission

Zone	B	C	D	E	F	G
No. of compartments:	4	6	6	8	8	12
Correction (g.u.):	Heights (meters)					
0.01	0.5	1.9	3.3	7.6	11.5	24.9
0.02	0.7	2.6	4.7	10.7	16.3	35.1
0.03	0.8	3.2	5.8	13.1	19.9	43.1
0.04	1.0	3.8	6.7	15.2	23.0	49.8
0.05	1.1	4.2	7.5	17.0	25.7	55.6
0.06	1.2	4.6	8.2	18.6	28.2	60.9
0.07	1.3	5.0	8.9	20.1	30.4	65.8
0.08	1.4	5.4	9.5	21.5	32.6	70.4
0.09	1.5	5.7	10.1	22.9	34.5	74.7
0.10	1.6	6.0	10.6	24.1	36.4	78.7
0.20	2.4	8.7	15.1	34.2	51.6	111.6
0.30	3.2	10.9	18.6	42,1	63.3	136.9
0.40	3.9	12.9	21.7	48.8	73.2	158.3
0.50	4.6	14.7	24.4	54.8	82.0	177.4
0.60	5.3	16.5	26.9	60.2	90.0	194.7
0.70	6.1	18.2	29.3	65.3	97.3	210.7
0.80	6.9	19.9	31.5	70.1	104.2	225.6
0.90	7.8	21.6	33.7	74.7	110.8	239.8
1.00	8.7	23.4	35.7	79.1	117.0	253.2
	H	I	J	K	L	M
	12	12	16	16	16	16
0.01	32	42	72	88	101	125
0.02	46	60	101	124	148	182
0.03	56	74	125	153	186	225
0.04	65	85	144	176	213	262
0.05	73	95	161	197	239	291
0.06	80	104	176	216	261	319
0.07	86	112	191	233	282	346
0.08	92	120	204	249	303	370
0.09	96	127	216	264	322	391
0.10	103	134	228	278	338	413
0.20	146	190	322	394	479	586
0.30	179	233	396	483	587	717
0.40	206	269	457	557	679	828
0.50	231	301	511	624	759	926
0.60	253	330	561	683	832	1015
0.70	274	357	606	738	899	1097
0.80	293	382	648	790	962	1173
0.90	311	405	688	838	1020	1244
1.00	328	427	726	884	1076	1312

Note: These tables list the exact height differences which, assuming a density of 2000 kg/m^3 will produce the tabulated terrain effects. Thus, a height difference of 32 m between gravity station and average topographic level in one compartment of zone E would be associated with a terrain effect of 0.20, or possibly 0.19, g.u. Almost all commercial gravity meters have sensitivities of 0.1 g.u. but an additional decimal place is necessary if large 'rounding off' errors are to be avoided in summing the contributions from all the compartments. The inner radius of zone B is 2 m. Zone outer radii are: B: 16.6 m. C: 53.3 m. D: 170 m, E: 390 m, F: 895 m, G: 1530 m, H: 2.61 km, I: 4.47 km. J: 6.65 km, K: 9.9 km, L: 14.7 km, M: 21.9 km

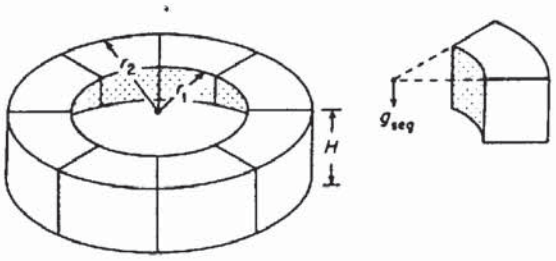

Figure 2.21 Segmented cylindrical ring used to compute terrain corrections. From Robinson and Coruh (1988), by permission

chart is estimated. The outer radius of the furthest zone is 21.9 km beyond which the effect of topography on g is negligible. In some cases, the range of the chart is extended to 50 km. Special tables (Table 2.8) are used to derive the terrain correction in g.u. for each segment, and then all the values are summed to produce a statistically weighted terrain correction for a given gravity station, each ring of the Hammer chart having a different weighting. For example, for a mean height difference of 34.7 m between the gravity station and a segment in zone D, a terrain correction of 0.95 g.u. can be determined from Table 2.8.

The terrain correction method works on the principle of determining the value of g at the centre of an annulus of inner and outer radii r_1 and r_2 (Figure 2.21) using the equation given in Box 2.13. Although topographic maps can be digitised and the terrain corrections calculated by computer (Bott 1959; Kane 1962) for the outer rings of the Hammer chart, it is still necessary to compute the terrain corrections for the innermost rings manually.

Box 2.13 Gravity of a Hammer chart segment (see Figure 2.21)

Gravity of a Hammer chart segment (δg_{seg}):

$$\delta g_{seg} = \frac{2\pi\rho G}{N}[r_2 - r_1 + (r_1^2 + z^2)^{1/2} - (r_2^2 + z^2)^{1/2}] \text{ (g.u.)}$$

where N is the number of segments in the ring, z is the modulus of the difference in elevation between the gravity station and mean elevation of the segment, and ρ is the Bouguer correction density (Mg/m^3).

There is no theoretical reason as to why the terrain correction needs to be calculated on the basis of a circular division of the terrain. It is computationally better for a regular grid to be used, in which case digitised topographic data can be used quite readily. Ketelaar (1976) has suggested a method in which the topography is represented by square prisms of side length D with an upper surface sloping at an

angle α. The terrain correction due to each prism can be calculated using the expression in Box 2.14. An example of computer analysis of terrain corrections for micro-gravity surveys has been given by Blizkovsky (1979) in which he also considers the gravitational effects of walls, vertical shafts and horizontal corridors. In micro-gravity surveys, an area of radius 2 m centred on the measurement station should be flat. For terrain effects of less than 1 μGal, height variations of less than 0.3 m in Hammer zone B and up to 1.3 m in zone C can be tolerated.

Box 2.14 Terrain correction for a square prism

Terrain correction due to a square prism of side length D:

$$\delta g_{\text{prism}(i,j)} = G\rho D(1 - \cos\alpha)K(i,j)$$

where $K(i,j)$ is the matrix of prism coordinates within the grid.

The calculation of terrain corrections is labour-intensive, time-consuming and adds considerably to the total cost of the survey. It is only undertaken when dictated by the roughness of the local topography. In built-up areas, care has to be taken in estimating the likely effect of neighbouring buildings. Modern, thin-walled buildings may contribute only a small effect (of the order of 1–5 μGal), but older thick-walled constructions may give rise to a terrain correction effect of 10–30 μGal. In these cases, it is preferable to position the gravimeter more than 2.5 m away from such a building in order to keep the effect to less than 5 μGal. Otherwise, specific calculations of the terrain corrections of the buildings concerned becomes necessary. An alternative approach is to measure the gravity effect around a comparable building, assuming one exists, away from the survey area and to carry out an empirical adjustment of the actual survey data. Budgetary constraints may preclude detailed data reduction, in which case the effectiveness of the micro-gravity survey may be jeopardised. Such considerations need to be made at the design stage of the survey. In some cases, the effects of adjacent buildings are assumed to be negligible and are ignored unjustifiably as they are thought to be too difficult to determine. Yet the magnitude of the anomalies being sought may be of the same order of magnitude as the terrain correction. There is scope for collaboration between geophysicists and members of the construction industry!

2.5.7 Eötvös correction

For a gravimeter mounted on a vehicle, such as a ship or a helicopter, the measured gravitational acceleration is affected by the vertical

component of the Coriolis acceleration which is a function of the speed and the direction in which the vehicle is travelling. To compensate for this, gravity data are adjusted by applying the Eötvös correction, named after the Hungarian geophysicist Baron von Eötvös who described this effect in the late 1880s.

There are two components to this correction. The first is the outward-acting centrifugal acceleration associated with the movement of the vehicle travelling over the curved surface of the Earth, and the second is the *change* in centrifugal acceleration resulting from the movement of the vehicle relative to the Earth's rotational axis. In the second case, an object that is stationary on the Earth's surface is travelling at the speed of the Earth's surface at that point as it rotates around the rotational axis in an east–west direction. If that same object is then moved at x km/h towards the east, its speed relative to the rotational velocity is increased by the same amount. Conversely, if it travels at a speed of y km/h in a westerly direction, its relative speed is slowed by the same amount. Any movement of a gravimeter which involves a component in an east–west direction will have a significant effect on the measurement of gravity. For shipborne gravimeters the Eötvös correction can be of the order of 350 g.u. For airborne gravity measurements, where speeds over 90 km/h (about 50 knots) are common, the Eötvös correction can be as high as 4000 g.u. The expression governing the Eötvös correction is given in Box 2.15, with a fuller mathematical explanation in Box 2.16.

Box 2.15 Eötvös correction

The Eötvös correction is given by:

$$\delta g_{EC} = 75.08\, V \cos\phi \sin\alpha + 0.0416\, V^2 \text{ (g.u.)}$$

or

$$\delta g_{EC} = 40.40\, V' \cos\phi \sin\alpha + 0.012\,11\, V'^2 \text{ (g.u.)}$$

where ϕ is the degree of geographic latitude, α is the azimuth in degrees, and V and V' are the speeds of the vehicle in knots and kilometres per hour respectively.

The error in the Eötvös correction $[d(\delta g_{EC})]$ in g.u. due to errors in speed (dV) and azimuth $(d\alpha)$ is:

$$d(\delta g_{EC}) = (0.705\, V' \cos\phi \cos\alpha) d\alpha + (40.40 \cos\phi \sin\alpha + 0.024\,22\, V') dV'.$$

At a latitude of 25°, a change of 0.1 knot (0.2 km/h) with a half a degree shift off course will result in over 7 g.u. difference in

Eötvös correction while on an easterly course ($\alpha = 90°$), or 3 g.u. on a northerly course ($\alpha = 0°$), assuming a speed of 10 km/h. Consequently, for an airborne survey to be accurate to within 10 g.u., extremely tight controls need to be kept on nagivation and on the general movement (roll, pitch, yaw, etc.) of the helicopter or plane; such accuracies are now thought to be routinely achievable (Hammer, 1982, 1984). From the last equation in Box 2.15, it can be seen that there is the greatest sensitivity to errors in speed in an east–west direction, and to errors in azimuth on a north–south course. Recent tests of airborne gravity have been discussed by Halpenny and Darbha (1995).

Box 2.16 Derivation of the Eötvös correction equation
(see Figure 2.22)

In general, the centrifugal acceleration a_1 is (velocity)$^2/d$. The total east–west speed of the vehicle is the linear speed of rotation of the Earth (v) plus the *east–west* component of the speed of the vehicle (V_E). Thus the centrifugal acceleration $a_1 = (v + V_E)^2/d$.

Centrifugal acceleration (a_2) along the radius vector, due simply to the movement of the vehicle in a *north–south* direction, is $a_2 = V_N^2/R$.

However, it is the *change* in acceleration that is required, so the centrifugal acceleration acting on a static body (a_3) needs to be removed: $a_3 = v^2/d$.

The total change in acceleration acting in a vertical sense is:

$$\delta g_E = a_1 \cos\phi + a_2 - a_3 \cos\phi \quad \text{(equation (4)).}$$

We note that:

$$d = R\cos\phi$$
$$v = \omega R \cos\phi$$
$$V = (V_N^2 + V_E^2)^{1/2} \quad \text{(from Pythagoras' theorem)}$$
$$V_E = V \sin\alpha, \text{ where } \alpha \text{ is the bearing to True North.}$$

Substituting into equation (4) we obtain:

$$\delta g_E = \frac{(v + V_E)^2}{R\cos\phi}\cos\phi + \frac{V_N^2}{R} - \frac{v^2\cos\phi}{R\cos\phi}.$$

Simplifying, this becomes

$$\delta g_E = [(v + V_E)^2 + V_N^2 - v^2]/R$$

continued

continued

which reduces to

$$\delta g_E = [2vV_E + (V_E^2 + V_N^2)]/R.$$

Rewriting this in terms of ω, R, ϕ, and α using the above expressions, this becomes:

$$\delta g_E = 2\omega V \cos\phi \sin\alpha + V^2 R \quad \text{(equation (5))}.$$

Given the following values:

$$\omega = 7.2921 \times 10^{-5} \text{ radians/s}$$
$$R = 6.371 \times 10^8 \text{/cm}$$
$$1 \text{ knot} = 51.479 \text{ cm/s}$$
$$1 \text{ Gal} = 10^4 \text{ g.u.}$$

then equation (5) can be rewritten (in terms of g.u.) as:

$$\delta g_E = 2(7.2921 \times 10^{-5} \times 51.479 \times 10^4)V \cos\phi \sin\alpha + (51.479V)^2 \times 10^4/6.371 \times 10^8$$

Finally:

$$\boldsymbol{\delta g_E = 75.08\, V \cos\phi \sin\alpha + 0.0416\, V^2 \text{ (g.u.)}.}$$

2.5.8 Isostatic correction

If there were no lateral variations in density in the Earth's crust, the fully reduced gravity data, after application of all the corrections so far outlined, would be the same. However, where there are lateral variations, a gravity anomaly results which is known as the *Bouguer anomaly* (discussed in more detail in Section 2.5.10). The average Bouguer anomaly in oceanic areas is generally positive, while over mountainous regions it is usually negative. These effects indicate that the rock beneath the oceans is more dense than normal while that beneath the mountains is less dense.

Two hypotheses were proved in the 1850s to account for this large-scale systematic variation in density (Figure 2.23). The geodesist G.B. Airy (1855) proposed that while mountain chains had deep roots, beneath the oceans the crust, which was assumed to have constant density everywhere, was thin. In contrast, an English Archdeacon J.H. Pratt (1859) thought that the crust extended to a uniform depth below sea level but that density varied inversely with the height of the topography.

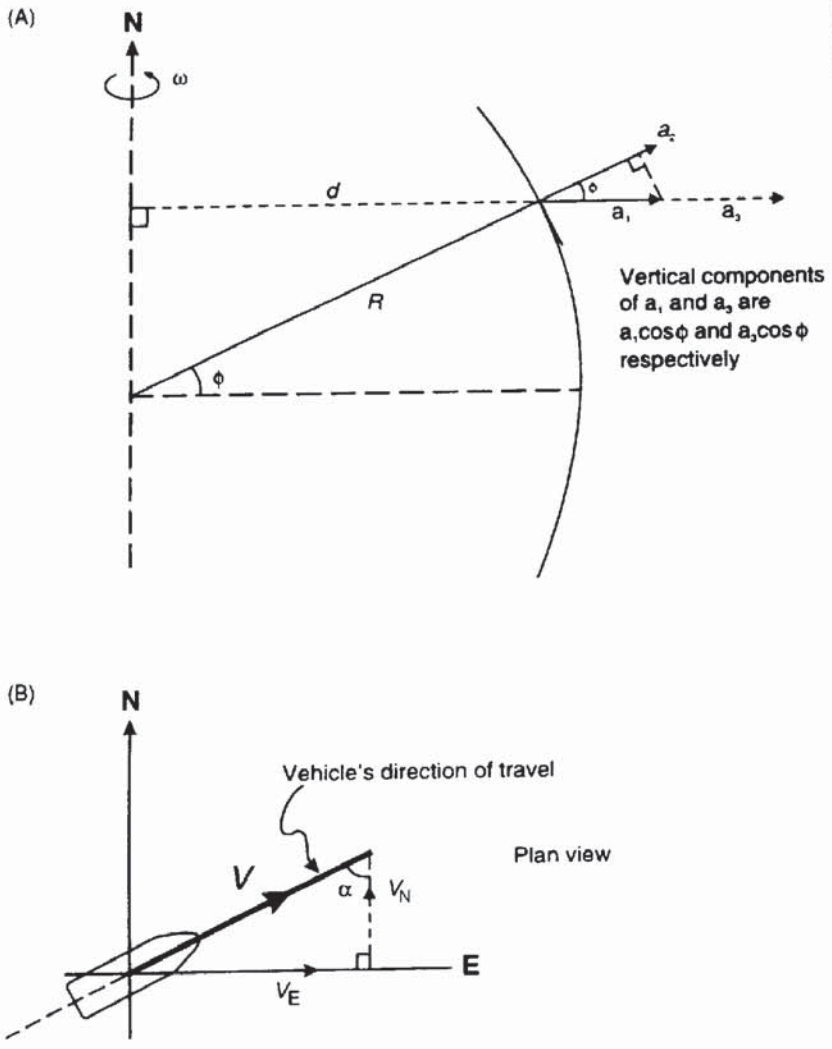

Figure 2.22 Schematic illustrating the components which contribute to the Eötvös correction (see box 2.16)

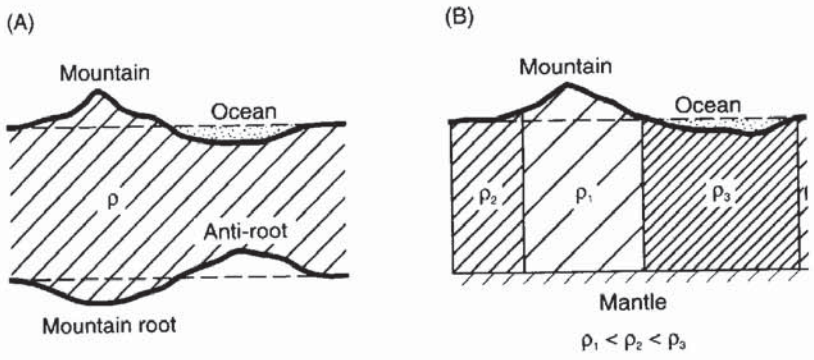

Figure 2.23 (A) Airy and (B) Pratt's models for isostacy

Airy's isostatic model is preferred geologically and seismologically, whereas Pratt's model is easier to use to calculate the isostatic (e.g. Rimbert *et al.* 1987), but the results are similar. Pratt's model has been developed by Heiskanen (1938) who suggested that density changes laterally with variable thickness of crust and that density increases gradually with depth. The aim of the isostatic correction is that effects on g of the large-scale changes in density should be removed, thereby isolating the Bouguer anomaly due to lateral variations in density in the upper crust (Hayford and Bowie 1912). The isostatic correction is discussed in more detail by Garland (1965), and the implications for isostatic rebound due to crustal loading and the viscosity of the mantle are discussed by Sharma (1986).

2.5.9 Miscellaneous factors

In Sections 2.5.1–2.5.8, calculable corrections to gravity data have been discussed. Gravimeters are sensitive not only to these factors but also to several others which tend to be erratic, temporal and difficult to quantify so that they may constitute gravitational noise. Such factors are: meteorological loading produced by atmospheric pressure changes; inertial acceleration caused by seismic and microseismic waves, including the effect of wind pressure on the gravimeter, and vibration from traffic and industrial machinery; and electrical noise from the gravimeter itself. Changes in atmospheric pressure can be corrected for by using -0.03 g.u. per millibar. Modern gravimeters used in micro-gravity surveys can filter out most noise above 10 Hz, and reject the microseismic noise between 0.1 and 2 Hz, so that standard deviations on gravity readings can be as small as 0.04 g.u. (4 μGal) (Thimus and van Ruymbeke, 1988).

2.5.10 Bouguer anomaly

The main end-product of gravity data reduction is the *Bouguer anomaly*, which should correlate only with lateral variations in density of the upper crust and which are of most interest to applied geophysicists and geologists. The Bouguer anomaly is the difference between the observed gravity value (g_{obs}), adjusted by the algebraic sum of all the necessary corrections (Σcorr; see Table 2.7 and Box 2.17), and that at some base station (g_{base}). The variation of the Bouguer anomaly should reflect the lateral variation in density such that a high-density feature in a lower-density medium should give rise to a positive Bouguer anomaly. Conversely, a low-density feature in a higher-density medium should result in a negative Bouguer anomaly.

Box 2.17 Bouguer anomaly

The Bouguer anomaly (Δg_B) is the difference between the observed value (g_{obs}), duly corrected, and a value at a given base station (g_{base}), such that:

$$\Delta g_B = g_{obs} + \Sigma(\text{corr}) - g_{base}$$

with

$$\Sigma(\text{corr}) = \delta g_L + (\delta g_F - \delta g_B) + \delta g_{TC} \pm \delta g_{EC} \pm \delta g_{IC} - \delta g_D$$

where the suffices refer to the following corrections:

L = latitude; F = free-air; B = Bouguer;
TC = terrain correction; EC = Eötvös correction;
IC = isostatic correction; and D = drift (including Earth tides).

2.6 INTERPRETATION METHODS

There are two approaches to the interpretation of Bouguer anomaly data. One is *direct* where the original data are analysed to produce an interpretation. The other is *indirect*, where models are constructed to

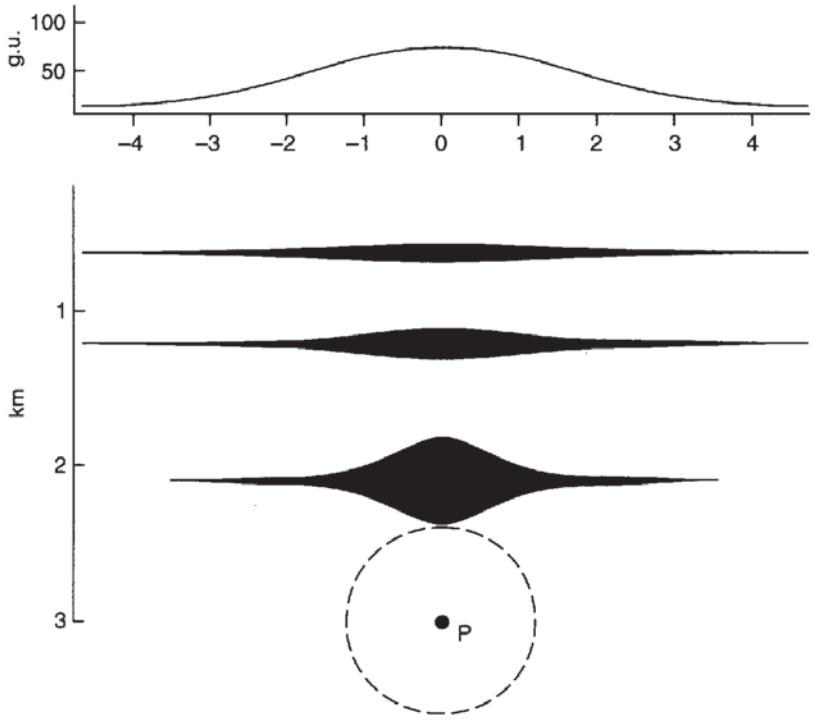

Figure 2.24 Ambiguity in geological models, all of which produce the gravity anomaly shown at the top. The lens-shaped bodies have a gravity anomaly identical to that of a sphere at P of radius 600 m and density contrast 1.0 Mg/m^3. The thickness of the bodies is exaggerated by a factor of 3. From Griffiths and King (1981), by permission

compute synthetic gravity anomalies which are compared in turn with the observed Bouguer anomaly. The model producing the best fit, however, will not be unique as several alternative models may be found which also produce an equivalent fit (Figure 2.24). It is because of this type of ambiguity, which has already been discussed in Section 1.2 (see also Figure 1.1), that different geophysical methods are used together to constrain the geologic model.

2.6.1 Regionals and residuals

Bouguer anomaly maps are rather like topographic maps with highs and lows, linear features and areas where the contours (*isogals*) are closely packed and others where they are further apart. There may be a gentle trend in the gravity data, reflecting a long-wavelength gravity anomaly attributable to deep-seated crustal features; this is known as a *regional anomaly*. Shorter-wavelength anomalies arising from shallower geological features are superimposed on the regional anomaly, and it is these anomalies that are often to be isolated for further analysis. Separation of the regional from the Bouguer anomaly will leave a *residual anomaly* (Figure 2.25).

There are a number of different methods with varying degrees of complexity and effectiveness by which residual anomalies can be isolated (Nettleton, 1954). These range from curve-sketching, which is purely subjective, through to computer-based analytical methods. Graphical methods include sketching in estimated regional trends by eye on a profile (Figure 2.25A) or calculating the residual from estimated isogals on a map. Figure 2.25B illustrates how the residual is calculated. The 5.0 mGal isogal, which has been highlighted, intersects several estimated regional isogals. At points A and B, the difference (i.e. the residual) between the 5.0 mGal line and those it crosses are respectively +0.2 and +0.4 mGal and contours are drawn of the same residual value.

An example of the quantitative analytical method consists in fitting a low-order polynomial expression to the Bouguer anomaly data and then subtracting the calculated values from those observed to produce residual values, which are then plotted in map form. A more sophisticated method is the application of Fourier analysis by which a power spectrum is obtained for the Bouguer anomaly (Spector and Grant 1970; Syberg 1972). This highlights the different wavelengths of anomaly present and so allows a form of filtering to be undertaken to remove the unwanted anomalies (e.g. Granser *et al.* 1989). Dobrin (1976), Grant and West (1965) and Telford *et al.* (1990) discuss the various techniques in more detail.

Although the analytical methods appear more rigorous and thorough, there are occasions when the manual interpretation can take into account known variations in local geology more readily than an automated system.

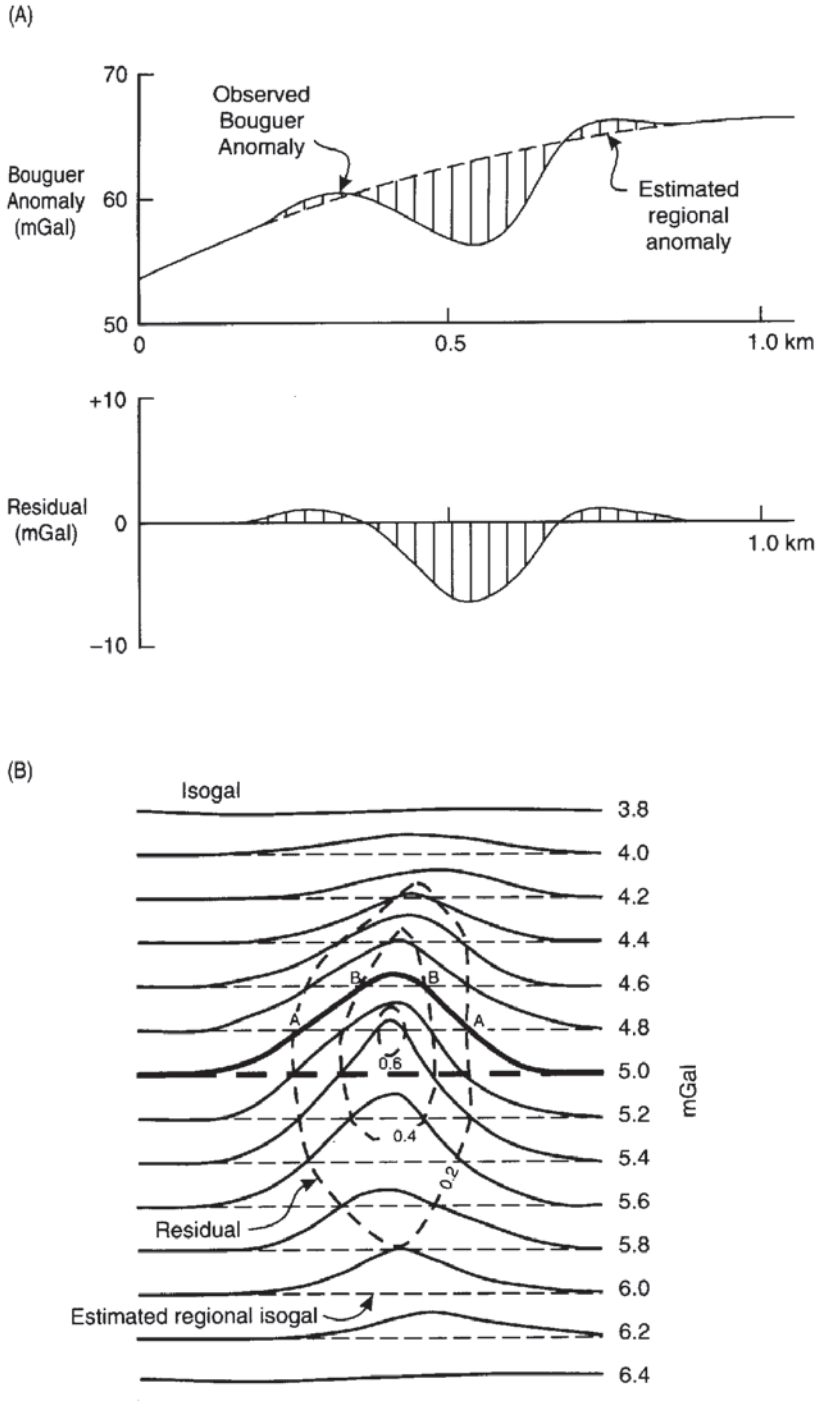

Figure 2.25 (A) Removal of a residual gravity anomaly from a regional profile, and (B) how a residual gravity map is constructed (see text for an explanation). After Dobrin (1976), by permission

2.6.2 Anomalies due to different geometric forms

Certain geologic structures can be approximated to models with known geometric forms (Nettleton, 1942). For example, a buried cavity may be represented by a sphere, a salt dome by a vertical cylinder, a basic igneous dyke by an inclined sheet or prism, etc. Another factor to be considered is whether the target to be modelled should be considered in two or three dimensions. If g is computed across a profile over a buried sphere, then that profile should hold true for any direction across the sphere. However, if the profile is across a buried horizontal cylinder, then the profile along the long-axis of the cylinder will be quite different from that across it. Also, if the strike length of the feature is greater than 20 times any other dimension, then it may be considered a two-dimensional body. Where this does not hold true, any profile will also sense the effects of the third dimension ('edge effects') and thus will not be modelled accurately if considered only in two dimensions.

Several common geometrical forms are illustrated in Figure 2.26, with their associated gravity profiles and the types of geologic features they approximate. The equations used to calculate the maximum anomaly for each geometric feature are given in Box 2.18. No attempt is made here to explain the derivations of these formulae, all of which are discussed much more fully by Dobrin (1976), Telford *et al.* (1990) and Parasnis (1986). The equations in Box 2.18 are intended only as guides to estimate the maximum values of the associated gravity anomalies. The use of the half-width ($x_{1/2}$) is discussed in more detail in Section 2.6.3 and 2.6.4.

The range of geometric forms given above is by no means complete. Details of other forms and their interpretations, such as by the use of characteristic curves, are given by Grant and West (1965) and Telford *et al.* (1990).

Calculation of gravity anomalies using the above methods should be regarded as a first step in the interpretation process. There are other, more sophisticated, and commonly computerised methods of gravity anomaly analysis. However, it is worth noting that for more complicated geological features of irregular shape which do not approximate to any of the geometrical forms, two other broad approaches can be adopted. The first is the use of graphical methods, and the second is an analytical approach. In the graphical methods, a template, which is divided into segments, is superimposed on an irregular cross-section of the geological feature to be modelled. The gravity at a point on the surface can be calculated by summing the effects of all the individual segments covering the cross-section of the feature.

Graphical methods can also be used for three-dimensional bodies. In this case, the appropriate template is superimposed on contours of the geological feature in the horizontal plane, thereby dividing it into

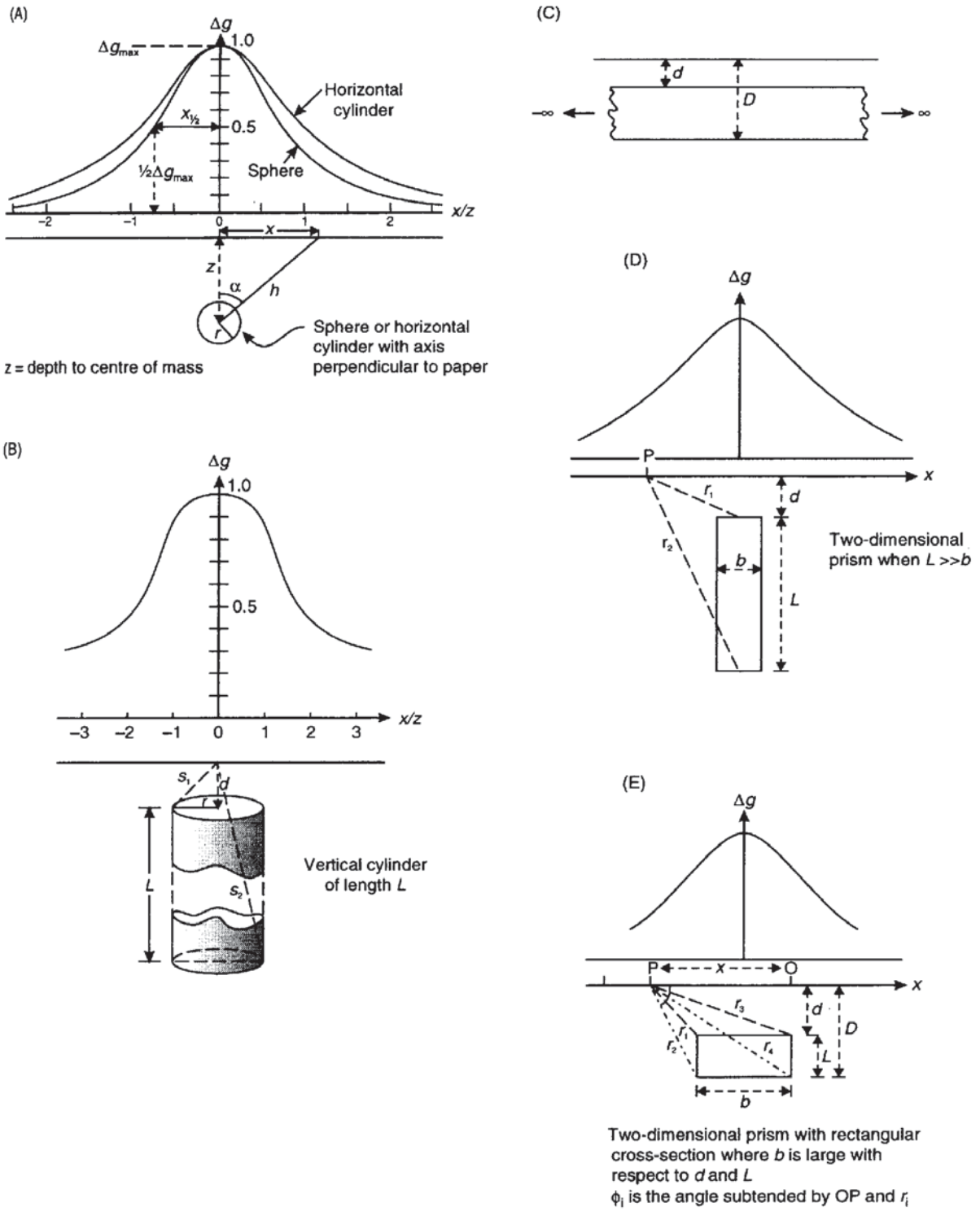

Figure 2.26 Representative gravity anomalies over given geometric forms: (A) a sphere or horizontal cylinder with its long axis perpendicular to the paper; (B) a vertical cylinder; (C) a semi-infinite horizontal slab (a Bouguer plate when $d = 0$); (D) a vertical rectangular prism; and (E) a horizontal rectangular prism

Box 2.18 Gravity anomalies associated with geometric forms
(see Figure 2.26)

Models	Maximum gravity anomaly	Notes
Sphere	$\Delta g_{max} = (4/3)\pi G\delta\rho r^3/z^2$	$z = 1.305x_{1/2}$ (m)
Horizontal cylinder	$\Delta g_{max} = 2\pi G\delta\rho r^2/z$	$z = x_{1/2}$
Vertical cylinder	$\Delta g_{max} = 2\pi G\delta\rho\,(s_1 - d)$	If $L \rightarrow$ infinity
	$\Delta g_{max} = 2\pi G\delta\rho r$	If $d = 0$
	$\Delta g_{max} = 2\pi G\delta\rho\,(L + s_1 - s_2)$	If L finite
		$z = x_{1/2}\sqrt{3}$
Buried slab (Bouguer plate)	$\Delta g_{max} = 2\pi G\delta\rho\, L$	For $L = 1000$ m and $\delta\rho = 0.1$ Mg/m^3, $\Delta g_{max} = 42$ g.u.
Infinite slab	$\Delta g_{max} = 2\pi G\delta\rho\,(D - d)$	
Horizontal rectangular prism	$\Delta g_p = 2G\delta\rho\left[x\ln\left(\frac{r_1 r_4}{r_2 r_3}\right) + b\ln\left(\frac{r_2}{r_1}\right) + D(\phi_2 - \phi_4) - d(\phi_1 - \phi_3)\right]$	
Vertical rectangular prism	$\Delta g_{max} = 2G\delta\rho[b\ln(d/L)]$	$L \gg b$
Step	$\Delta g_{max} = 2G\delta\rho\,[x\ln(r_4/r_3) + \pi(D - d) - D\phi_4 + d\phi_3]$	

All distances are in metres unless stated otherwise; Δg_{max} in mGal and $\delta\rho$ in Mg/m^3, and the factor $2\pi G = 0.042$.

a pile of horizontal slabs each with a thickness equal to the contour interval.

Most computer-based analytical methods (e.g. Bott 1960) are based on the premise proposed by Talwani *et al.* (1959), that a cross-section of a two-dimensional body can be approximated by representing it by a multisided polygon (Figure 2.27A). This was developed by Talwani and Ewing (1960) for three-dimensional bodies (Figure 2.27B) which are approximated by a stack of polygonal laminae. The gravity effect of each lamina is computed and summed to give a total gravity anomaly. Enhancements of these methods have largely been centred on improving the ease of use of the software on computers that have dramatically increased in power and efficiency, and on the portability of software from mainframe machines to personal microcomputers (Busby 1987).

A development of the three-dimensional approach is to consider a geological body as a stack of cubic blocks of uniform size, each

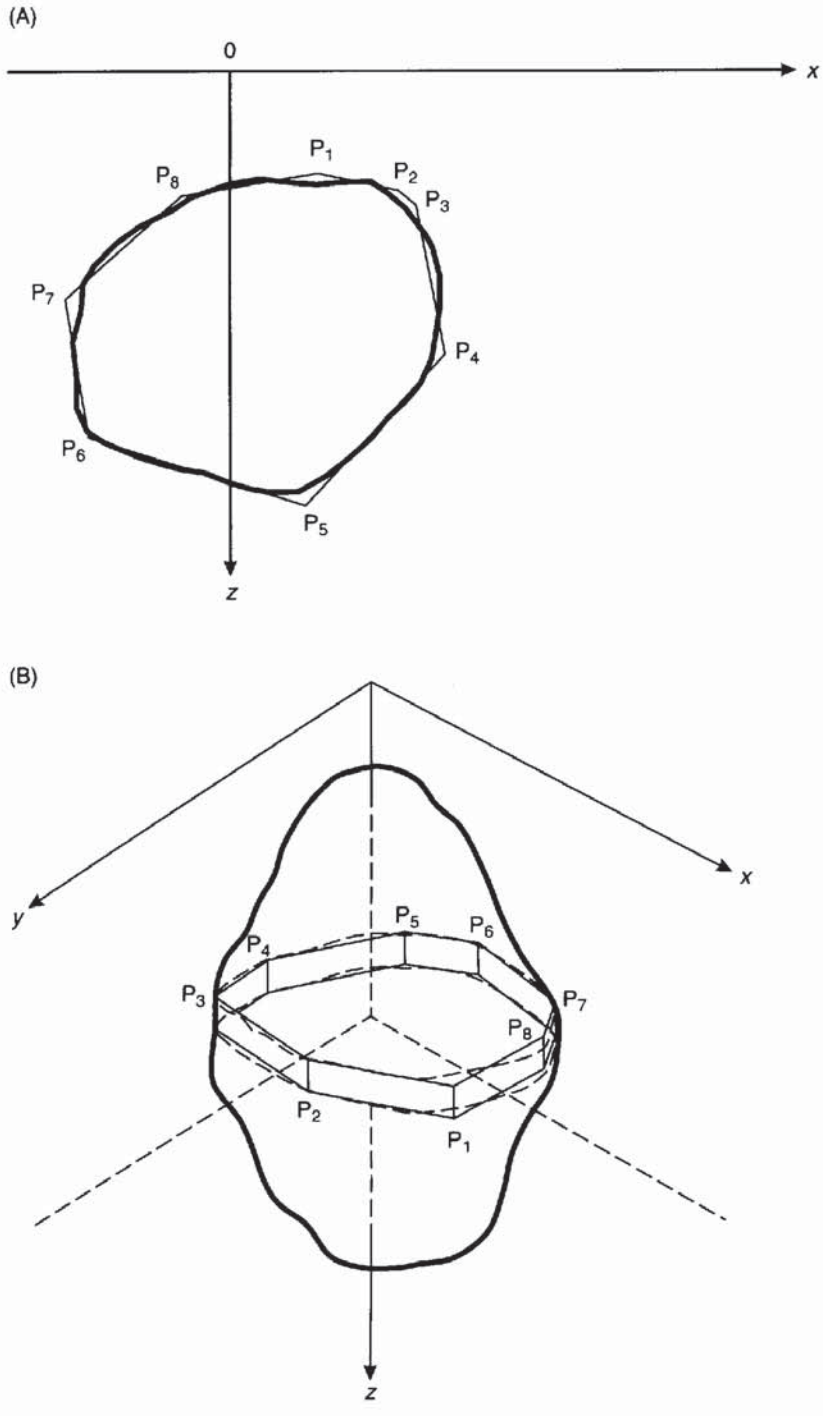

Figure 2.27 (A) Polygonal representation of an irregular vertical section of a two-dimensional geological feature. (B) Representation of an irregular three-dimensional geological feature by polygonal laminae

having a specified density contrast. Each little cube is considered as a point mass and thus the total gravity anomaly for the entire body is obtained by summing the constituent gravity components for each mini-cube. The resultant gravity anomaly is compared with that

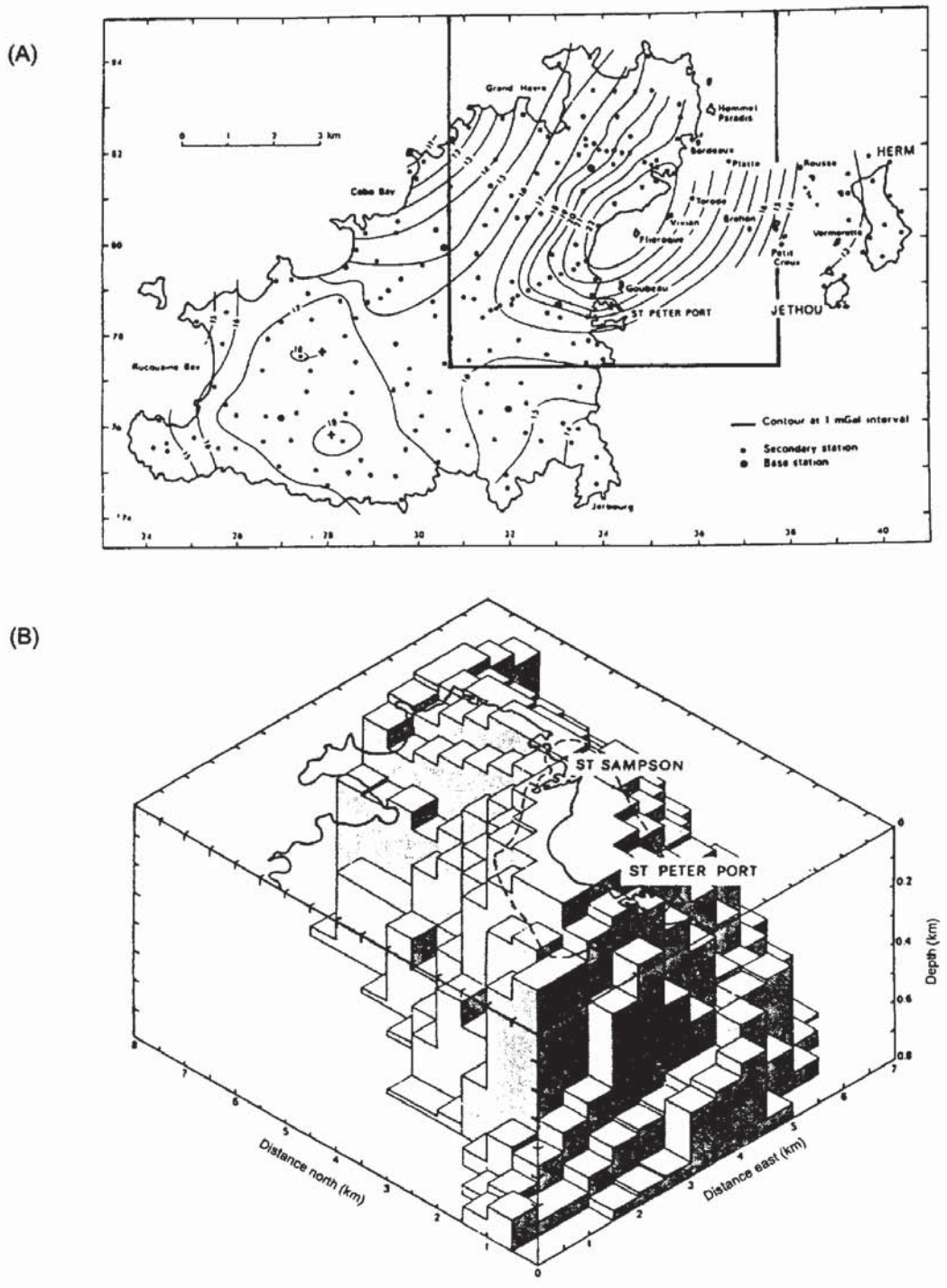

Figure 2.28 (A) Bouguer anomaly map for Guernsey, Herm and Jethou, Channel Islands, and (B) a three-dimensional model of the underlying St Peter Port Gabbro (density contrast 0.27 Mg/m^3, vertical exaggeration 5:1). The coastline and the outline of the gabbro outcrop are indicated. The gabbro is thus interpreted as a laccolith approximately 4 km in diameter and 0.8 km thick. From Briden *et al.* (1982), by permission

observed and, if necessary, the model is adjusted by trial-and-error or by automatic iterative methods (e.g. non-linear optimisation (Al-Chalabi 1972)) until the differences between the computed and observed anomalies are reduced to an acceptable, statistically defined level. Better resolution is obtained by reducing the size and increasing the number of individual cubes within the model. By having a regular cube size, the computation is eased considerably. An example of the application of this technique is given in Figure 2.28, where gravity data from Guernsey, Channel Islands, have revealed that a gabbro body, which outcrops to the north-east of the island near St Peter Port, has the form of a laccolith 0.8 km thick and about 4 km in diameter (Briden *et al.* 1982).

2.6.3 Depth determinations

Of major importance in the interpretation of any gravity data is the determination of depth to the centre of mass and/or to the top of the body causing the anomaly. The maximum depth at which the top of any particular geological body can be situated is known as the *limiting depth*. Methods of obtaining this information depend on which interpretational technique and model are being used. Let us consider various *direct* or *forward* methods where the actual gravity anomaly data are used to derive depths and also estimates of anomalous masses of the features causing the anomalies.

The commonest rules of thumb concern the use of the half-width of the anomaly; that is, the half-width ($x_{1/2}$) of the anomaly where the amplitude is half the maximum value (see Figure 2.26). Some workers define the half-width as the entire width of the anomaly at half peak amplitude and the form of the depth and mass determination equations will differ accordingly. Whichever formulae are used, care should be taken when calculating the limiting depth. The causative body has finite size and its mass is not concentrated at its centre of mass, and thus any estimate of depth will be overestimated. Also, the method will only give an approximation of depth in cases where all the constituent components have the same sense of density contrast (i.e. all negative or all positive). These formulae will also not be effective for compact mineral bodies. Formulae for a selection of given geometric forms are given in Box 2.19A and an example of one calculation is given in Box 2.19B.

Several basic 'rules', known as the *Smith Rules* after their originator (Smith 1959, 1960), have become established in the calculation of limiting depths. Two rules (1 and 2 in Box 2.20) use a *gradient–amplitude ratio* method. Consider any geological body that gives an isolated gravity anomaly (Figure 2.30) entirely of either sign with a maximum gravity (Δg_{max}) that varies along the line of the profile and thus has a horizontal gradient which reaches a maximum value at $\Delta g'_{max}$. The Smith Rules describe the various relationships between

the limiting depth d to the top of any geological body and the maximum gravity (Δg_{max}) and its horizontal gradient ($\Delta g'_{max}$) as listed in Box 2.20.

Box 2.19A Depth estimates for given geometric forms

Form	Formula	Notes
Sphere	$z = 1.305x_{1/2}$ $d = z - r$	z is depth to centre of mass d is depth to top of sphere of radius r $r^3 = \lvert\Delta g_{max}\rvert z^2/(0.028\delta\rho)$ from Box 2.18
Horizontal cylinder	$z = x_{1/2}$ $d = z - r$	z is depth to cylinder axis d is depth to top of cylinder of radius r $r^2 = \lvert\Delta g_{max}\rvert z/(0.042\delta\rho)$ from Box 2.18
Vertical cylinder	$z = 1.732x_{1/2}$	z is depth to top end of cylinder (overestimates z)
Thin dipping sheet	$z \approx 0.7x_{1/2}$ $z \approx x_{1/2}$	z is depth to top of sheet When $z \approx$ dip length of sheet When $z \gg$ dip length of sheet *When length of sheet is very large or sheet dips at less than 60°, no solution is possible*
Thick prism	$z = 0.67x_{1/2}$ $z = 0.33x_{1/2}$	z is depth to prism top = prism width, and depth to prism base is twice width When depth to prism base is 10 times prism width *In both cases, estimates of z are unreliable*

Box 2.19B Example of calculation for a sphere

An air-filled cavity in rock of density 2.5 Mg/m^3 can be modelled by a sphere of radius r and depth to centre of mass, z (m). The resultant gravity anomaly is shown in Figure 2.29. Given $\Delta g_{max} = 0.048$ mGal, $x_{1/2} = 2.2$ m, and $\delta\rho = 2.5$ Mg/m^3:

$$z = 1.305 \times 2.2\,\text{m} = 2.87\,\text{m}.$$

Radius of sphere = r:

$$r^3 = 0.048 \times (2.87)^2/(0.0286 \times 2.5) = 5.53\,\text{m}^3.$$

continued

continued

So $r = 1.77$ m. Depth to top of sphere $d = 2.87 - 1.77 = 1.10$ m. *An air-filled cavity of this size so close to the surface could constitute a hazard*

Box 2.20 Smith Rules

(1) Where the entire anomaly has been isolated:

$$d \leqslant C.\ \Delta g_{max}/\Delta g'_{max}$$

where $C = 0.65$ for a 2-D body and $C = 0.86$ for a 3-D body.

(2) When only part of an anomaly is isolated, for any point x:

$$d \leqslant K\ \Delta g_x/\Delta g'_x$$

where $K = 1.00$ for a 2-D body and $K = 1.50$ for a 3-D body.

(3) For a maximum density contrast $\delta\rho_{max}$ and a maximum value of the second horizontal gradient ($\Delta g''_{max}$) (that is, the rate of change of $\Delta g'$ with x):

$$d \leqslant 5.4\, G\delta\rho_{max}/\Delta g''_{max}.$$

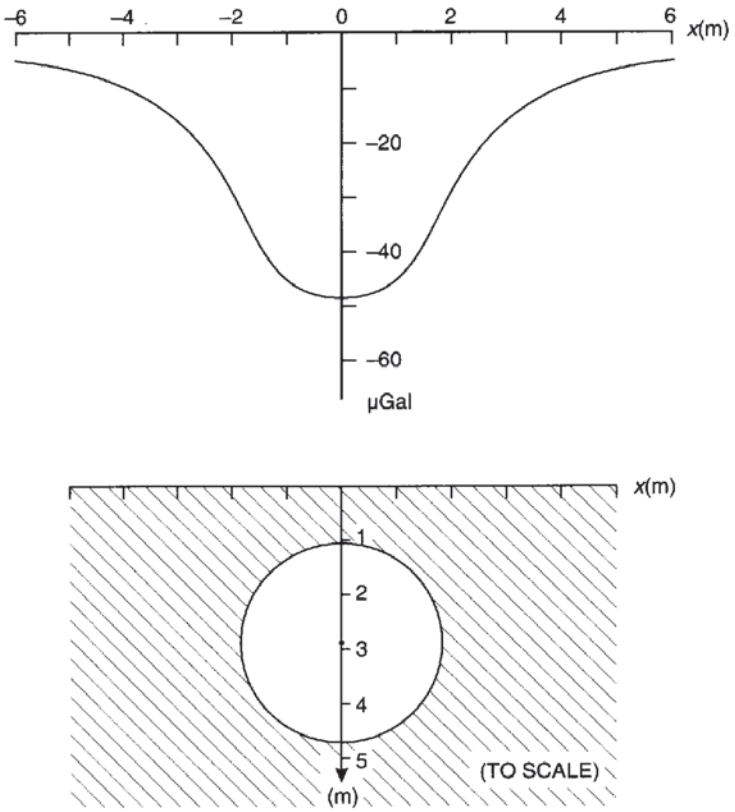

Figure 2.29 Gravity anomaly over an air-filled cavity of radius 1.77 m and 2.87 m depth to centre, in rock of density 2.5 Mg/m^3

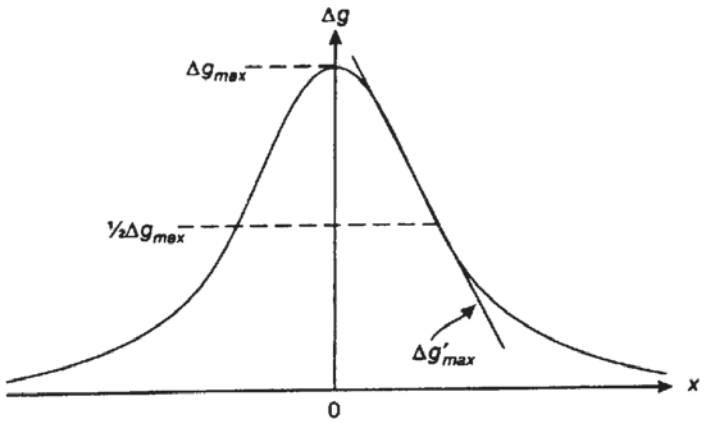

Figure 2.30 Limiting depth calculations: half-width method and gradient–amplitude ratio method (see text for details)

The third Smith Rule adopts a second-derivative method which uses the rate at which the gravity gradient changes along the profile. It is thought that second-derivative methods produce more accurate estimates of limiting depths. Second derivatives are discussed in more detail in Section 2.6.5.

2.6.4 Mass determination

Anomalous mass is the difference in mass between a geological feature and the host rock. There are two basic methods of calculating either an excess mass due to a high-density body or a mass deficiency caused by a body with a lower density.

The first method uses a rule of thumb based on the gravity anomaly half-width ($x_{1/2}$) and an assumption that the geological feature approximates to a given geometric form, such as a sphere (Box 2.21). The anomalous mass can be calculated by subtracting the mass due to a sphere (density times volume) from the mass estimated using gravity data. In the example below, the actual mass of an air-filled cavity is negligible, so the mass deficiency calculated is the mass of the missing rock.

Box 2.21 Mass of a sphere

Total mass $M \approx 255\ \Delta g_{max} (x_{1/2})^2$ tonnes

where Δg_{max} is in mGal and $x_{1/2}$ in metres.

Example
For an air-filled cavity described in Box 2.19B, the total mass deficiency of the sphere is equal to the mass of the rock that

continued

continued

would have been in the cavity, times its density (2.5 Mg/m^3):

$$\text{Mass} = \text{density} \times \text{volume} = 2.5 \times (4/3)\pi\ 1.77^3 = 58 \text{ tonnes.}$$

Using the gravity data:

$$\text{Mass} \approx 255 \times 0.048 \times 2.2^2 = 59 \text{ tonnes.}$$

The second method is based on Gauss's Theorem in potential theory (Grant and West 1965) and is particularly important for two reasons. First, the total anomalous mass of a geological feature can be calculated from the associated gravity anomaly without any assumptions being necessary about the body's shape or size. Secondly, the total anomalous mass can be very important in the determination of tonnage of ore minerals (Hammer, 1945). For this method to work effectively, it is important that the regional gravity field be removed and that the entire residual anomaly be isolated clearly. The survey area is divided into a series of rings each of which is further divided into segments of area δA. The gravity effect of each segment is determined and the total for each ring is obtained and summed together (Box 2.22). Having determined the excess mass, it is then a simple matter to calculate the actual mass (M) if the densities of the host rock (ρ_0) and the anomalous body (ρ_1) are known.

Box 2.22

(1) Total anomalous mass (M_E):

$$M_E = 23.9\Sigma(\Delta g \delta A) \text{ tonnes}$$

where Δg is in mGal and δA in metres.

(2) Actual mass of a geological body (M):

$$M = M_E \frac{\rho_1}{(\rho_1 - \rho_0)} \text{ tonnes } (\rho_1 > \rho_0).$$

Parasnis (1966) gives an example where the total anomalous mass of the Udden sulphide orebody in northern Sweden was calculated to be 568 820 tonnes. Assuming the densities of the ore and host rock to be 3.38 and 2.70 Mg/m^3 respectively, the actual mass of the ore was found to be 2.83 million tonnes, a value consistent with drillhole estimates.

2.6.5 Second derivatives

2.6.5.1 Second vertical derivative (SVD) maps

One of the problems inherent within the interpretation of Bouguer anomaly maps is that it is difficult to resolve the effects of shallow structures from those due to deeper seated ones. The removal of the effect of the regional field from the Bouguer anomaly data results in an indeterminate and non-unique set of residuals. It is possible to separate the probable effects of shallow and deeper structures by using second vertical derivatives.

The gravity field (g) which is measured by gravimeters varies with height; that is, there is a vertical gradient ($\delta g/\delta z = g'$). Over a non-uniform earth in which density varies laterally, the vertical gradient changes and the *rate* of change ($\delta g'/\delta z$) is thus the second vertical derivative of the gravity field ($\delta^2 g/\delta z^2$. This quantity is very sensitive to the effects of shallow features (and to the effects of noise and topography).

As an illustration of how the gravity effects of shallow and deep structures can be separated, consider two equal point masses (m) at two different depths, say at depths of 1 unit and 4 units. The value of g for a point mass at a depth z is simply equal to the product of the gravitational constant (G) and the mass divided by the depth z squared, so $g = Gm/z^2$). If this is differentiated twice with respect to z, it becomes $g'' = 6Gm/z^4$. This tells us that the second derivative of the two masses, g'', is inversely proportional to z^4. Hence the ratio of the two derivatives will be, for $z_1 = 1$ and $z_4 = 4$, $g''_1/g''_4 = 256$.

It is possible to compute and plot maps of the second vertical derivative of Bouguer anomaly data. The zero-contour should indicate the edges of local geological features. The contours have units where 10^{-6} mGal/cm$^2 \equiv 10^{-9}$ cm^{-1}s$^{-2} \equiv 1$ E cm^{-1}. (E stands for an Eötvös unit $= 10^{-6}$ mGal/cm, which is a measure of gravitational gradient.)

It should be emphasised that it is not possible to undertake any quantitative analyses of SVD maps except to produce characteristic profiles over known geometric forms. The main advantage of SVD maps is to highlight and clarify features spatially, as can be seen from Figures 2.31 and 2.32. In the first of these, the Bouguer anomaly map appears to have a consistent trend in the direction of the gravity gradient (increasingly positive to the east) with isogals aligned in a NW–SE direction. There is no obvious major feature evident on the Bouguer anomaly map. In contrast, the SVD map shows a major ENE–WSW linear feature with three closures, and it has picked out the outline of the Cement field in Oklahoma extremely well. Figure 2.32 illustrates the case when a single Bouguer anomaly is really the envelope of several smaller anomalies. In this atypical and rather extreme case, several deep boreholes were drilled on the large minimum indicated on both the Bouguer and the residual anomaly maps;

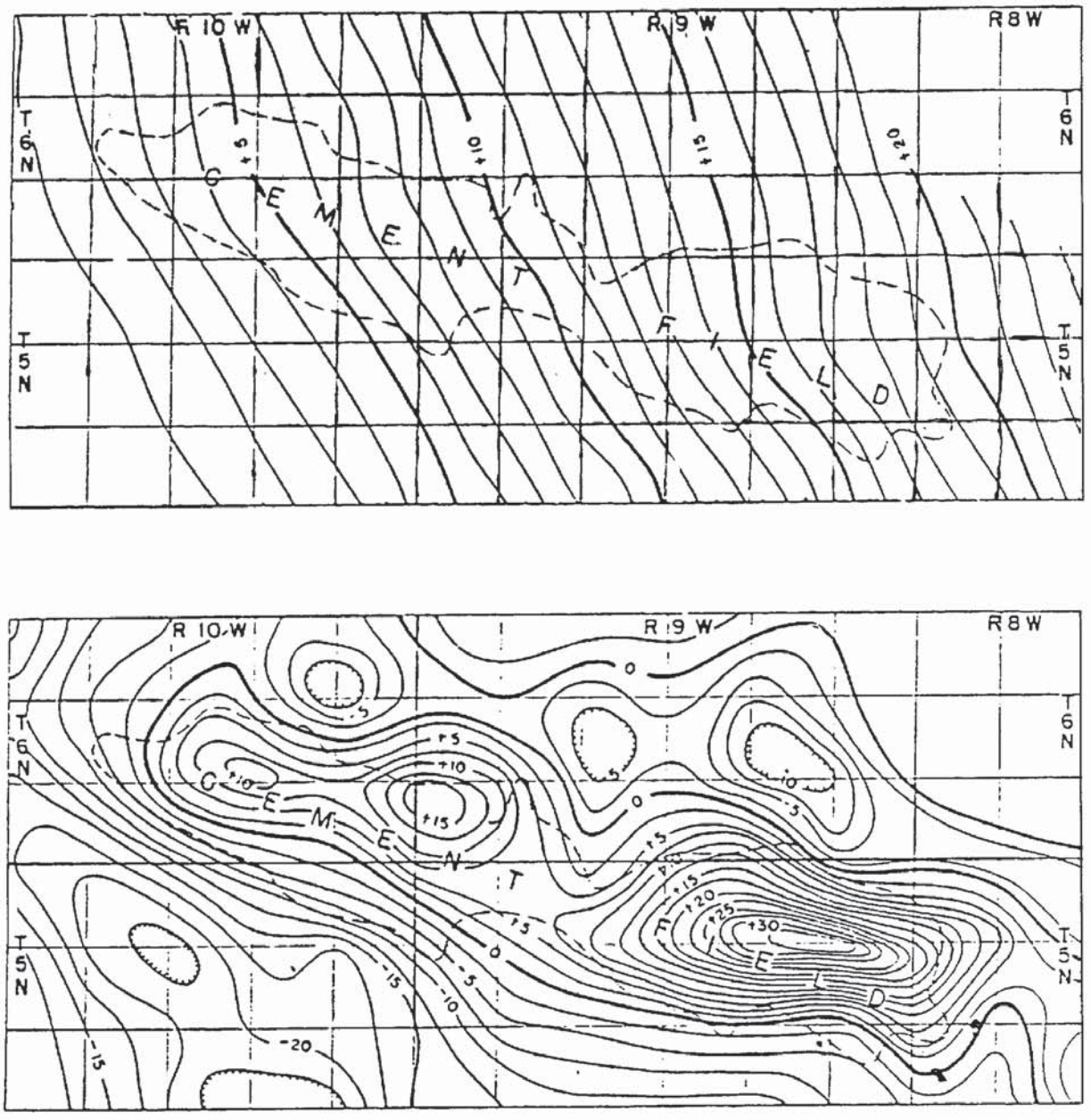

Figure 2.31 Observed Bouguer anomaly (contour interval 1 mGal) and second vertical derivative (contour interval 2.5×10^{-15} c.g.s.u.) maps over a Cement field in Oklahoma. From Elkins (1951), by permission

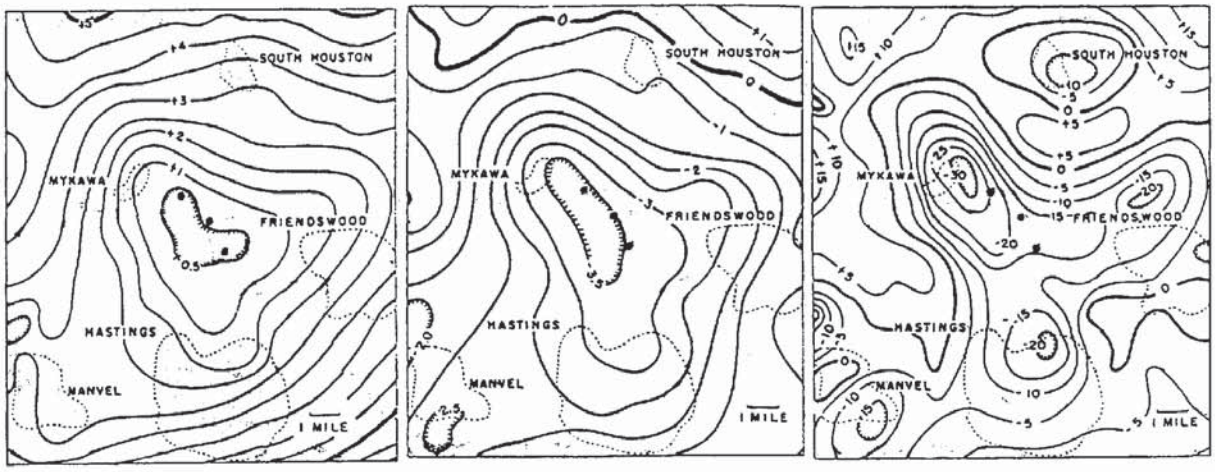

Figure 2.32 (A) Observed gravity, (B) residual gravity (contour interval 0.5 mGal), and (C) second vertical derivative (contour interval 5×10^{-15} c.g.s.u.) maps for Mykawa, Texas Gulf Coast. • indicate dry boreholes. From Elkins (1951), by permission

they were found to be dry, having missed the appropriate target, presumed to be a single salt dome. In contrast, the SVD map highlights three salt domes accurately.

Unfortunately, SVD also amplifies noise and so can produce many second-derivative anomalies that are not related to geology. Consequently, in some cases, SVD analyses provide no real advantage over the Bouguer anomaly map. An example of where extraneous anomalies shroud the geologically related features is given in Figure 2.33. Although it is possible to see on the SVD map the two main features present on the Bouguer anomaly map of the J-jaure titaniferous iron-ore region in Sweden, the SVD map also has a number of small maxima and minima that are of no structural interest. To resolve which anomalies are of geological importance, it is necessary to go back to the original gravity map and to any other source of geological information. It may even be prudent to refer back to the raw observations and corrections.

2.6.5.2 *Downward and upward continuation*

The effect on gravity of a geological mass at considerable depth is far less than if it were close to the surface (see Figure 2.24). the *principle of continuation* is the mathematical projection of potential field data (gravity or magnetic) from one datum vertically upwards or downwards to another datum. Effectively, the continuation process simulates the residual Bouguer anomaly at levels below or above sea level as if the gravity data had been obtained at those levels.

Upward continuation is relatively straightforward as the projection is usually into free space. Upward continuation serves to filter out the shorter-wavelength anomalies and reduce their amplitudes and decrease noise.

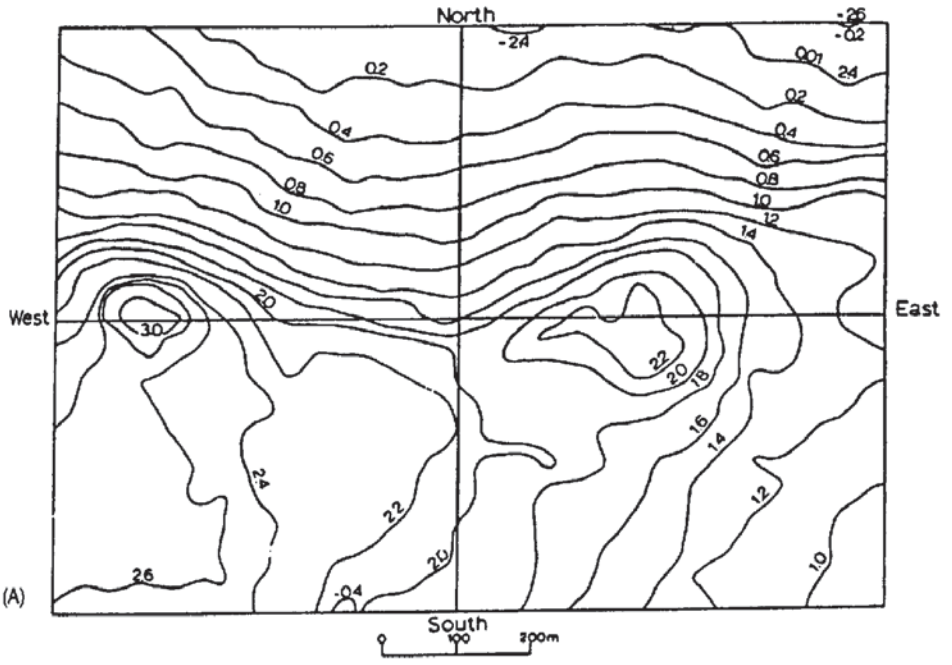

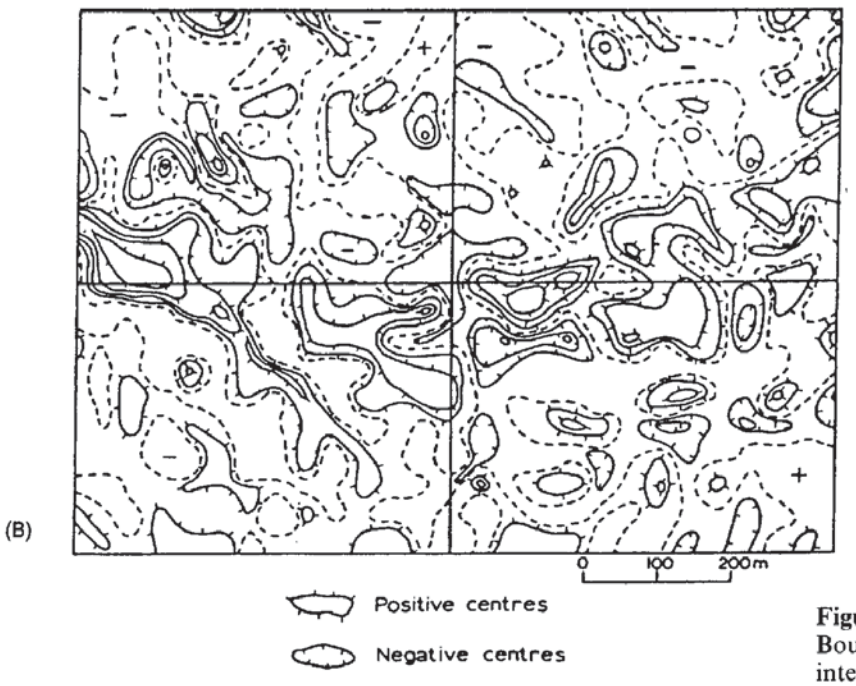

Figure 2.33 An example where the Bouguer anomaly map (A) (contour interval 2 mGal) exhibits more detail than the corresponding second vertical derivative map (B) for the J-jaure titaniferous iron-ore region in Sweden. Contours: 0 (dashed), ± 0.1, ± 0.2, ± 0.4 in units of 0.0025 mGal/m^2). From Parasnis (1966), by permission

Downward continuation is far more problematical as there is an inherent uncertainty in the position and size of the geological features as represented by the Bouguer gravity data. Furthermore, downward continuation aims to reduce each anomaly's wavelength and increase its amplitude. This mathematical amplification will also work on noise within the data and the resultant information may prove unsuitable for further analysis.

Continuation also forms a method of gravitational stripping (Hammer, 1963) where the gravity effects of upper layers are necessarily removed to reveal the anomalies due to deeper seated geological structures (e.g. Hermes 1986; Abdoh *et al.* 1990). The method uses the concept of an equivalent stratum (Grant and West, 1965). The Bouguer gravity field is continued downwards to a level that corresponds to a previously identified interface, such as from seismic reflection surveys, and an equivalent topographic surface is constructed at that level. This equivalent stratum should account for any residual anomalies at the surface arising from the interface. Continuation is discussed in much more detail by Grant and West (1965) and by Telford *et al.* (1990).

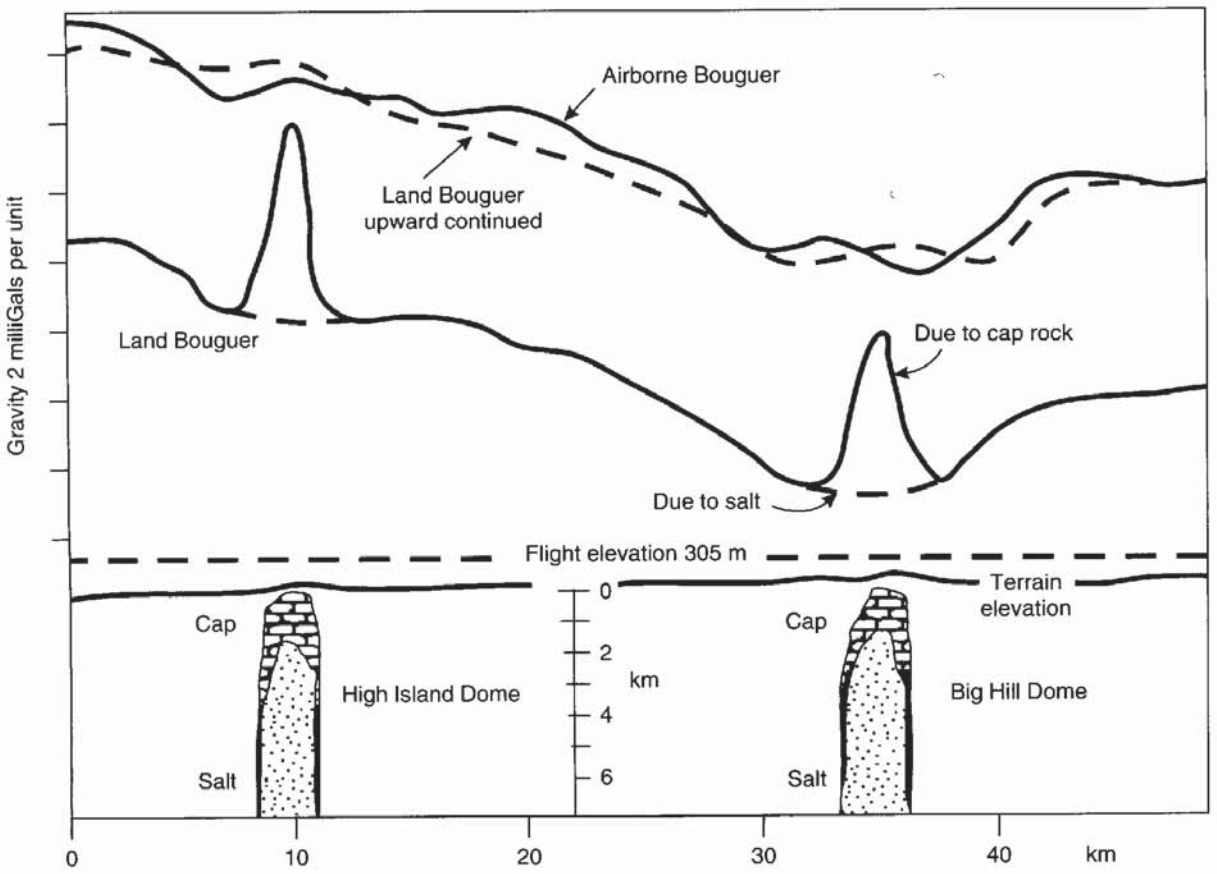

Figure 2.34 Comparison of airborne and upward continued land Bouguer gravity data with those obtained by airborne gravity surveying. From Hammer (1984), by permission

Upward continuation is used in comparisons of ground-based gravity anomalies with airborne data. It is usual to continue ground data upwards rather than to work downwards so as not to amplify noise. An example of such a comparison is shown in Figure 2.34 (Hammer 1982, 1984). Two gravity minima associated with low-density salt have shorter-wavelength maxima superimposed which are due to the high-density cap rocks. These maxima attenuate with increased elevation and the agreement between the upwardly continued land Bouguer data and the airborne is better than 5 g.u. except in the immediate vicinity of the cap rocks.

One of the major considerations in the interpretation of particularly regional gravity data is the amount of computer processing required. Considerable effort has been expended in developing computer-based methods of data enhancement. For example, image processing of data on computer-compatible tapes (CCTs) permits considerable manipulation of the data for display purposes to aid analysis and interpretation. Processes include edge enhancement to highlight lineaments (e.g. Thurston and Brown 1994), amplitude displays and spectral modelling (Figure 2.35). It is usually only economically viable to undertake such sophisticated processing on very large data sets.

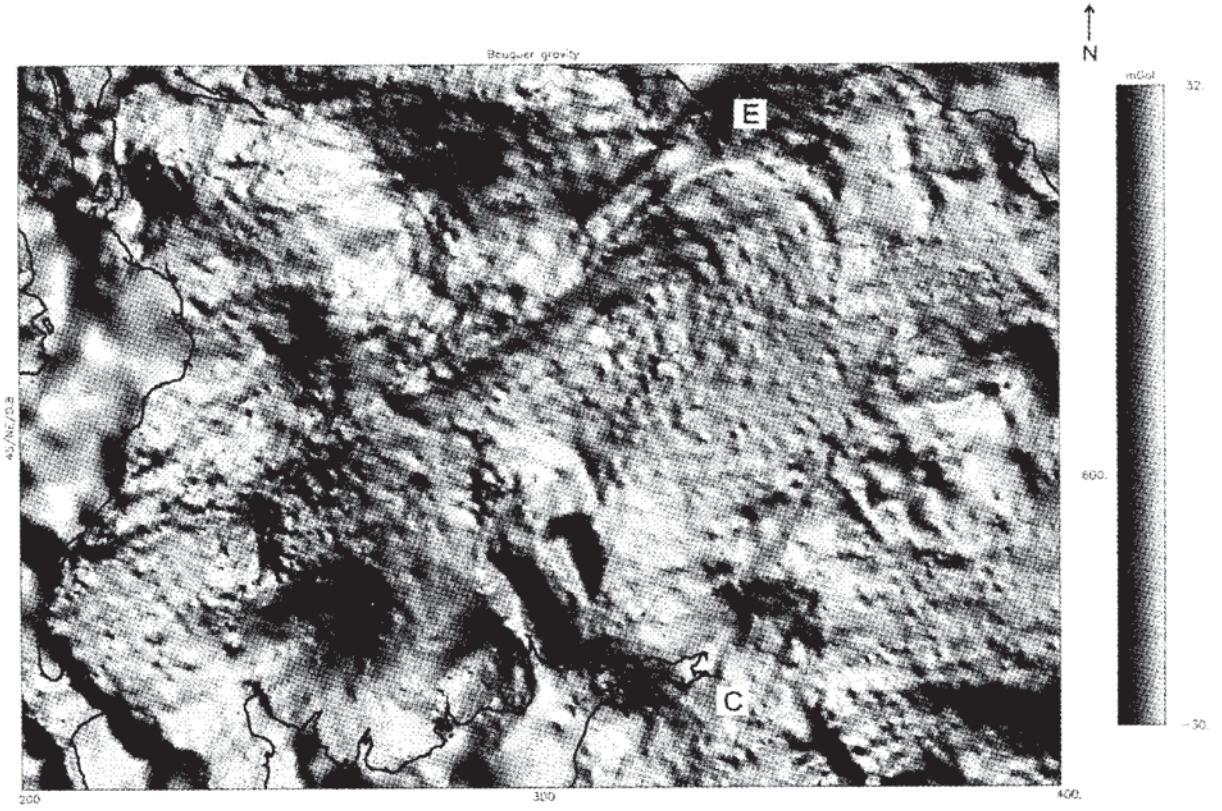

Figure 2.35 Structural analysis, based on lineations from a series of colour and greyscale shaped-relief images of geophysical data can provide a basis for reassessment of regional structure, mineralisation potential and fracture patterns. This image is of observed regional Bouguer gravity data, over an area of 200 km × 140 km of the Southern Uplands. Scotland (C: Carlisle; E: Edinburgh). The data have been reduced to Ordnance Datum using a density of 2.7 Mg/m^3, interpolated to a square grid of mesh size 0.5 km and displayed as a greyscale shaded-relief image. Sun illumination azimuth and inclination are NE and 45° respectively. A series of NE trending features paralled to the regional strike and the Southern Uplands fault have been suppressed by the NE illumination, whereas subtle NW trending features linked to development of the Permian basins are enhanced and seen to be more extensive. For comparison, see Figure 3.48. Image courtesy of Regional Geophysics Group, British Geological Survey

2.6.6 Sedimentary basin or granite pluton?

It is very important in the interpretation of gravity data for hydrocarbon exploration to be able to distinguish between a sedimentary basin (a good possible hydrocarbon prospect) and a granitic pluton (no prospect for hydrocarbons), as both can produce negative gravity anomalies of comparable magnitude.

For example, Arkell (1933) interpreted a minimum in an initial Bouguer gravity survey in the Moray Firth, north-east Scotland, as being due to a granite pluton. It was only after further geological work (Collette, 1958) and gravity work (Sunderland, 1972) that it was realised that the minimum was due to a sedimentary basin. Simultaneously, the Institute of Geological Sciences undertook seismic reflection surveys and initiated some shallow drilling. It was not until 1978 that the Beatrice Field was discovered (McQuillin *et al.* 1984). Had the 1933 interpretation been different, the history of the development of the North Sea as a major hydrocarbon province might have been very different.

In 1962, Bott proposed a set of criteria to distinguish between a sedimentary basin and a granite boss as interpretations of gravity minima. His argument was based on the second vertical derivative of the gravity anomaly due to a semi-infinite two-dimensional horizontal slab with a sloping edge. He found that the ratio of the moduli of the maximum and minimum second vertical derivative ($|g''_{max}|/|g''_{min}|$) provides a means of distinguishing between the two geological structures, as outlined in Box 2.23 and illustrated in Figure 2.36. McCann and Till (1974) have described how the method can be computerised, and the application of Fourier analysis to Bott's method. Some authors calculate the second *horizontal* derivative ($\delta^2 g/\delta x^2$) (e.g. Kearey and Brooks 1991; figure 6.19) which responds in exactly the same way as the *vertical* derivative except that the maxima and minima are reversed, as are the criteria in Box 2.23. In order for the method to work, the gravity anomaly attributed to the appropriate geological feature (sedimentary basin or granitic pluton) needs to be clearly isolated from adjacent anomalies due to other features. The method is not applicable, however, in cases where extensive tectonic activity has deformed either a sedimentary basin by basin-shortening or a granitic pluton by complex faulting, thereby changing the gradients of the flanks of both types of model.

Box 2.23 Bott criteria (see also Figure 2.36)

(1) For a sedimentary basin:

$$|g''_{max}|/|g''_{min}| > 1.0.$$

Basin sides slope *inwards*.

continued

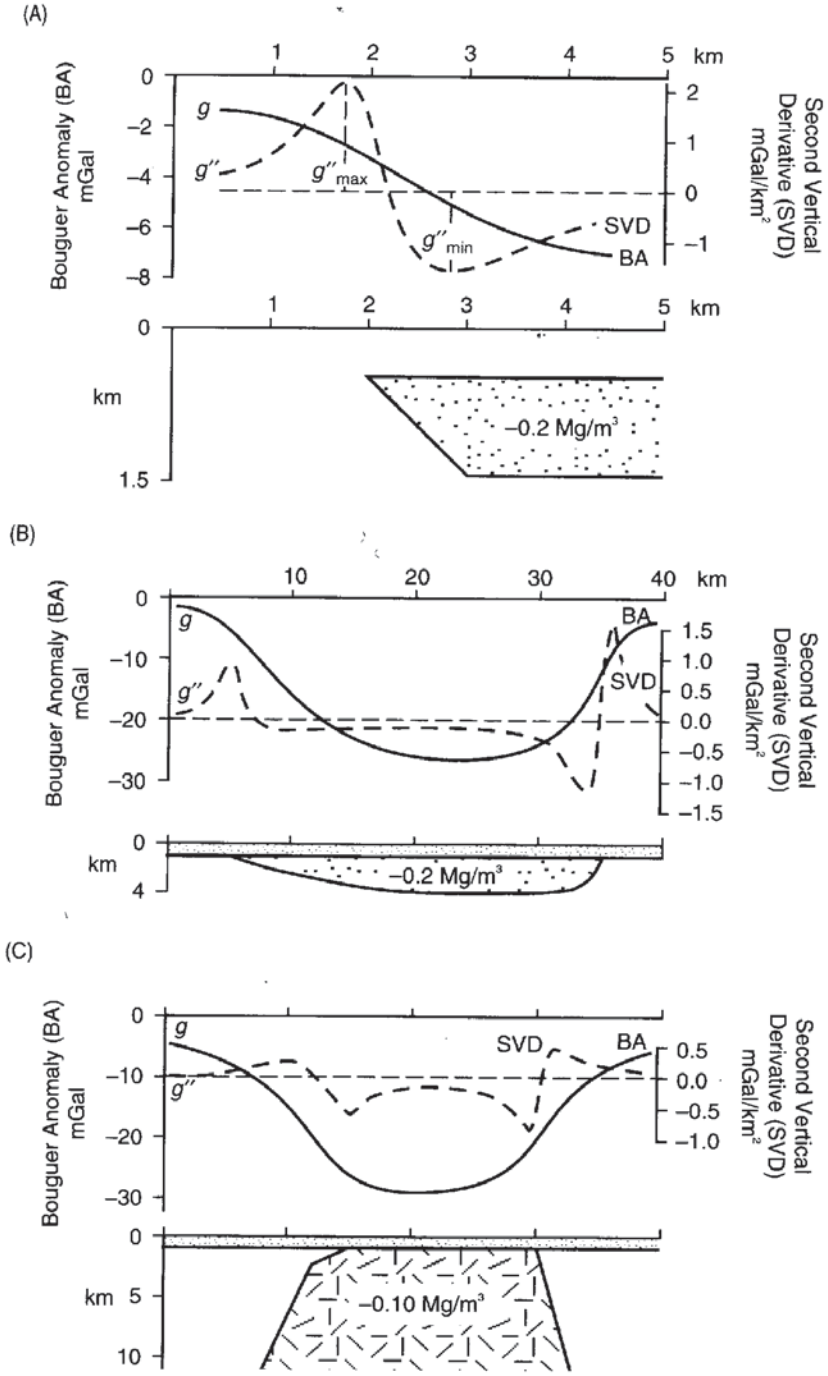

Figure 2.36 Bott criteria to distinguish between the Bouguer gravity profile over (A) a horizontal prism, (B) a sedimentary basin, and (C) a granitic pluton. After Bott (1962), by permission

continued

(2) For a granite pluton:

$$|g''_{max}|/|g''_{min}| \leqslant 1.0.$$

Granite pluton sides slope *outwards*.

The vertical variation of density of sediments with depth in a sedimentary basin can be represented in a number of ways. Moving away from Bott's uniform density model, consideration of the variation in density in terms of exponential and hyperbolic density contrast has been given by Rao *et al.* (1993) and Rao *et al.* (1994), for example.

2.7 APPLICATIONS AND CASE HISTORIES

In this section, a limited number of case histories are described to illustrate the diversity of applications to which the gravity method can be put. Other geophysical methods are discussed as appropriate, where they have been used in conjunction with, or to contrast with, the gravity results. These other methods are explained in their respective chapters.

2.7.1 Exploration of salt domes

2.7.1.1 Mors salt dome, Denmark (waste disposal)

An original interpretation of the Bouguer anomaly (Figure 2.37) over the Mors salt dome in northern Jutland was made in 1974, five years before any seismic results were known (Sharma, 1986). The investigation was connected to a feasibility study for the safe disposal of radioactive waste in the salt dome, but the methodology is identical had the study been for hydrocarbons.

The salt dome was approximated by a sphere. The values of $\Delta g_{max} \approx 16$ mGal and the half-width ≈ 3.7 km were obtained from profiles across the feature (Figure 2.38A) used to determine the depth to the centre of mass ($z = 4.8$ km). In order to calculate the depth to the top of the sphere, an estimate of the density contrast of the salt with the surrounding material had to be made. For a density contrast ($\delta\rho$) of -0.25 Mg/m^3, this gave the radius of the sphere as 3.8 km and thus depth to the top of the sphere is about 1 km (4.8 km minus 3.8 km); with $\delta\rho = -0.2$ Mg/m^3, the radius is 4.1 km and depth to the top is 0.7 km (4.8 km -4.1 km). This was later found to be in good agreement with the seismic results (Figure 2.38B). If the salt dome approximated to a vertical cylinder of length 5300 m, depth to top 700 m, and radius 4400 m, and density contrast -0.2 Mg/m^3, the expected value of Δg_{max} is around 19 mGal, compared with an observed value of 16–18 mGal; but this is still close enough to be a reasonable approximation to the actual shape.

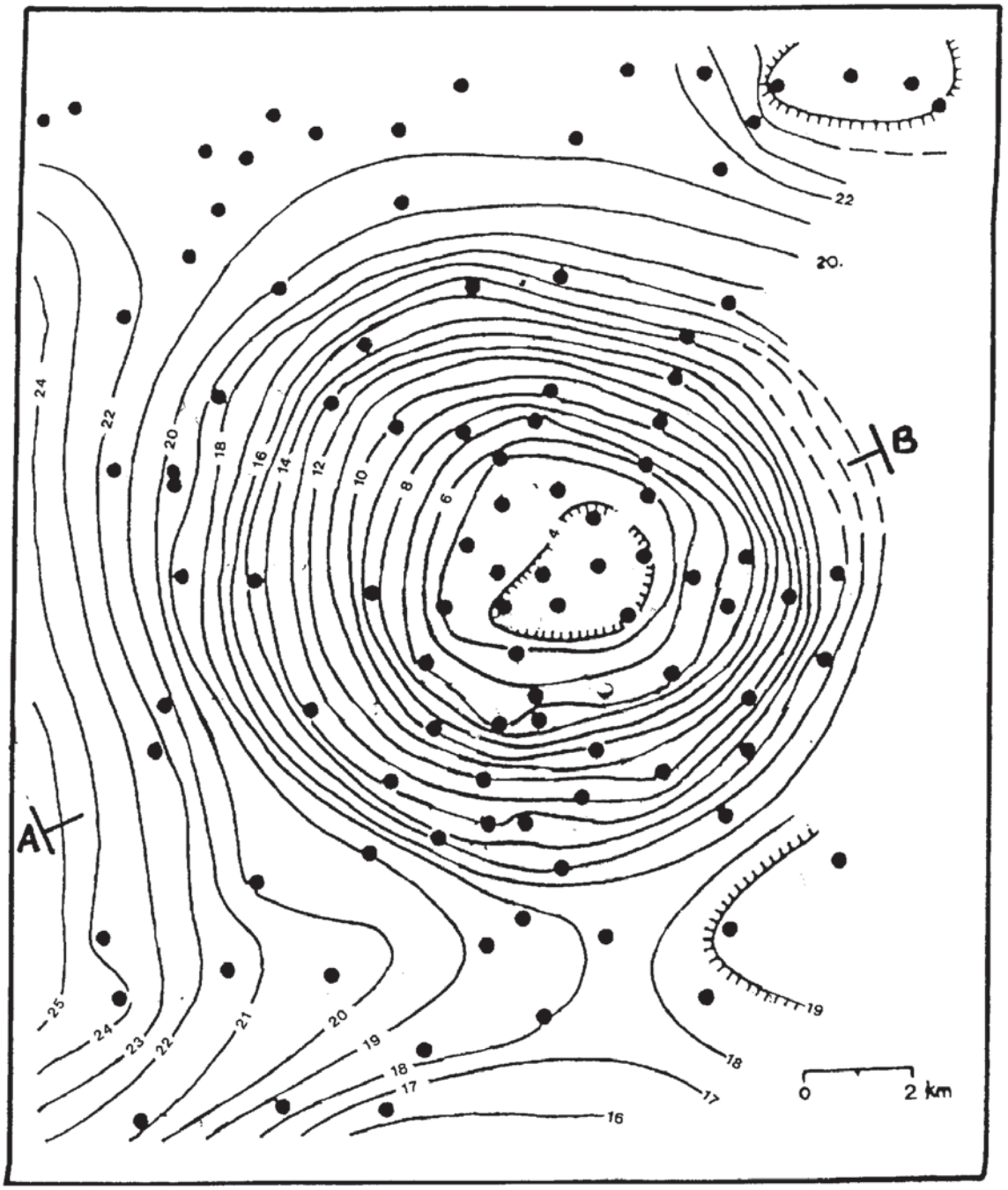

Figure 2.37 Bouguer anomaly map of the Mors salt dome, Jutland, Denmark. Solid dots represent observation points. Contour interval = 1 mGal. From Saxov (1956) and Sharma (1986), by permission

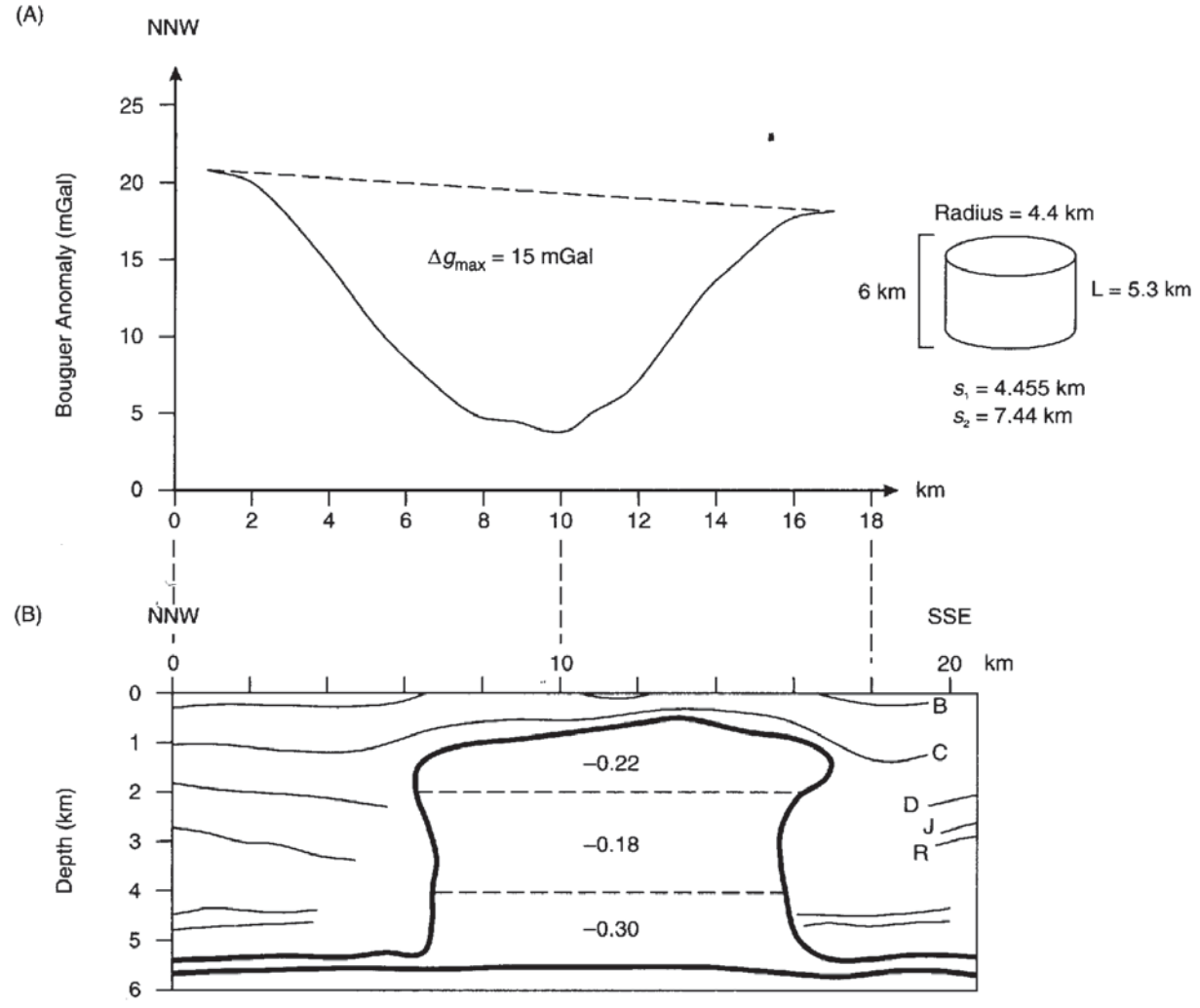

Figure 2.38 (A) Bouguer anomaly profile and (B) corresponding seismic section across profile A–B in Figure 2.37. After Kreitz (1982), LaFehr (1982) and Sharma (1986), by permission

Uncertainty in the density contrast is the biggest problem in interpretation. Subsequent drilling into the salt dome and the use of the seismic profiles undertaken radially across the salt dome enabled the geological model to be enhanced. It was found that the density contrast within the salt dome could be divided into three sections with slightly different density contrasts (Figure 2.38B). The seismic sections did not give a very good image of the top of the salt dome, which is mushroom-shaped and so causes the slight discrepancies between the sphere and vertical cylinder approximations. The combined use of seismic data and gravity modelling has resulted in a much more realistic geological model.

However, it should always be remembered that any geophysical model is only a crude approximation of what can be a very complex geological structure. Consider how well (or otherwise) a vertical cylinder

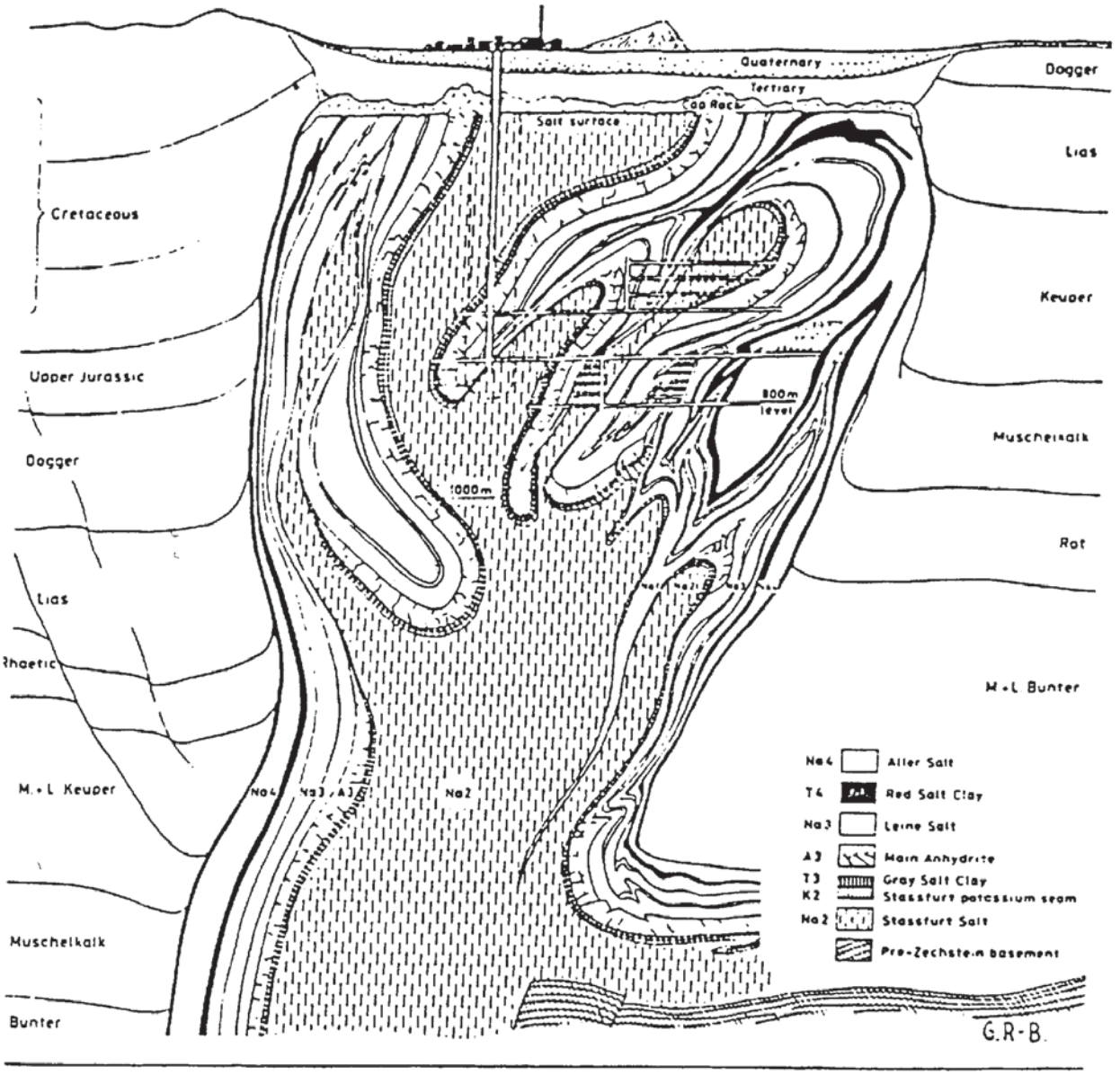

model would represent the salt dome illustrated in Figure 2.39. It is clear that much fine geological detail would not be resolvable unambiguously by the interpretation of geophysical data (Sorgenfrei 1971; Richter-Bernburg 1982).

Figure 2.39 Schematic cross-section through a salt dome structure in north-west Germany, illustrating known complexities in contrast to the usual assumed geophysical model of a vertical cylinder with a uniform density distribution. From Sorgenfrei (1971) and Richter-Bernburg (1982), by permission

2.7.1.2 Salt domes in NW Germany (hydrocarbons)

Another example of gravity anomalies over salt domes is given in Figure 2.40, which is taken from part of a survey over north-west Germany (Hermes, 1986). The intention was to derive the gravity field

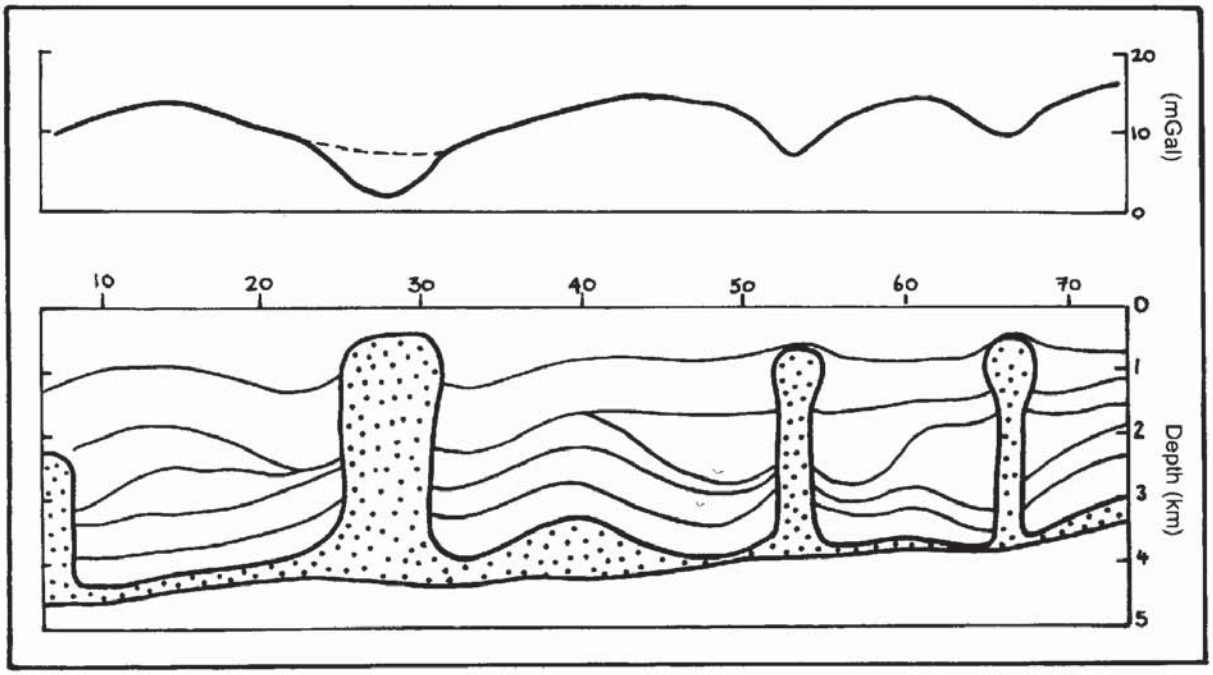

Figure 2.40 A typical Bouguer anomaly profile compared with the corresponding sub-surface geology associated with the Zechstein in northern Germany. From Hermes (1986), by permission

due to the pre-Zechstein and remove it, akin to gravity stripping, to be able to investigate what lies beneath it. Seismic reflection profiling has been singularly unsuccessful both in penetrating through this layer and in producing much useful information. The amplitudes of the Bouguer anomaly minima are clearly associated with the size of the salt domes, the smallest having the lowest amplitude (≈ 5 mGal). The largest minimum is a compound anomaly comprising a minimum associated with the syncline through which the low-density salt has risen. This emphasises the fact that the Bouguer anomaly map of this area is strongly influenced by the structures within the post-Zechstein and by the salt domes and walls. To determine the gravity effect of the pre-Zechstein it is thus essential that these effects be removed. Gravity stripping appears to succeed where filtering methods have been less successful.

2.7.2 Mineral exploration

Gravity surveys fulfil two roles in exploration for minerals: (1) for search and discovery of the ore body, and (2) as a secondary tool to delimit the ore body and to determine the tonnage of ore.

2.7.2.1 Discovery of the Faro lead–zinc deposit, Yukon

An integrated airborne and land geophysical exploration programme, of which gravity surveying was an integral part, led to the discovery of

the Faro lead–zinc deposit in the Yukon, northern Canada (Brock 1973). Gravity was found to be the best geophysical method to delimit the ore body (Figure 2.41). It was also used to obtain an estimate of the tonnage (44.7 million tonnes), which compared very well with a tonnage proven by drilling of 46.7 million tonnes (Tanner and Gibb 1979). In contrast, vertical magnetic mapping provided an anomaly with too shallow gradients to be used, as Figure 2.41 shows.

2.7.2.2 Pyramid ore body, North West Territories

The Pyramid lead–zinc ore body, at Pine Point in the North West Territories, Canada, was discovered using the 'induced polarisation' (IP) method (Seigel *et al.* 1968). For further details of IP, see Chapter 9. Gravity was used to optimise development drilling since the gravity anomalies (Figure 2.42) correlated extremely well with the distribution of the mineralisation within the ore body. Additionally, the gravity data were used successfully to estimate total ore tonnage. Electrical resistivity (see Chapter 7) produced low-amplitude anomalies with a broad correlation with the position of the ore body, and a TURAM electromagnetic survey (see Chapters 10 and 11) was singularly unsuccessful and produced virtually no anomaly at all. The induced polarisation chargeability produced a spectacular anomaly.

2.7.2.3 Sourton Tors, Dartmoor, SW England

This is an example of where gravity did not work at all in association with a known occurrence of mineralisation (Figure 2.43), whereas electrical, electromagnetic and magnetic methods all produced significant anomalies (Beer and Fenning 1976; Reynolds 1988). The reason for the failure of the gravity method in this case is twofold:

- The scale of mineralisation, which is a stockwork of mineralised veins, was of the order of only a few metres wide.
- The sensitivity of the gravimeter was insufficient to resolve the small density contrast between the sulphide mineralisation and the surrounding rocks.

Had a gravimeter capable of measuring anomalies of the order of tens of μGal, and the station interval been small enough, then the zone of mineralisation may have been detectable. At the time of the survey (1969), such sensitive gravimeters were not as widely available as they are today.

2.7.3 Glacier thickness determination

For a regional gravity survey to be complete in areas such as Antarctica and Greenland, measurements have to be made over ice

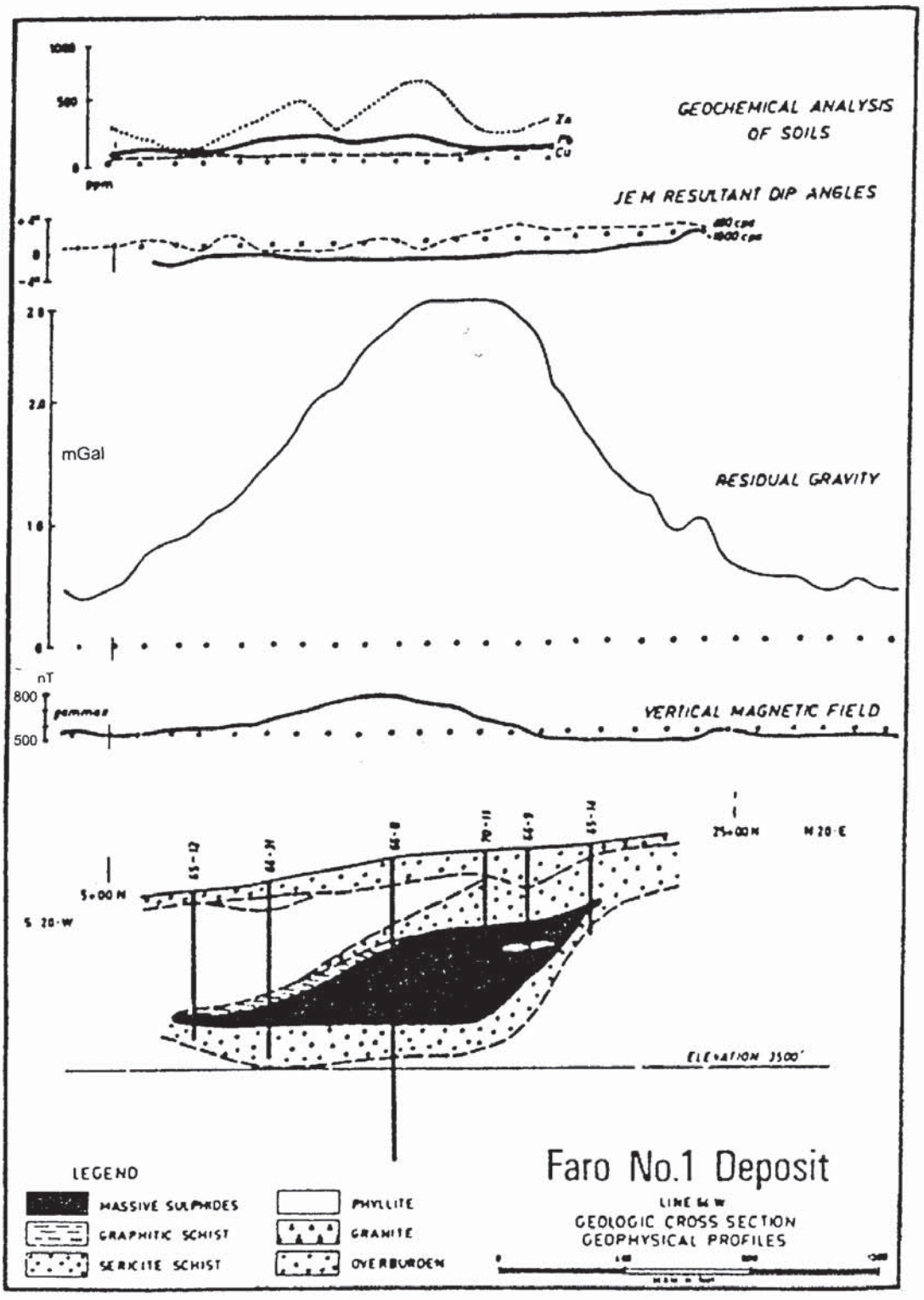
GEOCHEMICAL ANALYSIS OF SOILS
Zn
Cu
ppm
JEM RESULTANT DIP ANGLES
mGal
RESIDUAL GRAVITY
nT
gammas
VERTICAL MAGNETIC FIELD
S 20°W
N 20°E
ELEVATION 3500'
LEGEND
MASSIVE SULPHIDES
GRAPHITIC SCHIST
SERICITE SCHIST
PHYLLITE
GRANITE
OVERBURDEN
Faro No.1 Deposit
LINE 66 W
GEOLOGIC CROSS SECTION
GEOPHYSICAL PROFILES

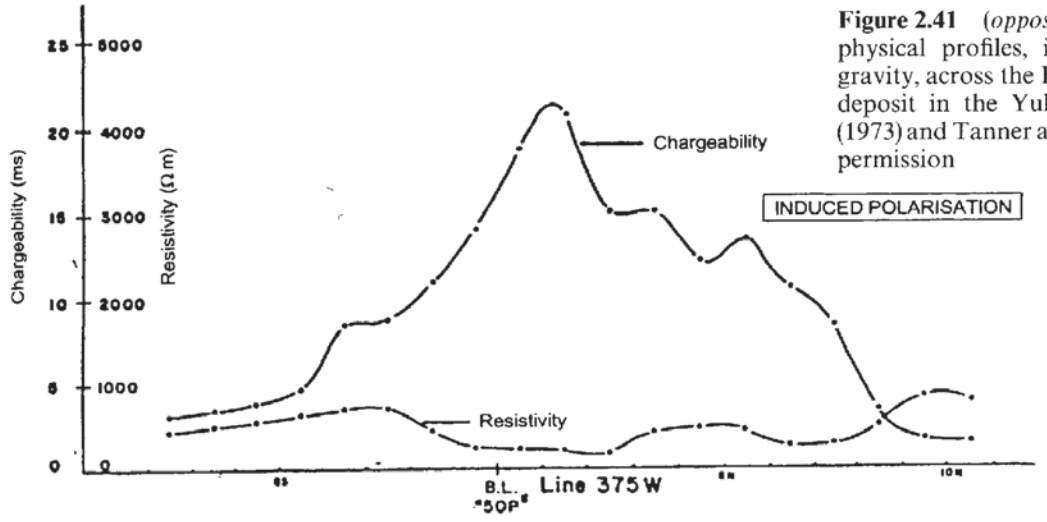

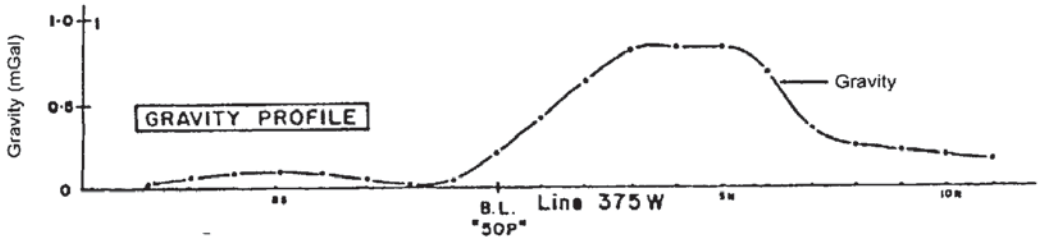

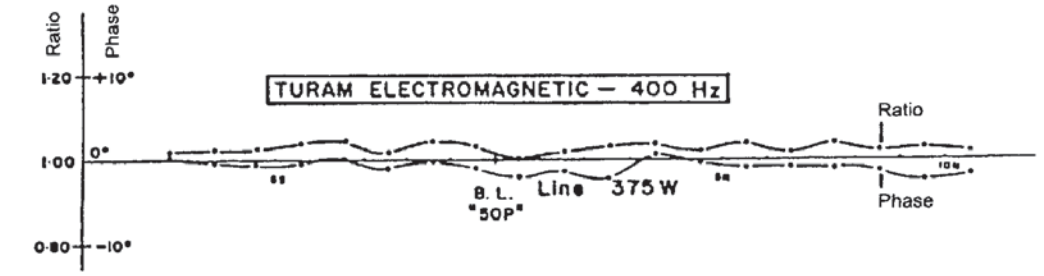

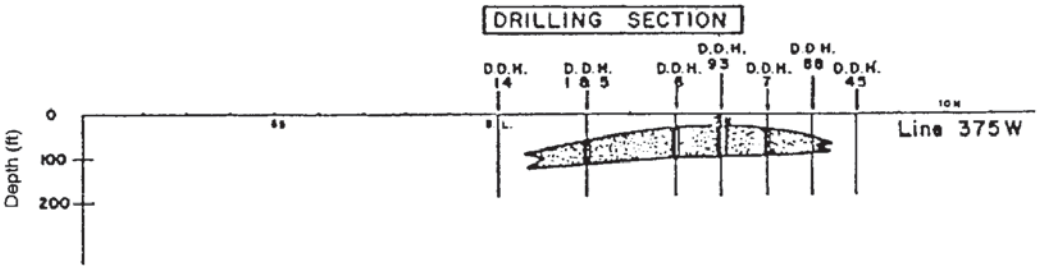

Figure 2.41 (*opposite*) Various geophysical profiles, including residual gravity, across the Faro lead–zinc ore deposit in the Yukon. From Brock (1973) and Tanner and Gibb (1979), by permission

Figure 2.42 Various geophysical profiles including residual gravity, across Pyramid no. 1 ore body. From Seigel *et al.* (1968), by permission

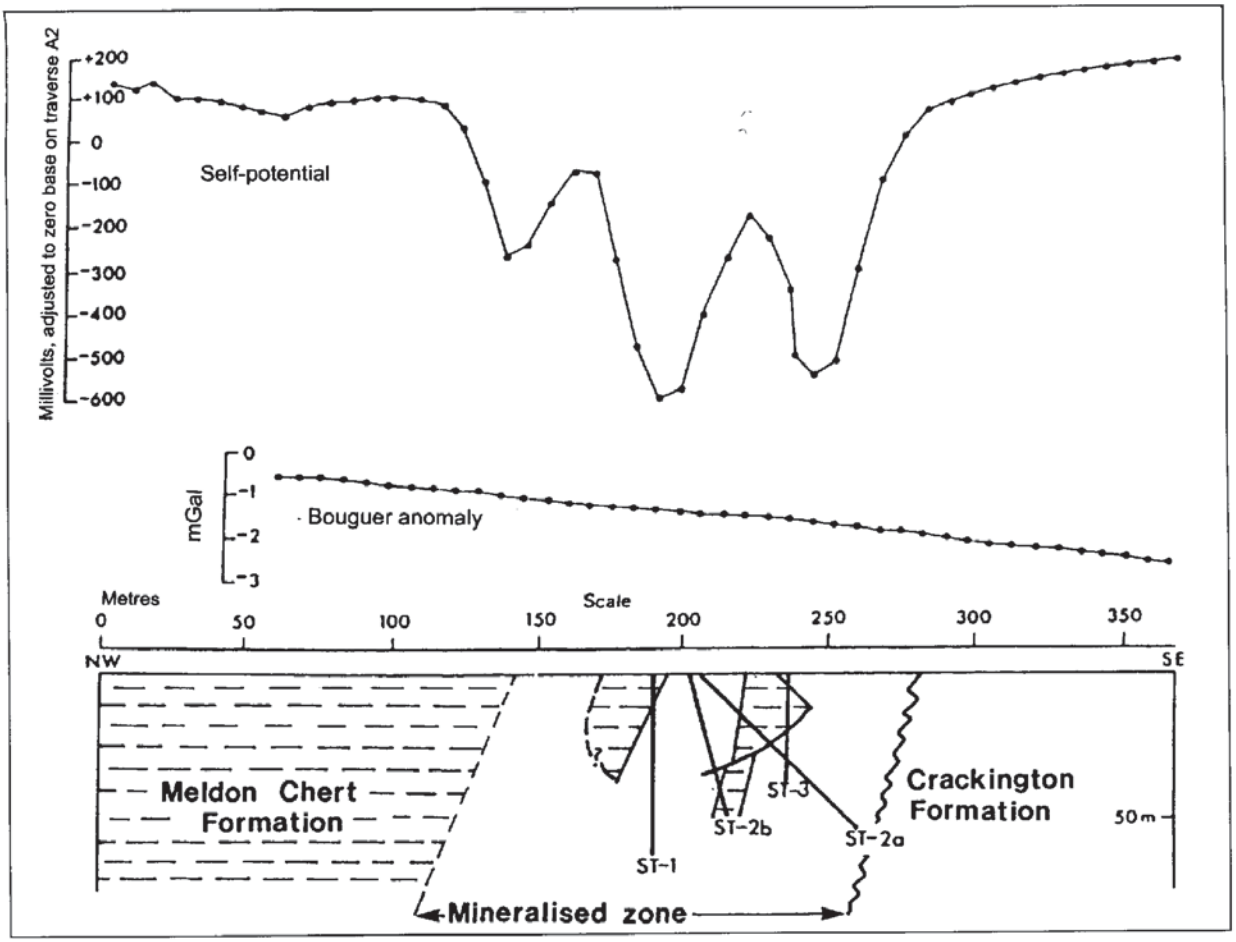

Figure 2.43 A Bouguer gravity profile across mineralised zones in chert at Sourton Tors, north-west Dartmoor, showing no discernible anomalies. From Beer and Fenning (1976), by permission

sheets and valley glaciers. Very often, these areas have incomplete information about the depth or volume of ice. The large density difference between ice (0.92 Mg/m^3) and the assumed average rock density (2.67 Mg/m^3) means that easily measured gravity anomalies can be observed and the bottom profile of the ice mass (i.e. the sub-glacial topography) can be computed.

An example of this has been given by Grant and West (1965) for the Salmon Glacier in British Columbia (Figure 2.44), in which a gravity survey was undertaken in order to ascertain the glacier's basal profile prior to excavating a road tunnel beneath it. A residual gravity anomaly minimum of almost 40 mGal was observed across the glacier, within an accuracy of ± 2 mGal due to only rough estimates having been made for the terrain correction. An initial estimate of local rock densities was 2.6 Mg/m^3 and the resultant depth profile across the glacier proved to be about 10% too deep (Figure 2.44B) compared with depths obtained by drilling. Considering the approxi-

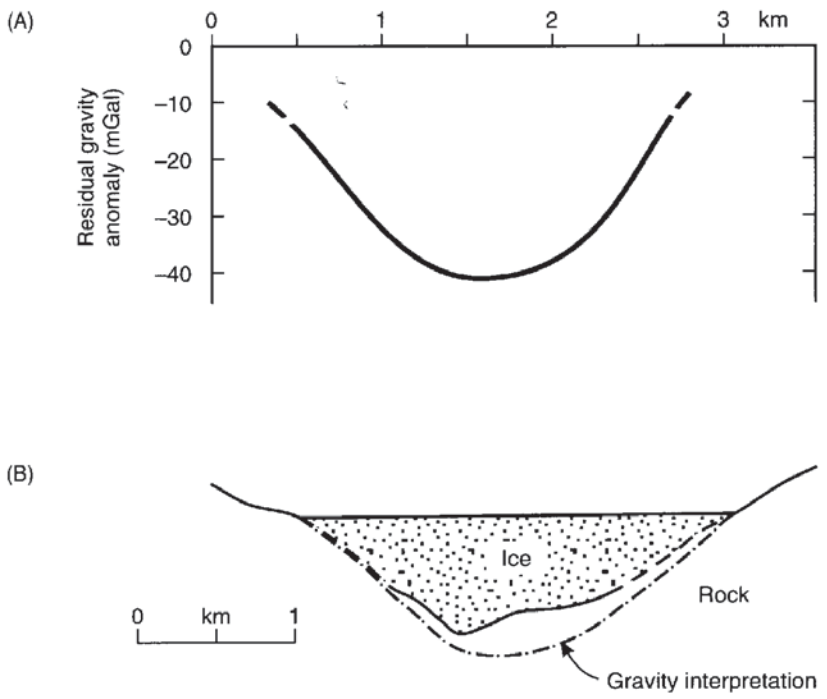

Figure 2.44 A residual gravity profile across Salmon Glacier, British Columbia, with the resulting ice thickness profile compared with that known from drilling. After Grant and West (1965), by permission

mations taken in the calculations, the agreement was considered to be fair. In addition, it was found that the average density of the adjacent rocks was slightly lower (2.55 Mg/m^3). This could have indicated that there was a significant thickness of low-density glacial sediments between the sole of the glacier and bedrock. However, had more detailed modelling been undertaken on data corrected fully for terrain, the discrepancy could have been reduced.

Increasingly, ice thickness measurements are being made by seismic reflection surveying (see Chapter 5), electromagnetic VLF measurements (see Chapter 9, Section 9.6.6.3) and radio echosounding (see Chapter 9, Section 9.7.4.2). Comparisons between the various geophysical methods indicate that agreements of ice thickness within 10% can be readily obtained. Gravity measurements over large ice sheets (e.g. Renner *et al.* 1985; Herrod and Garrett 1986) can be considerably less accurate than standard surveys for three reasons:

- The largest errors are due to the imprecise determination of surface elevations. Currently, heights can be determined to within 5–10 m.
- Inaccurate corrections for sub-ice topography vary by hundreds of metres, in areas without radio echosounding control. An error in estimated ice thickness/bedrock depth of 100 m can introduce an error of ± 74 g.u.
- As in all gravity surveys, the estimate of the Bouguer correction density is also of critical importance. Major ice sheets obscure the

local rock in all but a few locations, and the sub-ice geology, and its associated densities, may vary significantly.

Another glaciological application of the gravity method is the use of a gravimeter to measure oceanic tidal oscillations by the vertical movements of floating ice shelves in the Antarctic (Thiel *et al.* 1960; Stephenson 1984). The resulting tidal oscillation pattern can be analysed into the various tidal components and hence relate the mechanical behaviour of the ice shelf to ocean/tidal processes. If tidal oscillations are not found at particular locations, this may indicate that the ice shelf is grounded. Independent measurements with tilt meters, strain gauges and radio echosounding should be used to confirm such a conclusion (Stephenson and Doake 1982).

2.7.4 Engineering applications

The size of engineering site investigations is normally such that very shallow (<50 m) or small-scale (hundreds of square metres) geological problems are being targeted. Consequently, the resolution required for gravity measurements is of the order of μGals. The use of gravity is commonly to determine the extent of disturbed ground where other geophysical methods would fail to work because of particularly high levels of electrical or acoustic noise, or because of the presence of a large number of underground public utilities (Kick 1985). Additionally, gravity is used to assess the volume of anomalous ground, such as the size of underground cavities or of ice lenses in permafrost. There are often no records of where ancient quarrying or mining has been undertaken and the consequent voids may pose considerable hazards to people and to property. The increasing development of higher latitudes brings its own engineering problems, and the application of gravity surveying, amongst other applied geophysical methods, is playing a growing and important role in site investigations in these areas. Furthermore, it is also true to say that with the increased use of geophysical methods, the very geological phenomena under investigation are becoming better studied and better known.

2.7.4.1 Detection of back-filled quarries

Where there is sufficient density contrast between infill material and the surrounding rock, small-scale gravity surveys can be used successfully to locate backfilled quarries (Poster and Cope 1975), as the following example demonstrates.

A proposed new railway section in Newcastle-upon-Tyne, England, was routed through a built-up area which contained a number of backfilled, late-nineteenth century sandstone quarries. The design of the section of railway included a cut-and-cover tunnel, and so it was

extremely important to determine the position of the old quarry faces very accurately. The nature of the loose infill material (density 1.65 M/m^3) provided a strong contrast in physical properties with the local sandstone (of density 2.1 Mg/m^3) and a number of geophysical methods could have been employed. However, the site was criss-crossed by a large number of underground pipes and cables, and the superficial material contained significant amounts of scrap metal, all of which made it impractical to use electrical, electromagnetic or magnetic methods. High levels of acoustic noise which were generated by large volumes of traffic during the working day, and the lack of space due to extensive building cover, precluded the use of seismic methods. Consequently, the gravity method was selected and operated between the hours of midnight to 6 a.m., thus avoiding the problems of vibrations arising from both traffic and from heavy industrial plant, and ensuring better access through the reduction in the number of parked cars.

The contrast in density between the infill material and the local sandstone (0.5 Mg/m^3) produced small but detectable residual gravity anomalies of the order of 0.7 mGal. The gravity data were reduced and interpreted with the aid of data from one borehole and a preliminary archaeological investigation. A map of the residual gravity anomalies (Figure 2.45) clearly illustrates the locations of the faces of two quarries.

2.7.4.2 *Detection of massive ice in permafrost terrain*

The thawing of massive ice masses and associated ice-rich permafrost can cause severe engineering and environmental problems. The detection and identification of such ground phenomena is thus extremely important.

Kawasaki *et al.* (1983) provide an example of the use of gravity surveying to detect the presence and the volume of massive ice within an area of permafrost at Engineer Creek, near Fairbanks, Alaska, along the route of a proposed road cut. It is well known that large bodies of massive ice, such as occur within pingos, give rise to significant gravity anomalies (Mackay 1962; Rampton and Walcott 1974). Permafrost without discrete segregated ice has a density of about 1.6 Mg/m^3, compared with the density of solid ice (0.88–0.9 Mg/m^3) and with that of typical Alaskan soils (1.35–1.70 Mg/m^3) and should give rise to detectable residual gravity anomalies if measured with a sufficiently sensitive gravimeter.

Kawasaki and colleagues demonstrated that, although massive ice can be detected by correlation with the gravity minima along the profile shown in Figure 2.46, the measurements were also sensitive to variations of density within the schist bedrock.

The gravity method is considered an excellent tool for detailed investigation of construction sites where massive ice is suspected, but

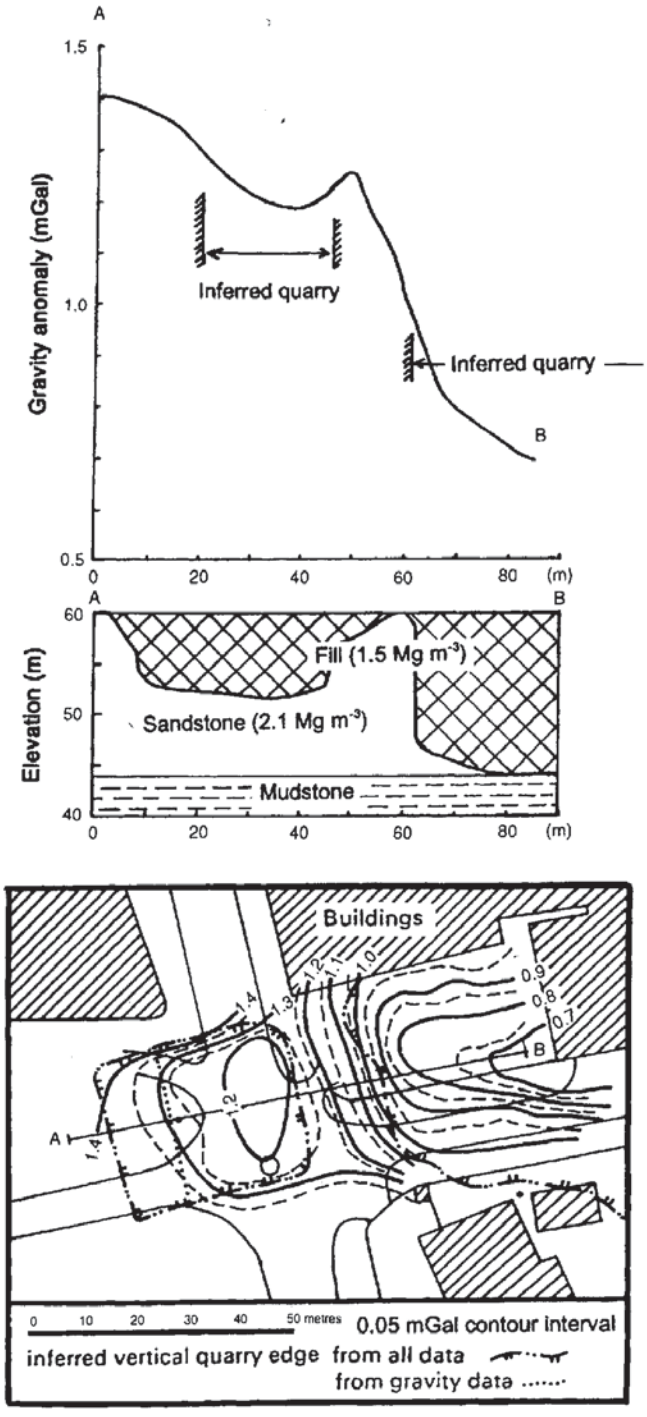

Figure 2.45 The top shows a residual gravity profile across infilled sandstone quarries in Newcastle-upon-Tyne. The cross-section and plan are also shown. After Poster and Cope (1975), by permission

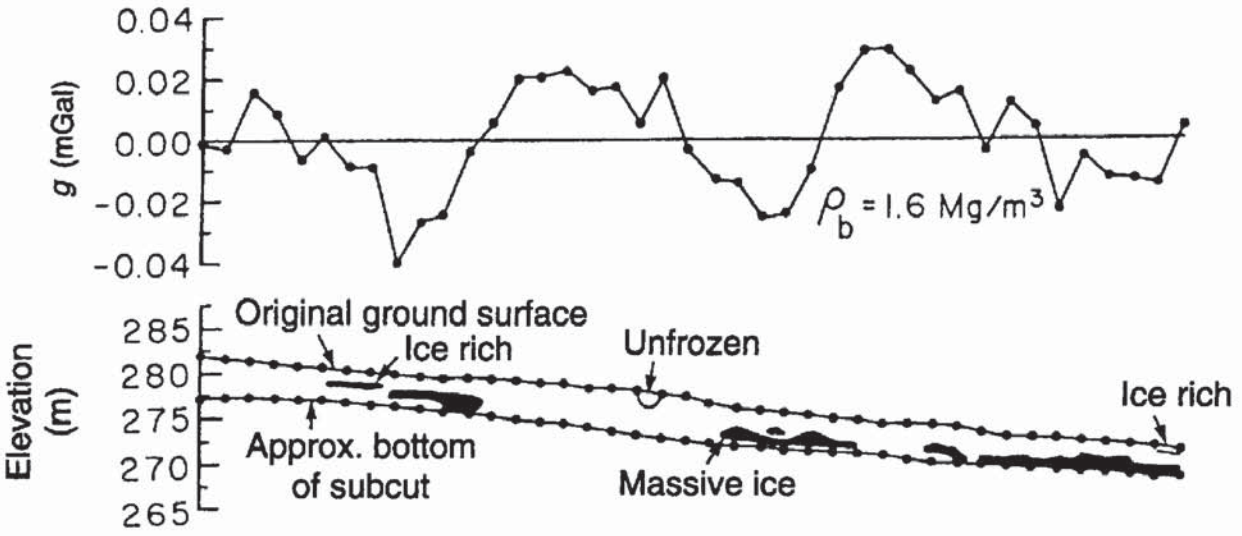

Figure 2.46 Gravity profile across massive ground ice in a road cut at Engineer Creek, near Fairbanks, Alaska. After Kawasaki *et al.* (1983), by permission

it is too slow a method for use as a reconnaissance tool over long profiles. Other geophysical methods such as electrical resistivity, electromagnetic ground conductivity and ground-penetrating radar are more efficient, particularly for reconnaissance (Osterkamp and Jurick 1980).

2.7.5 Detection of underground cavities

Hidden voids within the near-surface can become serious hazards if exposed unwittingly during excavation work, or if they become obvious by subsidence of the overlying ground (Figure 2.47). The detection of suspected cavities using gravity methods has been achieved in many engineering and hydrogeological surveys (e.g. Colley 1963). Gravimetry is increasingly of interest to archaeologists searching, for example, for ancient crypts or passages within Egyptian pyramids, such as has been achieved within the Kheops (see *First Break*, 1987 5(1): 3) with what is called 'endoscopic micro-gravity' (see also Lakshmanan 1991).

2.7.5.1 Hidden natural cavities

An example of the application of micro-gravimetry to the detection of underground cavities has been given by Fajklewicz (1986). Over many years he has investigated the gravity effect of both natural and man-made cavities and has helped to develop a method of detection based on calculating the vertical gradient of the gravity field. He has found that the amplitude of the gravity anomaly is commonly greater than that predicted (Figure 2.48) for reasons that are still not clear.

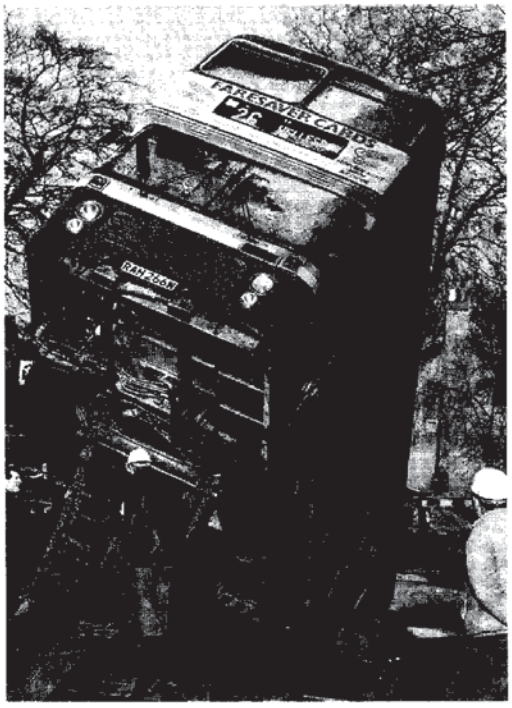

Figure 2.47 Catastrophic failure of the roof of an ancient flint mine in chalk in Norwich. Photo courtesy of Eastern Daily Press

A micro-gravity survey was carried out in the town of Inowrocław, Poland, where karst caverns occur to depths of around 40 m in gypsum, anhydrite, limestone and dolomite. The cavities develop towards the ground surface and have resulted in the damage and destruction of at least 40 buildings within the town. The density contrast between the cavity and the surrounding material in Figure 2.48A is $-1.8\ \mathrm{Mg/m^3}$ and for Figure 2.48B is $-1.0\ \mathrm{Mg/m^3}$, slightly lower due to the presence of rock breccia within the cavity. Fajklewicj has demonstrated that the cavity in Figure 2.48B should not have been detectable assuming that its gravity field is due entirely to a spherical cavity at the depth shown. Even the theoretical anomaly from the vertical gravity gradient is too broad to indicate the presence of a cavity, yet the observed anomaly is quite marked.

A similar approach can be taken using horizontal gravity gradients ($\Delta g/\Delta x$ or $\Delta g/\Delta y$), in which case the point at which the gravity anomaly reaches a minimum or maximum, the gradient goes through zero, and that point should lie over the centre of the body causing the anomaly (Butler 1984). An example of this (Figure 2.49) is given by Casten and Gram (1989) for a test case where gravity data were measured in a deep coal mine along an inclined drift which was known to pass at right-angles over a pump room.

Furthermore, micro-gravimetry can be used to determine the rate and extent of the development of strength-relaxation around underground excavations, as shown in Figure 2.50 (Fajklewicz 1986;

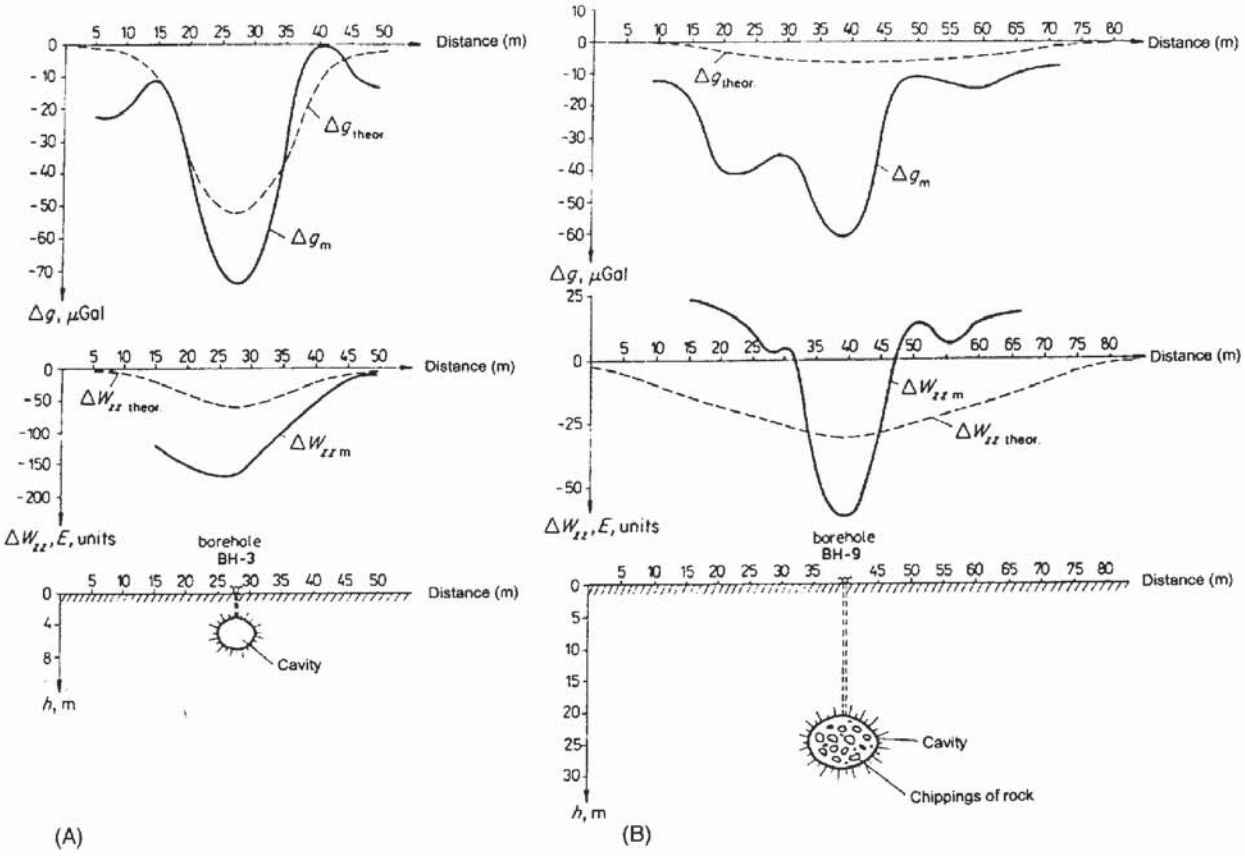

Figure 2.48 Δg_m and $\Delta W_{zz,m}$ micro-gravity anomalies and gravity gradient anomalies respectively–over (A) an air-filled cavity (BH-3), and (B) one partially infilled by rock fragments (BH-9). Curves labelled with suffix 'theor' represent the theoretical anomalies based on the parameters of the cavity alone. From Fajklewicz (1986), by permission

Gluśko *et al.* 1981). As the rock relaxes mechanically it cracks, thereby reducing its bulk density. As the cracking continues and develops, so the changes in density as a function of time can be detected using highly sensitive micro-gravimeters, and then modelled.

2.7.5.2 *Archaeological investigations*

Blizkovsky (1979) provides an example of how a careful micro-gravity survey revealed the presence of a suspected crypt within the St 'Venceslas church, Tovacov, Czechoslovakia, which was later proven by excavation work. The dataset consisted of 262 values measured on a $1\,m^2$ or $4\,m^2$ grid to an accuracy of $\pm 11\,\mu$Gal, corrected for the gravity effect of the walls of the building (Figure 2.51). Two significant gravity minima with relative amplitudes of $-60\,\mu$Gal were located which indicated mass deficiencies associated with the previously unknown crypts.

2.7.6 Hydrogeological applications

Gravity methods are not used as much as electrical methods in hydrogeology but can still play an important role (Carmichael

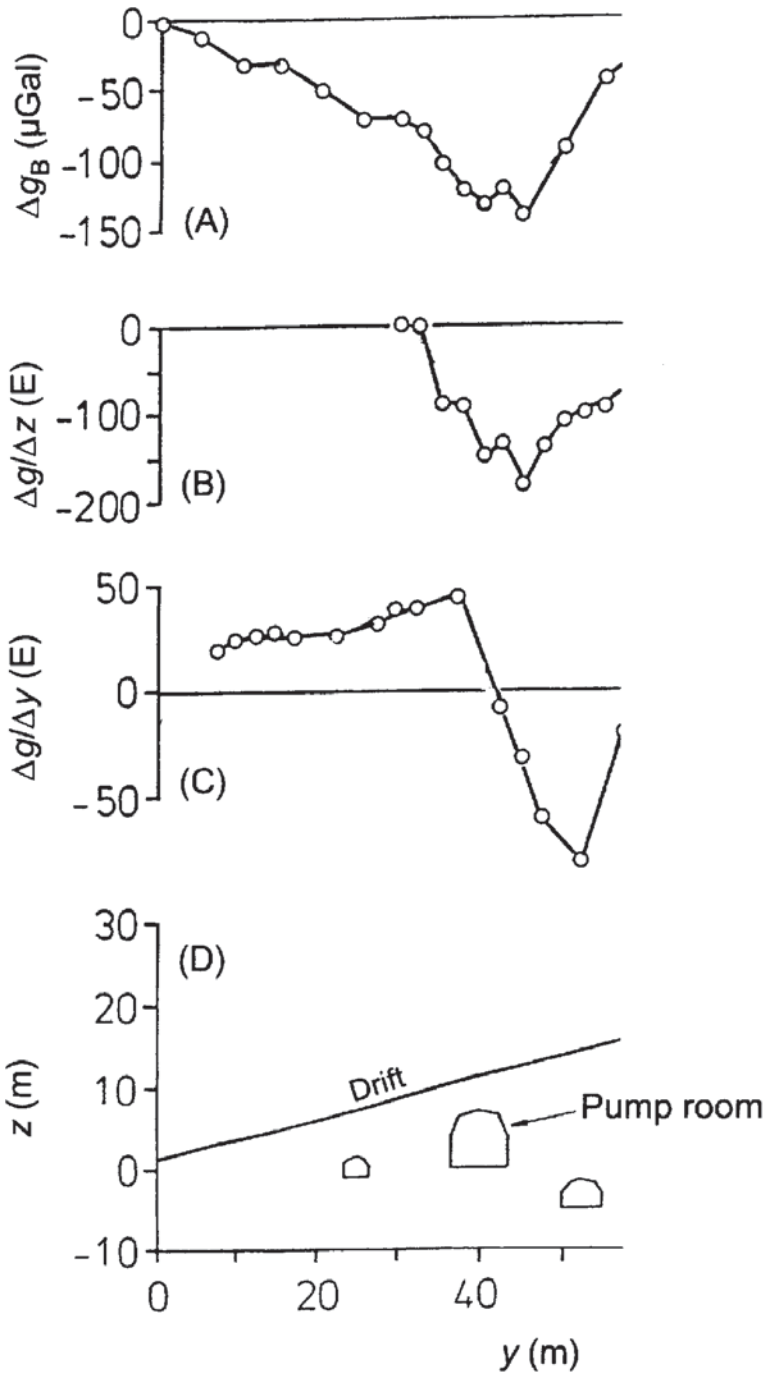

Figure 2.49 A micro-gravity survey within a deep coal mine as measured along a drift cut over a pump room and other known cavities. (A) shows observed residual gravity profiles; (B) observed and computed vertical gravity gradients; (C) observed horizontal gravity gradient, and (D) underground positions of known cavities from mine plans. From Casten and Gram (1989), by permission

and Henry 1977). Their more normal use is to detect low-density rocks that are thought to be suitable aquifers, such as alluvium in buried rock valleys (Lennox and Carlson 1967; van Overmeeren 1980).

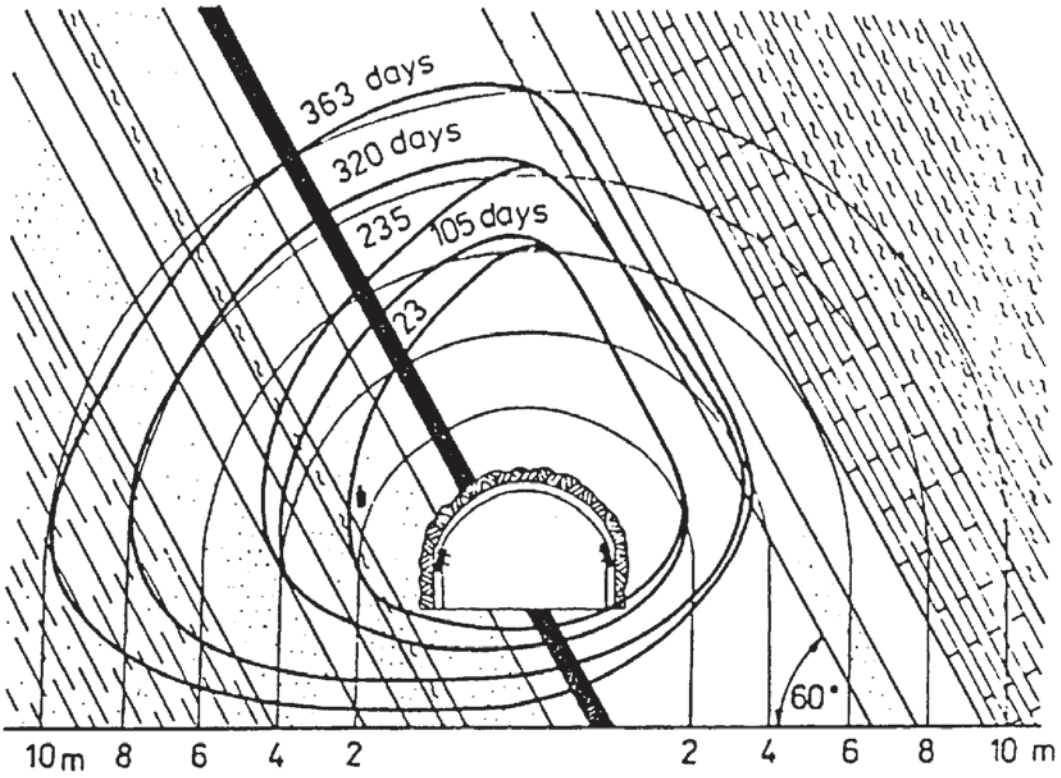

Figure 2.50 The time-dependent strength-relaxation around an underground gallery at 540 m depth as deduced from micro-gravity surveying in the Tchesnokov Colliery in the Don Basin over a period of 363 days. From Gluśko *et al.* (1981) and Fajklewicz (1986), by permission

Buried valleys, which have been incised into either bedrock or glacial till and are associated with the South Saskatchewan River, have been identified by their gravity effects (Hall and Hajnal 1962). The Bouguer anomaly across the current river valley shows a minimum considerably wider than the present-day valley (Figure 2.52), thus indicating the presence of low-density material – subsequently found by drilling to be silts and sand.

Rather than interpret Bouguer anomalies, it is possible to use a gravimeter to monitor the effect of changing groundwater levels. For example, in a rock with a porosity of 33% and a specific retention of 20%, a change in groundwater level of 30 m could produce a change in g of 170 μGal. It is possible, therefore, to use a gravimeter to monitor very small changes in g at a given location. The only changes in gravity after corrections for instrument drift and Earth tides should be the amount of water in the interstices of the rock. Consequently, for an aquifer of known shape, a measured change in gravity, in conjunction with a limited number of water-level observations at a small number of wells, can be translated into an estimate of the aquifer's specific yield. Similarly, repeated gravity measurements have been used to estimate the volume of drawdown, degree of saturation of the steam zone (Allis and Hunt 1986) and the volume of

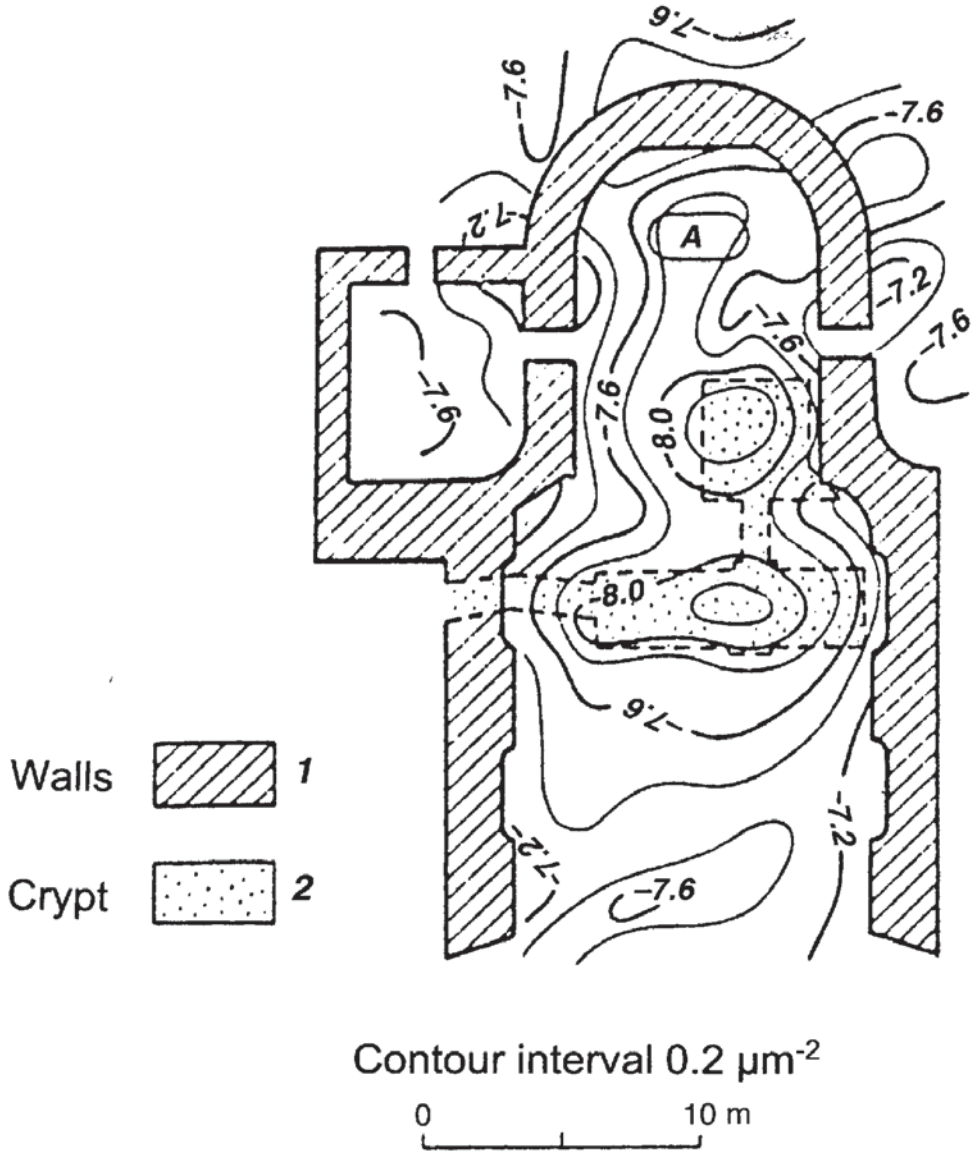

Figure 2.51 Micro-gravity map of St 'Venceslas Church, Tovacov, Czechoslovakia showing marked anomalies over previously unknown crypts. From Blizkovskt (1979), by permission

recharge of the Wairakei geothermal field, North Island, New Zealand (Hunt 1977).

2.7.7 Volcanic hazards

With the advent of highly accurate surveying equipment and methods, and the availability of very sensitive gravimeters, it is possible to monitor small changes in the elevations of the flanks of active volcanoes – ultimately with a view to predicting the next eruption. Such studies are often accompanied by seismic monitoring

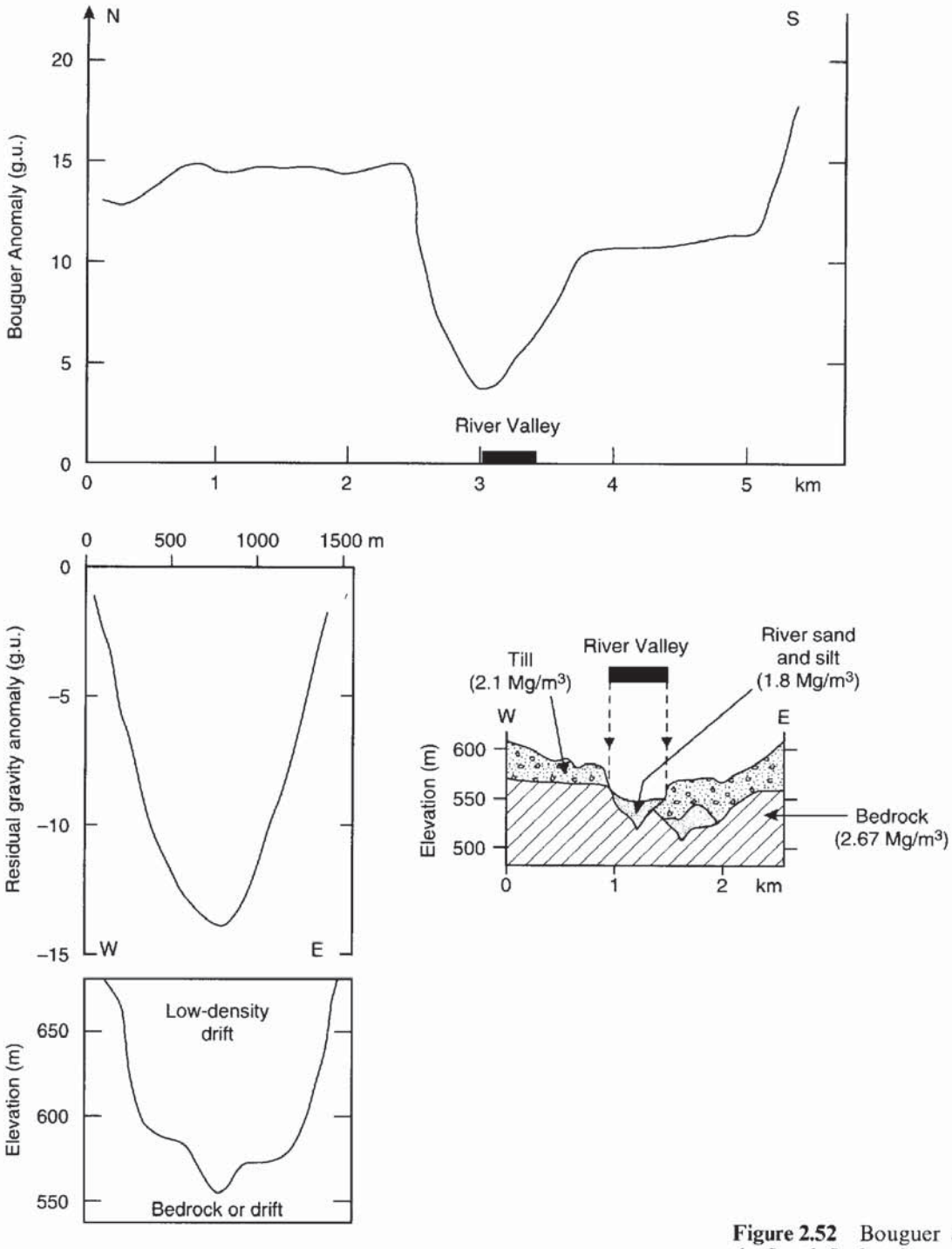

Figure 2.52 Bouguer anomaly over the South Saskatchewan River Valley, and the corresponding geological cross-section across the gravity minimum. After Hall and Hajnal (1962), by permission

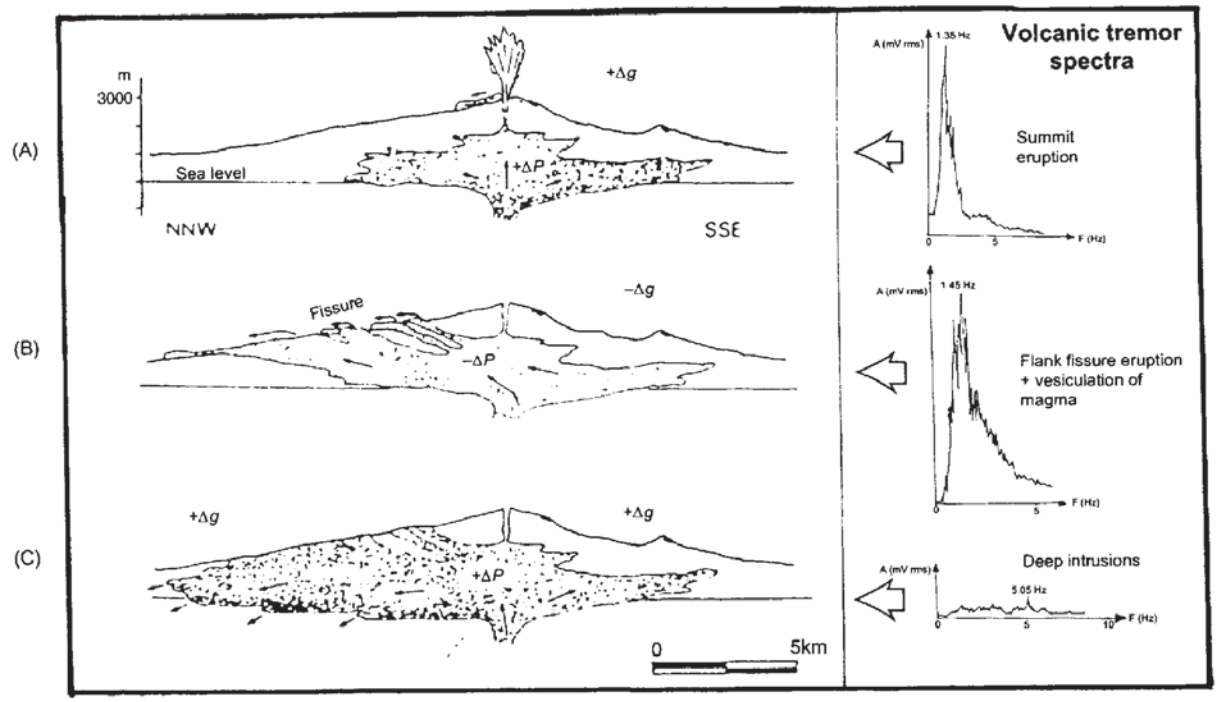

Figure 2.53 Sketches of the stages of fissure eruptions on Mt Etna, Sicily, with gravity trends and typical volcanic tremor spectra. From Sanderson *et al.* (1983) and Cosentino *et al.* (1989), by permission

(e.g. Cosentino *et al.* (1989). Sanderson *et al.* (1983) carried out such a gravity monitoring and levelling programme on Mount Etna, Sicily, during the period August 1980 to August 1981, during which time a flank eruption took place (17–23 March 1981) from which a lava flow resulted which narrowly missed the town of Randazzo. A series of schematic diagrams is shown in Figure 2.53 to illustrate the three clear stages of the fissure eruption.

Changes in gravity in association with elevation increases were interpreted as the injection of new magma at depth during the intrusion of a new dyke at about 1.5 km depth (Figure 2.53A). Gravity decreases were observed when eruptions took place because of the reduction in material (Figure 2.53B). Where increases in gravity were observed without an increase in elevation, this was interpreted as being due to the density of the magma increasing by the enforced emplacement of new material at depth (Figure 2.53C). The magnitude of the gravity changes (≈ 2–$25\,\mu$Gal) coupled with the known variations in elevation ($< \approx 20$ cm) provide a means of determining where within the volcano's plumbing the intrusions of new material and/or density changes are taking place.

Rymer and Brown (1987, 1989) have summarised the micro-gravity effects resulting from vertical movements of the magma/rock interface, vesiculation cycles with the magma column and radial changes in the dimensions of the magma body for Poás volcano in Costa Rica

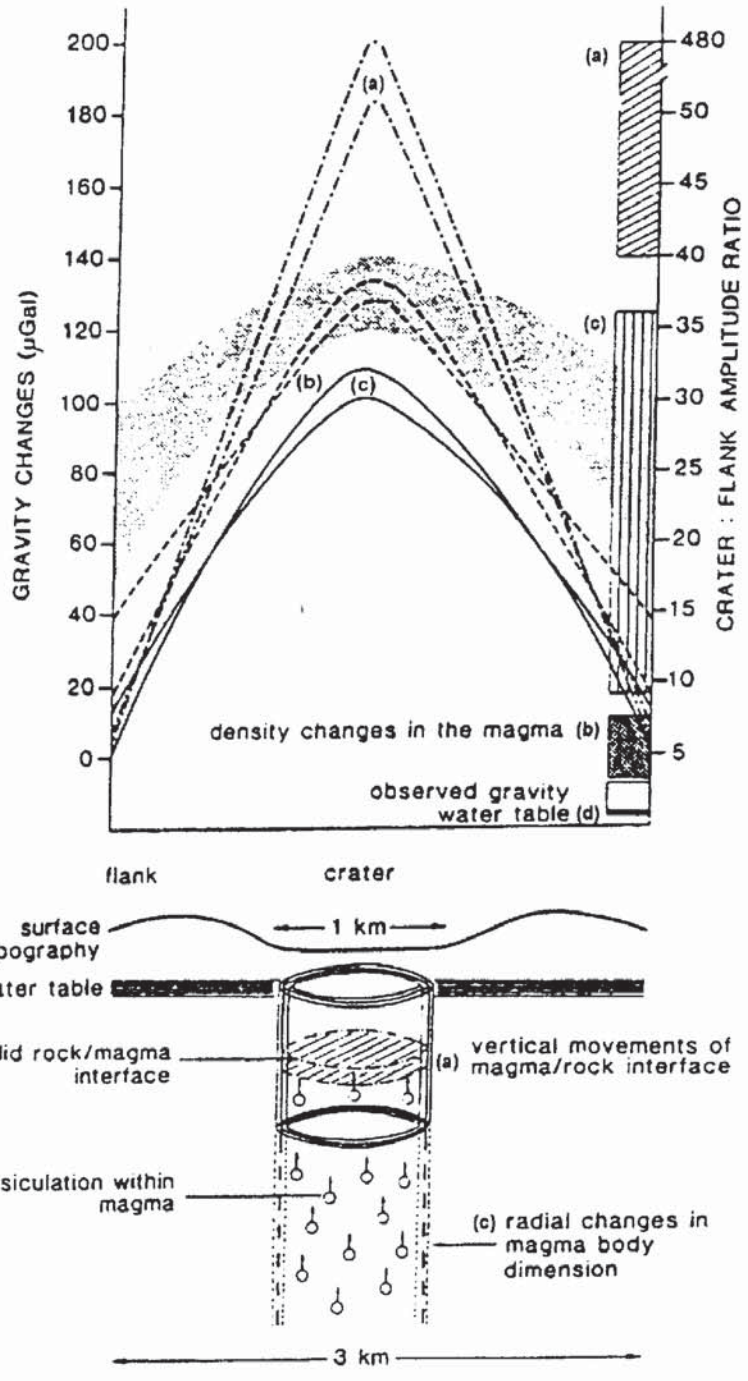

Figure 2.54 The top shows a schematic of the various gravity effects produced at the flank and summit of Poás volcano, Costa Rica (the observed range of gravity effects is shaded) and the ratio of the two (shown alongside in the vertical bar) as caused by different geological processes within the volcano (lower diagram). The processes are: (a) vertical movements of the magma/rock interface; (b) vesiculation cycles within the magma column; (c) radial changes in dimension of the magma column, and (d) variations in the level of the water table. From Rymer and Brown (1987), by permission

Figure 2.54). The individual internal processes in this particular volcano can be clearly differentiated by using the ratio of the gravity effects measured at the volcano flank and summit. However, not all sub-terrainian activity is associated with seismic signatures. Indeed,

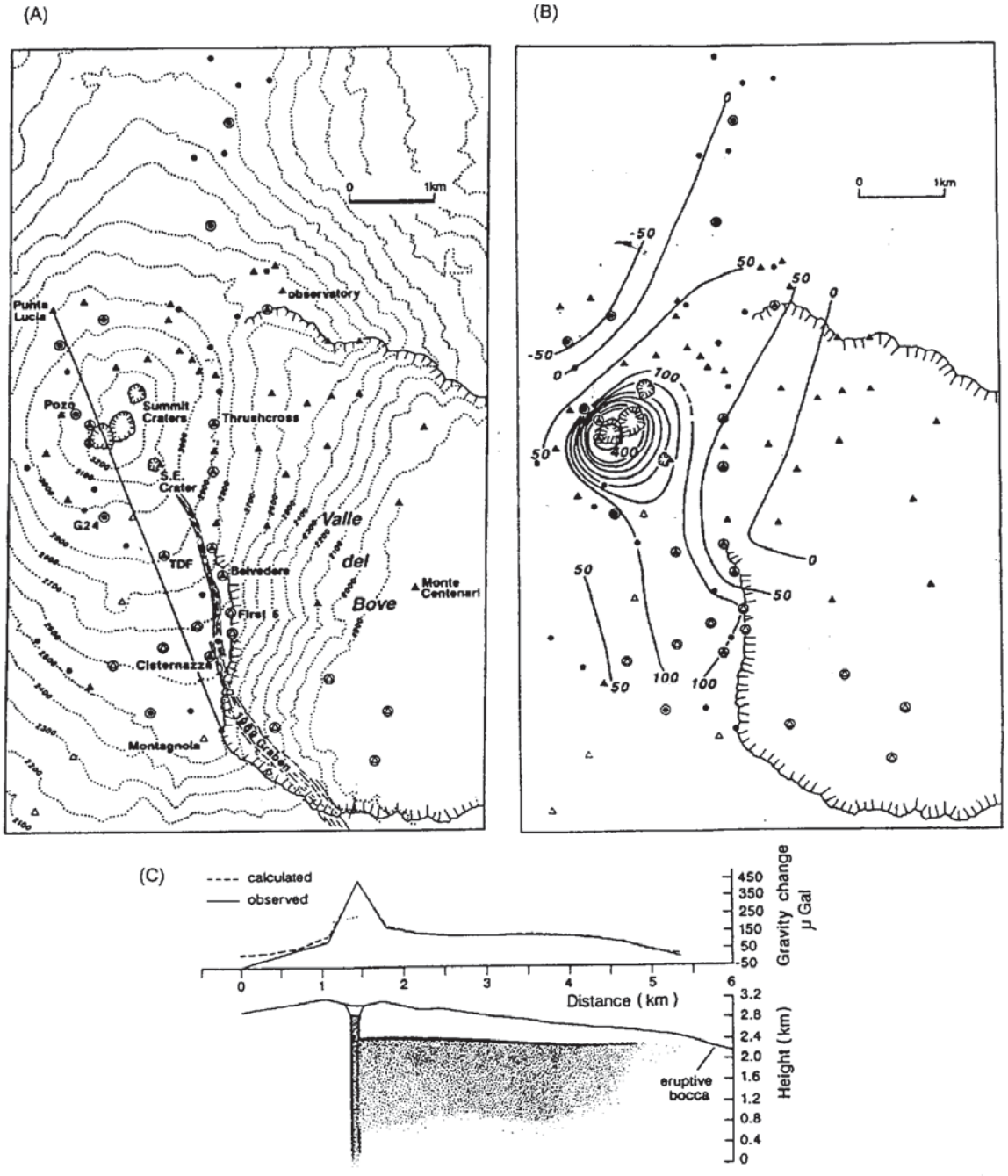

Figure 2.55 Maps showing (A) the locations of micro-gravity and ground deformation monitoring stations and (B) a contoured micro-gravity map of the summit area of Mt Etna, Sicily. The contour interval is 50 μGal. (C) Cross-section through the summit area of the Mt Etna along the profile indicated in (A). The best-fitting model for the observed gravity changes involved a dyke 4 m wide and a feeder pipe 50 m in diameter filling with magma at some time between the two sets of observations in June 1990 and June 1991. From Rymer (1993) and Rymer *et al.* (1993), by permission

Rymer (1993) reported on an increase in gravity at Mt Etna between June 1990 and June 1991 with no corresponding seismic activity. Large increases in gravity were observed around the summit craters and along an elongated zone following the line of a fracture formed during a previous eruption in 1989 (Figure 2.55). Surface elevation changes surveyed between 1990 and 1991 were only of the order of less than 3 cm. The gravity changes were an order of magnitude larger than would have been expected on the basis of elevation changes alone, which suggested that there must have been some sub-surface increase in mass. This was calculated to be of the order of 10^7 Mg and was caused by the intrusion of magma into fractures left by the 1989 eruption. The magma migrated passively into the pre-existing fractures so there was no corresponding seismic activity. Consequently, the micro-gravity measurements, in conjunction with elevations surveys, produced the only evidence of an impending eruption. The eruption of Mt Etna lasted for 16 months from 1991 to 1993, during which time lava poured out of the vent at a rate of $10\,m^3/s$, making this the largest eruption there for 300 years (Rymer 1993; Rymer *et al.* 1993).

Micro-gravity monitoring coupled with the distinctive patterns of the frequency of seismic activity (volcanic tremor spectra) are beginning to provide a very comprehensive model for volcanic eruptions, such as those at Mt Etna, and their associated processes. Many other volcanoes now have active monitoring programmes utilising gravity, seismic, and thermal investigations. Monitoring gas emissions is also proving to be a valuable additional indicator of impending volcanic activity (e.g. Pendick 1995, on the work of S. Williams). If these data can be obtained for individual volcanoes in conjunction with thermal radiation as measured by satellite, then the probability of identifying recognisable precursors to eruptions may be enhanced significantly, leading to a better prediction of volcanic activity and mitigation of potential hazards (Rymer and Brown 1986; Eggers 1987).

Chapter 3
Geomagnetic methods